

LEAP-RE

Research and Innovation Action (RIA)

This project has received funding from the European Union's Horizon 2020 research and innovation programme under grant agreement No 963530

Start date: 2020-10-01 Duration: 63 Months http://www.leap-re.eu/



Final report of task 9.2 on all surface data collected to be used in the Geothermal Atlas

Authors: Pr. Fiaschi DANIELE (UNIFI), Claudio Zuffi (UNIFI) Daniele Fiaschi (UNIFI)

LEAP-RE - Contract Number: 963530

Project officer: Bernardo Luis ABELLO GARCIA

Document title	Final report of task 9.2 on all surface data collected to be used in the Geothermal Atlas
Author(s)	Pr. Fiaschi DANIELE, Claudio Zuffi (UNIFI) Daniele Fiaschi (UNIFI)
Number of pages	89
Document type	Deliverable
Work Package	WP9
Document number	D9.3
Issued by	UNIFI
Date of completion	2024-03-30 20:10:49
Dissemination level	Error (13) !

Summary

The report outlines the LEAP-RE project's focus on developing and analyzing the Geothermal Atlas for Africa (GAA) within Work Package 9 (WP9), specifically Task 9.2, which examines engineering technologies for geothermal resources. Aligned with Task 9.1, which addresses geological-geophysical aspects and resource mapping, the objective is to create a tool for evaluating engineering applications for sustainable resource exploitation, considering energy, economic, and environmental factors. Methodologically, key parameters like temperature, mass flow rate, and ambient air temperature are selected to assess system performance in geothermal energy systems. Various energy system models are then validated to develop meta-models. Economic modeling analyzes plant component costs and evaluates initial investment and operation costs to determine the Levelized Cost of Energy (LCOE), while environmental modeling follows Life Cycle Assessment (LCA) methodology, focusing on Climate Change impact using the Environmental Footprint 3.1 methodology. Validation of thermodynamic and thermos-economic metamodels involves analyzing geothermal plants, facing challenges due to data scarcity. While the metamodels occasionally overestimate or underestimate parameters, they demonstrate low margin of error, ensuring reliability. Comparison of LCA results is complicated due to data variability, addressed by a meticulous analysis approach. Overall, the developed metamodels effectively forecast the size, cost, and environmental impact of geothermal energy systems, enhancing feasibility assessments. The final project mapping phase evaluates geographical areas for production potential, economic viability, and environmental feasibility, further enriching the tool's utility.

Approval	
Date	Ву
2024-03-30 20:11:56	Pr. Fiaschi DANIELE (UNIFI)
2024-04-03 17:54:01	Mr. Léonard LéVêQUE (LGI)



Research & Innovation Action

March 2024

Geothermal Atlas For Africa Deliverable D9.3

Task 9.2: Engineering Science

Version N°1

Authors:

Claudio Zuffi (University of Florence) Daniele Fiaschi (University of Florence)





Disclaimer

The content of this report reflects only the author's view. The European Commission is not responsible for any use that may be made of the information it contains.



Document information

Grant Agreement	963530				
Project Title	Long-Term Joint EU-AU Research and Innovation Partnership on Renewable Energy				
Project Acronym	LEAP-RE				
Project Coordinator	Vincent Chauvet (<u>Vincent.chauvet@lgi-consulting.com</u>) – LGI				
Project Duration	1 st October 2020 – 31 st December 2025 (63 Months)				
Related Work Package	Working Package 9: Geothermal Atlas for Africa				
Related Task(s)	Task 9.2: Engineering Sciences				
Lead Organisation	University of Florence (UNIFI)				
Contributing Partner(s)	UNIFI, Strathmore University (SU)				
Due Date	31/03/2024				
Submission Date					
Dissemination level					



History

Date	Version	Submitted by	Reviewed by	Comments
30/03/2024	1			



Table of contents

1.	Intro	ductio	on	.11
2.	Geot	herm	al tool	13
:	2.1	High	Enthalpy	16
	2.1.1		Flash / Dry steam	16
	2.1.2		Organic Rankine Cycle	19
:	2.2	Medi	ium and Low Enthalpy solution Heat and cold production	21
	2.2.1		High Temperature Heat Pump	21
	2.2.2		Refrigeration Absorption System	.23
:	2.3	Econ	nomic Evaluation	.24
:	2.4	Envi	ronmental assessment	.29
	2.4.1		Geothermal wells	.29
	2.4.2		Machinery	.33
		1.2.1 1.2.2	Power plant HTHP	
	2.4.3	}	Pipeline and Building	36
	2.4.4		Operation and Maintenance	37
	2.4.5	;	Case studies: Olkaria IV power plant	37
	2.4	1.5.1	Life Cycle Inventory: Olkaria IV	38
3.	Resu	lts		42
	3.1	High	Enthaply validation	42
	3.1.1		Thermodynamic	42
	3.1.2		Economic	43
	3.1.3	}	Environmental	44
	3.1.4		Metamodel results	47
	3.2	Medi	ium and Low Enthalpy validation	49
	3.2.1		Thermodynamic	50
	3.2.2		Economic	51
	3.2.3	;	Metamodel results	51
	3.2.4		Application and case studies	56
4.	Strat	hmor	e – Ken Gen Collaboration	61
4	4.1	LCA	Olkaria IV	61
4	1.2	Geot	thermal Power Plant in Kenya	66
4	1.3	Knov	wledge transfer and application cases with Strathmore University	67
5.	Conc	lusior	1	70
Αр	oendix:			73
Ref	erence			.79



List of figures

Figure 1: Lindal diagram for geothermal energy (DiPippo, 2016)	.14
Figure 2: Schematic diagram of the geothermal tool	15
Figure 3: T-s diagram of water representing the geothermal fluid inlet	16
Figure 4: Installation diagram of the Flash (A.1) and Dry-steam (A.2) power plant	17
Figure 5: T-s diagram and mass vapor fraction range	18
Figure 6: ORC binary power plant layout	20
Figure 7: High Temperature Heat pump layout	22
Figure 8: Refrigeration Absorption System layout	24
Figure 9: Correlation for number of geothermal wells	26
Figure 10: Material correlation for power plant machinery	34
Figure 11: Material correlation for High Temperature Heat Pump	35
Figure 12: Material correlation for Absorption System	36
Figure 13: thermodynamic power plant validation	43
Figure 14: LCOE metamodel validation	44
Figure 15: Comparison between Trend line, correlation proposed in the literature and primary de	
Figure 16: comparison with literature, primary data and trend-line of Climate change indicators.	
Figure 17: Levelized Cost Of Electricity metamodel results for different well depth (wd). A: wo =1000m; B: wd = 2000m; C: wd = 3000m; D: wd= 4000m (Power Plant)	
Figure 18: Climate Change metamodel results for different well depth (wd): A:wd =1000m; B: = 2000m; C: wd = 3000m; D: wd= 4000m (Power Plant)	
Figure 19: Column diagram of the validation of thermodynamic metamodel for the absorption cy	
Figure 20: Column diagram for validation of the economic metamodel for the absorption cycle \dots	51
Figure 21: thermodynamic metamodels of Coefficient of Performance and Evaporation Temperat	
Figure 22: Levelized Cost of Cold economic metamodels for different well depth (wd): A:wd = 00 B: wd = 500m; C: wd = 1000m; D: wd= 2000m (ABS)	m;
Figure 23: Environmental metamodels of climate change indicators for different well depth (wd A:wd =0m; B: wd = 500m; C: wd = 1000m; D: wd= 2000m (ABS)	•
Figure 24: Levelized Cost of Heat economic metamodels for different well depth (wd): A:wd = 0 B: wd = 500m; C: wd = 1000m; D: wd= 2000m (HTHP)	
Figure 25: environmental metamodels of climate change indicators for different well depth (wd A:wd =0m; B: wd = 500m; C: wd = 1000m; D: wd= 2000m (HTHP)	•
Figure 26: Potential exploitation for a cooking station in Malawi	59
Figure 27: Potential exploitation for Cassava Drying in Malawi	60
Figure 28: Potential exploitation for a cooking station in Ethiopia	61
Figure 29: Contribution analysis of high priority indicators	63
Figure 30: Monte Carlo analysis with different σ for Climate Change	64

Engineering Science Deliverable 9.3



Figure 31: Monte Carlo analysis with different σ for Ecotoxicity freshwater	.65
Figure 32: Comparison between: different geothermal Photovoltaic, Wind power plant, and natio electricity grid at single score level	
Figure 33: Direct use flow diagram	.68
Figure 34: Extent of Thermal Ground in Sectors of Olkaria and Eburru (Hochstein & Kagiri, 1997)) 68
Figure 35: P-h diagram for milk pasteurization analysis on EES	.69
Figure 36: Analysis for different temperatures for UHT pasteurization process	.69

Engineering Science Deliverable 9.3



List of tables

Table 1: Classification of energy systems according to geothermal temperature range	14
Table 2: Parameter of the thermodynamic cycle	18
Table 3: Main parameter fixed for High Temperature Heat Pump	23
Table 4: Economic Correlation for machinery and wells	25
Table 5: Economic correlations for Thermo-economic model	28
Table 6: Simplified LCI of geothermal wells in literature	31
Table 7: Environmental correlation for pLCI	32
Table 8: material and energy consumption for Building (LCI Building)	36
Table 9: material and energy consumption for Pipeline (LCI Pipeline)	37
Table 10: LCI drilling geothermal wells	39
Table 11: LCI wellhead	40
Table 12: LCI pipeline	40
Table 13: LCI Building	41
Table 14: LCI Maintenance	41
Table 15: LCI operation	42
Table 16: Comparison of statistical parameter of trend line against correlations in the literature	46
Table 17: Hot spring from Malawi and Aluto-Langano	57
Table 18: Life Cycle Impact Assessment of Olkaria IV	62
Table 19: Kenvan geothermal power plants	67



Abbreviations and Acronyms

Acronym	Description
WP	Work Package
Geothermal Atlas for Africa	GAA
Absorption System	ABS
High Temperature Heat Pump	НТНР
Mass flow rate	m
Temperature	Т
Enthalpy	h
Pressure	Р
Vapor Mass Fraction	VMF
Coefficient of Performance	COP
Levelized Cost of Energy	LCOEn
Levelized Cost of Electricity	LCOE
Levelized Cost of Heat	LCOH
Levelized Cost of Cold	LCOC
Life Cycle Inventory	LCI
Parametric Life Cycle Inventory	pLCI



Life Cycle Impact Assessment	LCIA
Life Cycle Assessment	LCA
Well Depth	wd

Summary

The report outlines the LEAP-RE project's focus on developing and analyzing the Geothermal Atlas for Africa (GAA) within Work Package 9 (WP9), specifically Task 9.2, which examines engineering technologies for geothermal resources. Aligned with Task 9.1, which addresses geological-geophysical aspects and resource mapping, the objective is to create a tool for evaluating engineering applications for sustainable resource exploitation, considering energy, economic, and environmental factors. Methodologically, key parameters like temperature, mass flow rate, and ambient air temperature are selected to assess system performance in geothermal energy systems. Various energy system models are then validated to develop meta-models. Economic modeling analyzes plant component costs and evaluates initial investment and operation costs to determine the Levelized Cost of Energy (LCOE), while environmental modeling follows Life Cycle Assessment (LCA) methodology, focusing on Climate Change impact using the Environmental Footprint 3.1 methodology. Validation of thermodynamic and thermos-economic metamodels involves analyzing geothermal plants, facing challenges due to data scarcity. While the metamodels occasionally overestimate or underestimate parameters, they demonstrate low margin of error, ensuring reliability. Comparison of LCA results is complicated due to data variability, addressed by a meticulous analysis approach. Overall, the developed metamodels effectively forecast the size, cost, and environmental impact of geothermal energy systems, enhancing feasibility assessments. The final project mapping phase evaluates geographical areas for production potential, economic viability, and environmental feasibility, further enriching the tool's utility.

Keywords: Geothermal tool, Geothermal energy, Power Plant, Heat Pump, Energy analysis; Life Cycle Assessment



1. Introduction

The global transition from the current fossil-fuel-dependent energy system towards a sustainable one, primarily based on renewable resources, necessitates evidence-based decision-making supported by green technology (Christensen & Hain, 2017). Technology transfer and the development of new technologies are crucial for sustainable development and mitigating climate change (Noailly & Shestalova, 2017). Geothermal energy has demonstrated significant potential as a renewable energy resource due to its low environmental impact, minimal greenhouse gas emissions, and technological feasibility (Templeton, 2014; Shortall, 2015).

Geothermal energy is derived from the heat stored beneath the Earth's surface, utilizing natural heat sources accumulated over millions of years (Sharmin et al. 2023) and are predominantly concentrated in three main areas: the circum-Pacific belt's west coast, the Mid-Atlantic Ridge, and the Mediterranean to the Himalayan region (Dincer & Ozturk, 2021). Numerous authors concur that geothermal energy qualifies as a renewable energy source (Armstead, 1978; DiPippo, 2012; Johansson, 1993), with significant potential, offering a reliable and abundant alternative to fossil fuels (Lund 2020). This heat is primarily stored in hot rocks at considerable depths beneath the Earth's surface (Chen et al., 2015; Yang et al., 2009), and it is also present in complex structures of hydrothermal reservoirs at high temperatures. Overall, brine has been identified as a heat medium suitable for both fluid and vapor, including steam (vapor-dominated systems) and mineral-laden hot water (brine) (Zarrouk, 2015). These fluids transport geothermal heat stored underground to the surface for electricity generation and non-electric purposes (direct uses) through wells drilled into localized high-temperature geothermal reservoirs (Eslami-Nejad et al., 2014).

The temperature differential known as the 'Geothermal Gradient' serves as the fundamental source of energy (Gupta & Harsh, 2007). Global geothermal energy distribution varies based on geological and geophysical parameters. According to the World Geothermal Congress 2020 (WGC 2020) held in Reykjavik, Iceland, the total installed capacity of geothermal energy has steadily increased over the years: 10,897 MWe in 2010, 12,283 MWe in 2015, and 15,950 MWe in 2020. Projections indicate a forecasted capacity of 19,361 MWe by 2025. The estimated annual compound growth rate of the geothermal industry from 2015 to 2060 is anticipated to range from 3.4% to 5.4% under various scenarios (Dincer & Ozturk, 2021). Presently, the total installed capacity of geothermal power plants worldwide stands at 12,729 MW and is forecasted to reach 21,443 MW by 2020. In 2020, the top ten nations in terms of installed geothermal power generation plants were documented, with the United States, Indonesia, and the Philippines leading the pack (Huttrer, 2021). Various configurations of the power conversion system transform geothermal heat flow into electricity or other forms of direct heating (Zarrouk et al., 2015; Eslami-Nejad et al., 2014).

Geothermal power plants utilize different configurations for electricity generation, including steam cycles and binary cycles, with dry steam, single flash, double flash, and advanced geothermal energy conversion systems being among them (Anderson & Rezaie, 2019). Geothermal power plants are classically categorized as binary (14%), back pressure (1%), single flash (14%), double flash (14%), back pressure (1%),

single flash (41%), double flash (19%), triple flash (2%), and dry steam plants (23%) (Bertani, 2016). Similarly, the global installed thermal capacity amounts to 70,885 MWT, distributed across nine direct-use geothermal energy applications (Lund, 2016).

Despite the widespread availability of geothermal reservoirs, only 32% of global geothermal resources are deemed suitable for energy production (Moya et al., 2018). Dry



steam plants constitute approximately 23% of the global geothermal capacity, with single flash and double flash plants comprising the majority of the remaining capacity (Moya et al., 2018). Dry steam plants are recognized as the most cost-effective and efficient among geothermal power plants (Moya et al., 2018).

Africa's estimated geothermal potential stands at approximately 15 GW, primarily concentrated in the Rift Valley, with Kenya and Ethiopia holding significant shares. In 2016, Africa's total installed geothermal capacity ranged from 606 to 653 MW, with Kenya contributing 95% of this capacity (Tole et al., 1996; IRENA, 2023). Africa, particularly Kenya, emerges as a key player in geothermal power generation, currently producing 949 MW of electricity. Kenya's strategic location within the Rift Valley, rich in volcanic activity, presents an estimated untapped geothermal electricity potential ranging from 4000 to 7000 MW (Simiyu et al., 2000). This potential has spurred collaborative efforts between private investors and the government to leverage this valuable resource for electricity generation. Although the significance of geothermal energy in Kenya's national power sector is evident, it has yet to reach the scale of solar and wind energy sources.

However, the development of geothermal power plants in Africa faces several challenges, including substantial initial capital requirements and the need for a well-connected transmission line network. As of 2018, Kenya remains the sole African country with operational geothermal power stations. Ambitious plans aim to increase total geothermal installations in East Africa by over 4 GW within the next decade (Tole 1996). Nevertheless, various challenges hinder the progress of geothermal development, such as high upfront costs, insufficient grants for research and drilling, a lack of technological advancements, and a shortage of trained workers. Commercial banks' financial support, particularly during the drilling and exploration phases, remains crucial.

The evolution of geothermal production from 2013 to 2022 indicates fluctuations in power generation, with a decline observed from 2019 onwards, possibly attributed to insufficient investments in the domain. Nonetheless, the period from 2013 to 2019 saw consistent growth in production, serving as a potential example for further resource exploitation and development. The East Africa Rift System (EARS) and the Comoros Island have reported exceptionally high temperatures reaching up to 400°C at depths of approximately 2300 meters (IRENA, 2020).

For this reason, it is necessary to develop tools that facilitate the development of systems that exploit energy resources on the African continent. The work that is presented in this report is the work that was carried out within the LEAP-RE project specifically for Working Package 9 (WP9) Geothermal Atlas for Africa (GAA) and in particular Task 9.2 Science Technologies related to geothermal resources. This task ties in with the work that has been done in Tasks 9.1 dealing with geological-geophysical issues and mapping of the resource. In fact, the goal is to be able to evaluate the resource with a comprehensive sustainability analysis that assesses the energy, economic and environmental performance of energy systems that exploit a geothermal resource. Several energy systems are analysed with respect to the classical technologies found in the literature for exploiting geothermal resources. The aim is to create a tool that enables rapid evaluation using only few input data. The tool presented here will be linked to the work done in Task 9.1 by obtaining engineering mappings with exploitation potential, economic cost and environmental impact in the final phase of the project. Also reported in the text is the work done in collaboration with Strathmore University-KenGen, which defined a summary of power plants in Kenya and applied some analyses to case studies.



2. Geothermal tool

In this section, the methodology applied for the development of the geothermal tool for sustainability analysis is outlined. The objective is to create a tool to evaluate the best engineering applications, namely energy systems, for the sustainable exploitation of the resource, and thus assessing the energy, economic, and environmental aspects. Developing a tool to rapidly assess the energy, economic, and environmental performance of geothermal systems requires input derived from data collected and evaluated from Tasks 9.1 and 9.4. The fundamental parameters for assessing the energy potential of a geothermal resource are the conditions of the resource itself and depend on multiple factors (Barbier, 2002; Williams et al., 2011; di Pippo 2008). The geothermal tool begins by taking inputs, assessing what type of energy system can exploit the resource characterized by the input values, evaluating the energy performance and size of the system, and then assessing its economic cost and environmental impact. In the Geothermal Tool, only a few fundamental parameters are selected for the thermodynamic model, two dependent on the resource and one dependent on external conditions:

- Temperature $(T_{geo,in})$, which defines the possible applications (electricity production / heat) and also the potential of the selected device.
- Mass flow rate (m_{geo}) , which defines the sizes of the energy systems and their components such as heat exchangers, turbines, and other mechanical components.
- Ambient air temperature (T_{air}), which defines the reference environmental temperature and the related interactions at the condenser and evaporative tower of powerplants.

For certain energy systems, all three inputs are required, whereas for others, only two are necessary. In the case of power plants, these three parameters play a crucial role in determining the plant's size and its power output. However, for systems focused on heat or cold production, only the temperature and mass flow rate of the resource are considered as inputs. The primary characteristic of a geothermal resource is its exploitable temperature (Tgeo,in). Usually, temperature ranges are established within boundaries where a technology can demonstrate thermodynamic feasibility (Soelaiman, 2016). Accordingly, the classification of geothermal resources is based on the Lindal diagram, which delineates temperature ranges for various applications, as shown in (Gupta and Roy, 2007). As depicted in the Figure 1, power production can be convenient when the temperature of the geothermal resource exceeds 100°C. For all the geothermal resources with temperatures between 60-150°C, potential uses for cold production can be outlined. Within the 60-100°C range, heat pumps or absorption cycles can cool buildings with air conditioning systems, while within the range of 100-150°C, cycles for industrial refrigeration or food preservation can be proposed. The temperature range between 50-100°C can be utilized for the application of hightemperature heat pumps to provide heat between 100 and 150°C to the user. Other applications such as aquaculture, greenhouse cultivation, agro-industrial processes, or industrial processes requiring heat at lower temperatures are suitable for geothermal temperature ranges ranging from 30-80°C.



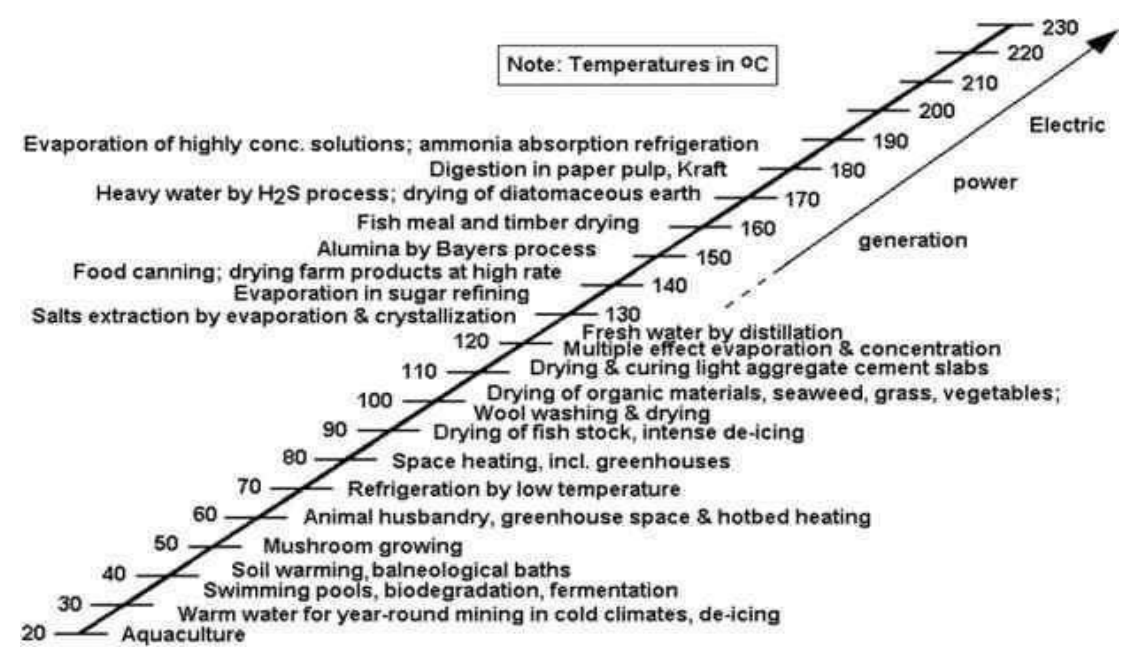


Figure 1: Lindal diagram for geothermal energy (DiPippo, 2016)

A variety of energy systems are selected for the developed geothermal tool, and they are formulated as thermodynamic blocks. The concept of a thermodynamic block refers to a simplified representation of a particular energy system. It is designed to take input data of the geothermal resource and can be arranged either sequentially or in parallel with other blocks. The simplified models are tailored for key applications, including power plants, cooling cycles, and heat generation plants. The energy system models developed for this project comply with the temperature classification outlined in Table 1.

Table 1: Classification of energy systems according to geothermal temperature range

T _{geo,in} range [°C]	m _{geo} range [kg/s]	T _{air} range [°C]	Energy Systems	Product	Final users
100 - 350	1-1200	15-50	Flash Power plant	electricity	National grid
100 - 350	1-1200	15-50	Dry-steam power plant	electricity	National grid
100-250	1-500	15-50	Binary Cycle power plant	electricity	National grid
80-150	1-100	-	Refrigeration Absorption System	Cold	Refrigeration, Building cooling
50-100	1-100	-	High Temperature Heat Pump	Heat	Industrial process, district heating, agro-industrial



By utilizing specific temperature ranges tailored to each energy system and integrating other inputs such as mass flow rate (mgeo) and air temperature (Tair), each within its respective range, a uniform input distribution is achieved. This uniform distribution occurs during the compilation of a dimensional matrix for each input parameter. For energy models that involve all three inputs, the resulting matrix has dimensions of $n_p \times n_p \times n_p$, whereas for energy models dependent solely on the temperature and flow rate of the geothermal resource, it is $n_p \times n_p$. The value of n_p varies depending on the specific case and has been chosen to create a dense input grid while avoiding redundancy. The precise value is provided in the subsequent paragraphs but typically falls within the range of 20-40. The models, once validated with literature values, are used to compute every combination of input grids $(n_p \times n_p \times n_p \text{ or } n_p \times n_p)$, thereby generating an output matrix. This process assigns each input combination a result in terms of mechanical component sizes (kW), parameters related to the chosen cycle (e.g., pressure level, temperature, mass flow rate, working fluid composition), and the outlet geothermal condition (temperature and mass flow rate). These output matrices are utilized for the generation of meta-models or surrogate models.

Meta-models are defined as mathematical models capable of providing computationally cost-effective evaluations of the input-output relationship of a system, particularly in computationally expensive tasks (Palar et al., 2019). Through the linear multidimensional interpolation methodology (Chan et al., 1997), a meta-model is created for the transition from the input matrix to the output matrix without requiring the reliance on the previously established calculation model.

The developed meta-model, serving as the computational core of the here discussed tool, is based on this classification but needs additional resource-specific details for a thorough assessment. Indeed, for both thermo-economic evaluation and environmental impact, additional parameters exert considerable influence on these indicators and should thus be incorporated into the generation of meta-models. Significant parameters include the useful life of the system, the capacity factor, and the depth and number of geothermal wells. As elaborated in the subsequent paragraphs, these parameters vary for each type of application.

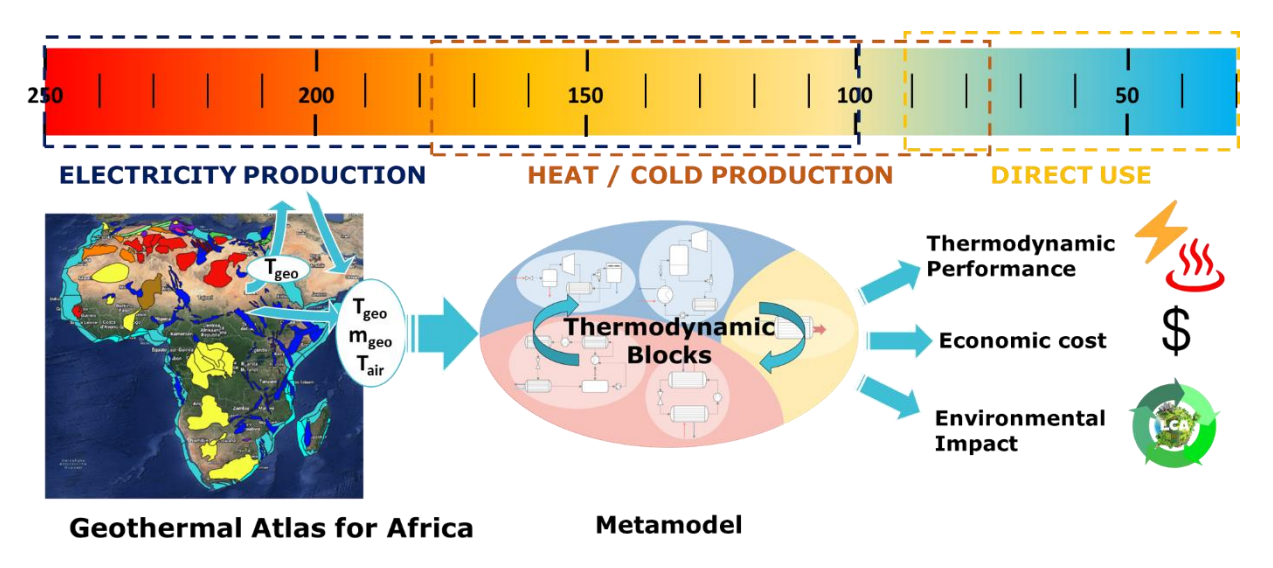


Figure 2: Schematic diagram of the geothermal tool

The following is a detailed description of each thermodynamic blocs and the relative simplified model evaluated.



2.1 High Enthalpy

For the utilization of high enthalpy resources, power generation plants are chosen based on three distinct technologies: Flash, Dry-steam, and ORC Binary Cycle. Both Flash and Dry Steam systems employ similar technology, differing primarily in their initial components, as elucidated in the subsequent paragraph. Specifically, the difference between these systems lies in the input conditions of the geothermal resource, which needs an explanation of the applied methodology.

Potential input resource conditions encompass subcooled liquid, saturated liquid, saturated vapor, or superheated vapor. Should the inlet brine be subcooled or the vapor superheated, the code automatically implements an isentropic expansion or compression to achieve the saturated state—either saturated liquid or saturated vapor, respectively. Thus, this procedure introduces a fictitious component which entails neither expended nor gained work. This approach obviates the necessity to consider pressure as a parameter, thereby streamlining the metamodel generation process.

In some case studies, particularly those used to validate the model, the initial dataset consists of temperature and a measurement of pressure or mass vapor fraction (VMF) at the wellhead. In such instances, the code operates in reverse mode to determine the inlet temperature. This procedure is delineated in Figure 3, where the initial data is denoted by point A, signifying the known temperature and mass vapor fraction, and consequently, the pressure level. To ascertain the conditions of the input resource, one follows the isenthalpic line until it intersects with the saturated liquid line (point B). Conversely, if the vapor is dry, the code considers the input temperature corresponding to the saturated vapor phase. In cases of dry steam, the code directly assumes the saturated vapor condition (point C).

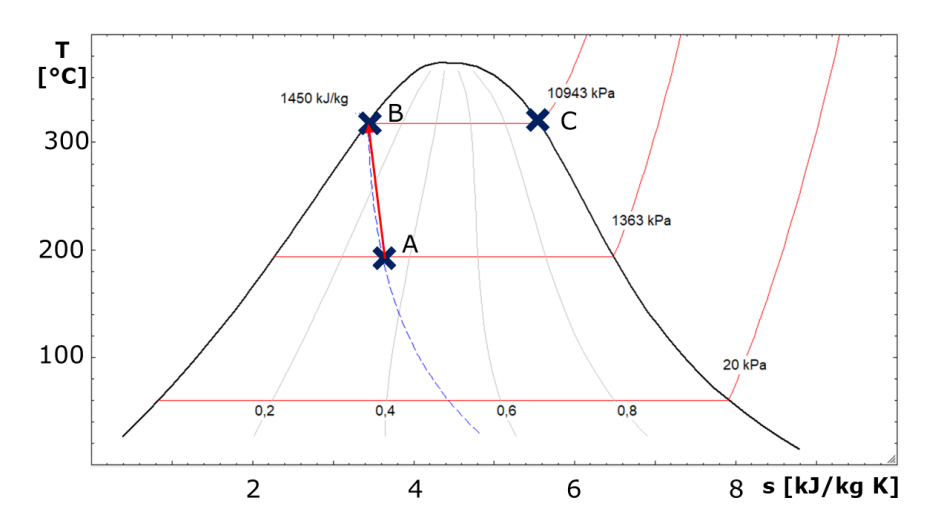


Figure 3: T-s diagram of water representing the geothermal fluid inlet

In the following section, the structure of the thermodynamic blocks of the Flash/Dry steam systems is described, followed by the ORC system, which have many differences between them.

2.1.1 Flash / Dry steam

The thermodynamic Calculation code for the flash and dry steam system is structured in two blocks, which are shown in Figure 4. The first distinguishing parameter between the Flash and Dry Steam systems is the thermodynamic block which models the system from



the geothermal well to the turbine outlet. Hence, the cycle comprises the geothermal well (1'), the wellhead valve (2'), the separator, which divides the steam phase directed to the turbine (3') from the liquid phase for reinjection or other purposes (5'), and finally, the turbine outlet (4'). In the Dry-steam cycle, the configuration remains the same except for the missing separator. Consequently, the wellhead valve (2') is directly linked to the turbine. The turbine outlet (4') connects to the second part of the cycle, consisting of the condenser (2"), two recirculation pumps (3"- 4"), and the cooling tower (7").

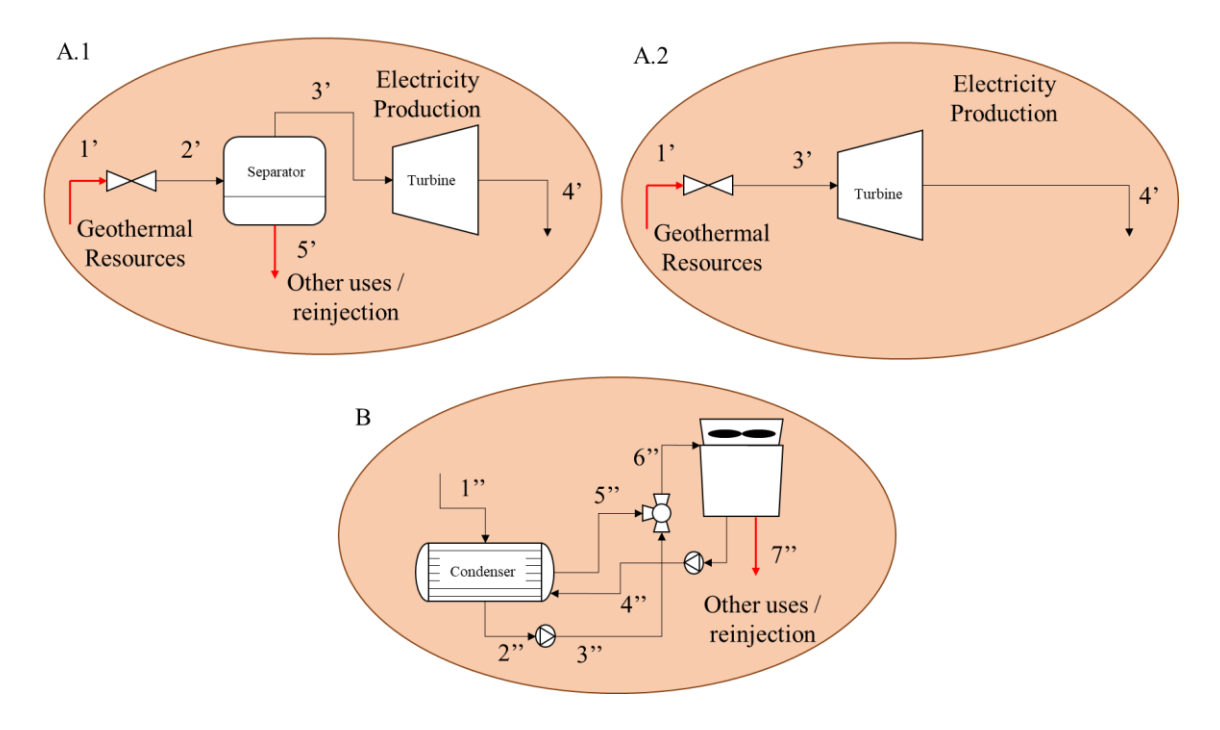


Figure 4: Installation diagram of the Flash (A.1) and Dry-steam (A.2) power plant

As previously mentioned, the conditions of the resource within the well are set relative to saturated liquid conditions for the flash block and saturated vapor conditions for the dry steam block before the expansion valve at the wellhead (1').

Furthermore, an important assumption is made within the Flash system separator. It emphasizes that a critical condition for determining the exploitability of geothermal resources is the presence of a pressure gradient and, consequently, an available enthalpy drop between the turbine's inlet and outlet. Accordingly, the acceptable pressure level within the separator is defined to range between P_1 and P_{cond} , where P_1 is the pressure at the wellhead upstream the expansion valve and P_{cond} is the condenser pressure, i.e., the pressure at the turbine outlet. To ensure that the pressure conditions are always met and so that the plant can produce energy, another parameter called x_{rel} is introduced, evaluated using E1. Here, x_{sep} indicates the mass vapor fraction within the separator, while x_{max} represents the maximum mass vapor fraction allowed to maintain the condition $P_{sep} = P_2$, exceeding P_{cond} . Specifically, x_{max} is determined by the mass vapor fraction of the fluid assigning the inlet enthalpy value ($h = h_1$) and the condenser pressure ($P = P_{cond}$). These maximum pressure levels and the range of mass vapor fractions are graphically represented in Figure 5, with an example of Initial Pressure at 10943 kPa and Condenser Pressure of 20 kPa.



$$x_{rel} = \frac{x_{sep}}{x_{max}} = \frac{x_{sep}}{x(h_{1}; P_{cond})}$$
 (E1)

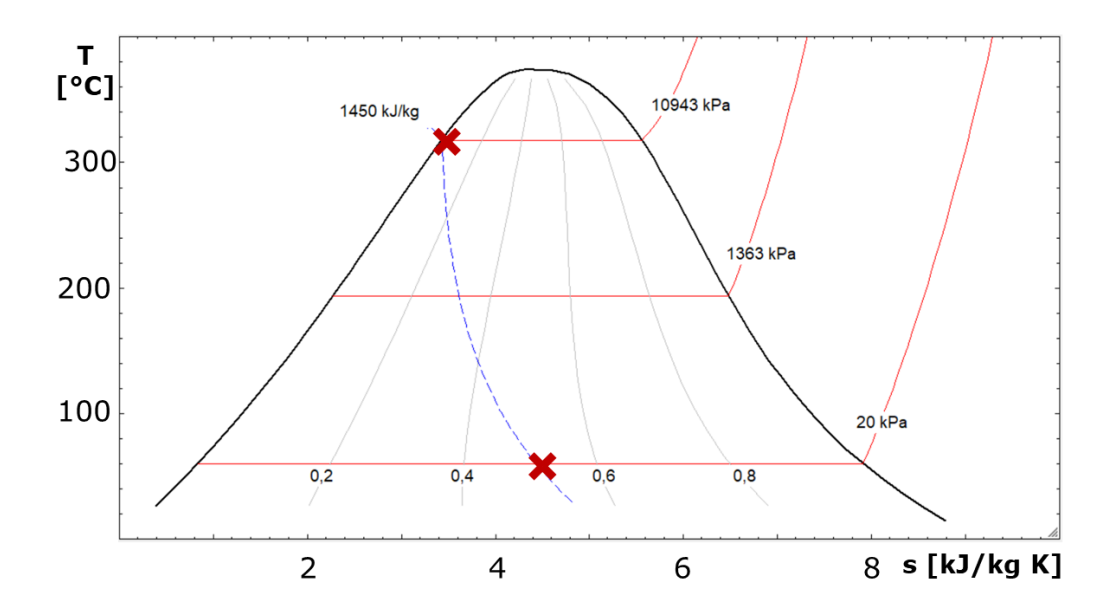


Figure 5: T-s diagram and mass vapor fraction range

The turbine outlet then connects to the second thermodynamic block consisting of the condenser and cooling tower. A predetermined condition is established at the turbine outlet, which is closely related to the ambient air temperature. Specifically, it is fixed to the condensing pressure (P_{cond}) at the specified temperature within the condenser (T_{cond}). The condenser is connected to the cooling tower and allow the heat exchange with the recirculating water flowing in and out of the tower. The temperature at the condenser, T_{cond} , is evaluated using E2, which considers various parameters.

$$T_{cond} = T_{air} + \Delta T_{approach} + \Delta T_{range} + \Delta T_{cond}$$
 (E2)

where T_{air} is an input parameter of the model representing the ambient air temperature, ΔT_{cond} is the fixed cooling water temperature difference between inlet and outlet of the condenser (e.g. the condenser range), $\Delta T_{approach}$ is the difference between cooling tower outlet water and air temperature, ΔT_{range} is the cooling tower range, e.g. the difference between water inlet and outlet. All these parameters are given in Table 2. They are set such that, for variations in T_{air} , the condenser and cooling tower inlet and outlet temperatures of the fluids do not overlap.

Table 2: Parameter of the thermodynamic cycle

Parameter [° C]	value	Parameter [° C]	value
ΔT_{cond}	4 °C	ΔT_{tower}	10 °C



$\DeltaT_{approach}$	5 °C	ηturb	0.82
ΔT_{range}	20 °C	η _{pump}	0.7

The main components are calculated through the related mass and energy balance using equations (E3-E8). Additionally, the model calculates the output conditions of the resource at 5' (Figure 4A). This functionality enables the model to work as a thermodynamic block, meaning that the conditions of the resource at 5' can serve as input for a second thermodynamic block. Indeed, this scenario arises when the resource at point 5' owns a suitable amount of energy for further exploitation, allowing, for example, the addition of a second block to achieve a double flash system.

$$W_{turb} = m_{3'} * (h_{3'} - h_{4'}) \tag{E3}$$

$$Q_{cond} = m_{1''} * (h_{1''} - h_{2''})$$
 (E4)

$$Q_{tower} = m_{6''} * h_{6''} - m_{7''} * h_{7''} - m_{4''} * h_{4''}$$
 (E5)

$$W_{pump} = m_{2''} * (h_{3''} - h_{2''})$$
 (E6)

$$Q_{geo,in} = m_{1'} * h_{1'} - m_{5'} * h_{5'}$$
 (E7)

$$\eta_I = \frac{W_{turb}}{Q_{geo,in}} \tag{E8}$$

2.1.2 Organic Rankine Cycle

The ORC binary system, depicted in Figure 6, consists of several fundamental components integral to its operation. These include a Heat Exchanger (HRSG) (3), which allows direct heat transfer between the geothermal fluid and the ORC working fluid, a Turbine (7), a condenser (1), and a recirculation pump (2). Of particular note is the presence of a separator in the plant schematic, a component not typically found in standard installations. By the way, it plays a strategic role in optimizing the energy system performance at variable input conditions. Specifically, the separator ensures that the turbine suitably works with saturated steam, thus ensuring a reliable expansion, regardless of resource conditions. It is important to underline that the separator, being a fictitious element necessary for evaluating a wide input network for meta-model generation, is not taken into account in calculations regarding economic cost and environmental impact. The main difference between the binary system and the flash one is that the latter directly utilizes geothermal fluid as the working fluid, whereas the binary cycle employs a heat exchanger to transfer heat from the geothermal fluid to the working fluid. This allows greater flexibility in the system for fluid selection based on thermodynamic characteristics (Zhai et al.,



2014). Various working fluids are viable options, each with its own set of thermodynamic characteristics. Some fluids have characteristics well-suited for geothermal applications, while also boasting optimal environmental profiles, such as a low Global Warming Potential (GWP) (Chitgar et al., 2023). Notably, the following working fluids were considered for our analyses: R1234ze(Z), R1233zd(E), R1234ze(E), Propylene, and R290. Each fluid responds differently to the condition of the geothermal resources, so for each one, both the flow rate (m_{cycle}) and the pressure which optimizes the cycle are evaluated through the use of an iterative procedure.

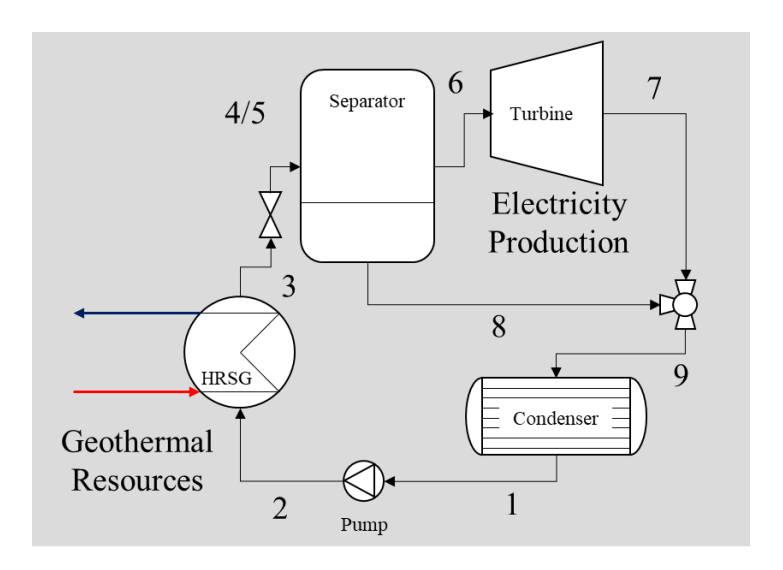


Figure 6: ORC binary power plant layout

The entire cycle operates based on the procedure devised for the HRSG heat exchanger, which relies on the temperature differential of the geothermal resource between inlet and outlet ΔT_{geo} . Initially, $\Delta T_{geo,max}$ is determined based on the incoming geothermal temperature: set at 90°C if T_{geo} exceeds 180°C, and half the temperature if T_{geo} is below 180°C. Subsequently, the outlet resource temperature is calculated using E9, along with the maximum heat of the geothermal resource which can be exchanged in the HRSG. If the ORC working fluid, at its specified flow rate, is capable of getting the entire supplied geothermal heat amount, these values are selected as accurate. Conversely, if the working fluid cannot get the whole supplied heat with $\Delta T_{geo,max}$, the code determines the maximum heat exchangeable to the working fluid and resets the ΔT_{geo} accordingly.

$$T_{geo,out} = T_{geo,in} - \Delta T_{geo} \tag{E9}$$

Thus, the heat transferred from the geothermal resource in the HRSG to the working fluid determines the conditions of the ORC fluid, which are calculated at points 3. At the same time, points 4 and 5 are evaluated under saturated vapor and saturated liquid conditions, respectively. So, to be able to evaluate the enthalpy at point 6, a verification is conducted: the maximum value between the enthalpies at points 3 (h_3) and 4 (h_4) is assessed. If the maximum value is h_3 , it indicates that the heat transferred from the geothermal fluid (Q_{geo}) has brought the working fluid to superheated vapor conditions, hence the entire fluid is in the vapor phase and can proceed to the turbine. Conversely, if h_4 is greater, it means that Q_{geo} is insufficient to completely vaporize the working fluid, therefore only the portion in the saturated vapor phase is directed to the turbine.



2.2 Medium and Low Enthalpy solution Heat and cold production

Thermodynamic blocks for the exploitation of medium and low enthalpy resources utilize an input from the resource, the conditions of which may vary from the input injected into the model. These conditions can range from subcooled liquid (at ambient pressure) for temperatures below 100°C to saturated liquid for temperatures exceeding 100°C. This flexibility allows for the application of these thermodynamic blocks in cases of surface exploitation of the resource or when connected to a high enthalpy thermodynamic block. Cases where the geothermal fluid is in the vapor phase with temperatures above 100°C have not been investigated. The thermodynamic blocks being analyzed are high-temperature heat pumps (HTHP) for heat production in two versions: a standard version and one with two pressure levels. For cooling production, a single-stage absorption system with water and ammonia is examined. Below is a detailed description of these systems. High-Temperature Heat Pumps (HTHP):

- Standard Version: This version of the HTHP system operates at high temperatures to produce heat efficiently. It utilizes a single pressure level to compress the refrigerant, which is then circulated through the system to extract heat from the heat source.
- Two-Pressure Level Version: In this variant, the HTHP system employs two pressure levels for compression, allowing for enhanced efficiency and heat production capabilities. By utilizing two stages of compression, the system can achieve higher temperatures and greater heat output compared to the simplest version.

Single-Stage Absorption System with Water and Ammonia for cooling production: this system utilizes a single-stage absorption process involving water and ammonia to produce cooling. Ammonia serves as the refrigerant, while water acts as the absorbent. The system operates by absorbing heat from the surroundings, causing the ammonia vapor to condense and release heat. The condensed ammonia then absorbs into the water, creating a solution with lower temperature and pressure (lean solution), which can be used for cooling applications.

These systems offer efficient and effective solutions for both heat production and cooling, catering to various industrial and commercial applications, using heat as primary energy resource in place of electricity.

2.2.1 High Temperature Heat Pump

In the simplest plant configuration, referred to as Cycle A in Figure 7, operating at a single pressure level, the geothermal fluid is introduced into the evaporator. Here, it transfers heat to the working fluid, which flows in counterflow. The temperature of the geothermal fluid exiting the evaporator ($T_{geo,out}$) and the specifications of two temperature differentials in the evaporator constructions ($\Delta T_{evap,in}$) and ($\Delta T_{evap,out}$) are fixed. Consequently, the temperature of the working fluid at the evaporator inlet is $T_{geo,out}$ - $\Delta T_{evap,in}$, and $T_{geo,in}$ + $\Delta T_{evap,out}$ at the outlet. This dependency on the temperature in geothermal well is evident. The working fluid, existing either as saturated steam (x=1) or superheated steam, enters the compressor, tasked with elevating the fluid pressure to match that of the condenser. The condenser's outlet pressure (x=0) and temperature (T_{cond}) are directly determined. Two distinct conditions are examined for the working fluids: the first with Low Temperature (LT) T_{cond} set at 105°C, and the second at High Temperature (HT), evaluating higher temperatures for the two HFO fluids with T_{cond} set at 140°C.



Assuming water is drawn at 50° C ($T_{w,in}$) from various sources such as residential, commercial, or industrial applications, it is raised to T_{cond} - $\Delta T_{cond,out}$. Utilizing the heat output provided by the condenser, the flow rate of hot water producible at this temperature is computed. The final component, the expansion valve, serves to revert the fluid to evaporator pressure, thereby completing the cycle.

In configuration (B), a separator is integrated into the cycle. Following the initial expansion undergone by the fluid in the high-pressure expansion valve, the separator segregates saturated liquid from saturated vapor. The former undergoes further expansion in a second expansion valve until it reaches the evaporator pressure. Meanwhile, the latter is blended with the fluid exiting the low-pressure compressor. This mixture is subsequently pressurized to match the condenser pressure by the high-pressure compressor. Table 3: reports the main parameters for both cycles. A parametric analysis for both fluids was carried out to determine the intermediate pressure optimizing the cycle.

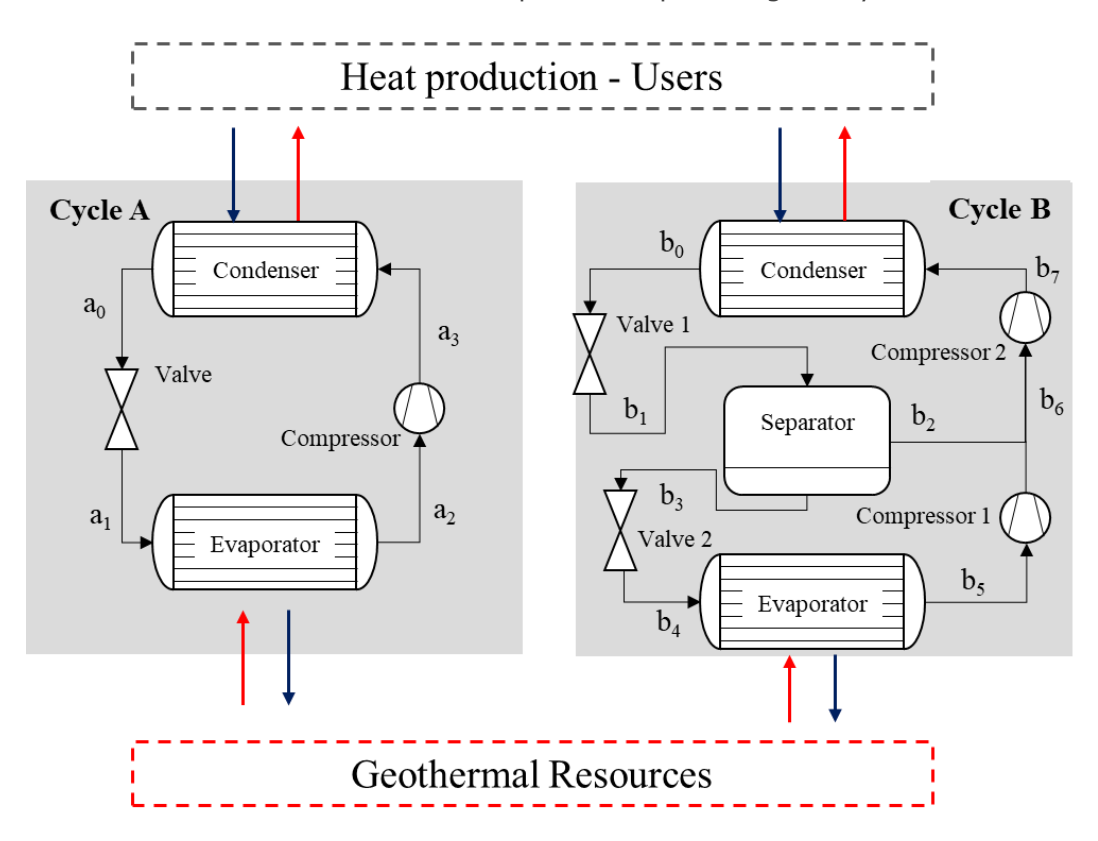


Figure 7: High Temperature Heat pump layout



Table 3: Main parameter fixed for High Temperature Heat Pump

Parameters		Value	Unit
Temperature of geothermal outlet	$T_{\text{geo,out}}$	45	°C
Evaporator inlet temperature difference	$\Delta T_{ ext{evap,in}}$	5	°C
Evaporator outlet temperature difference	$\Delta T_{\text{evap,out}}$	9	°C
Compressor isentropic efficiency	ηсотр	0.8	
Inlet temperature of the supplied water	Tw,in	50	°C
Temperature difference between critical point and condenser	ΔT_{cond}	10	°C
Subcooled temperature in the condenser	ΔT_{sub}	5	°C
Condenser outlet temperature difference	$\Delta T_{cond,out}$	5	°C
Separator pressure difference	ΔP_{sep}	2	bar

2.2.2 Refrigeration Absorption System

The thermodynamic block of the absorption system (ABS) is modelled for a single stage using a mixture of water and ammonia as working fluid and it is shown in Figure 8. The cycle consists of a heat generator (heat exchanger), a condenser, evaporator, absorber, recuperator and some valves and recirculation pumps. The heat generator is a heat exchanger with the geothermal fluid flowing on one side and the mixture of water and ammonia on the other. The geothermal fluid is modelled with the outlet temperature of the generator $T_{\rm geo,out}$ set at 50 °C and the inlet temperature in the range of 60-130 °C. The fluid is in the liquid phase by selecting 2 bar pressure for fluids with temperatures below 100°C and 4 bar for $T_{\rm geo} > 100$ °C. On the other hand, the working fluid enters the generator with a mass ratio of ammonia/mixture (r). The two generator outlets are pure ammonia in vapour phase on one side and a mixture with a low ammonia concentration on the other.



Thus, a total of three cycle lines can be distinguished: High concentration (Points 1-4), Initial concentration (5-0), Low concentration (7-9).

A correlation between the initial concentration and the inlet temperature has been developed after conducting a parametric analysis for each concentration level concerning the variation of T_{geo} . The COP curves have been determined for each level, and subsequently, all the points of maximum COP have been connected. Thus, the concentration sets the temperature at the evaporator and thus the target temperature level for the user side. This dependence occurs because the condition is set in such a way that the temperature at the condenser is equal to the temperature at the absorber, so the low pressure is calculated by evaluating the pressure of the mixture with concentration r at temperature T_{cond} under saturated liquid conditions. This low pressure and saturated vapour condition is set at the evaporator to calculate the evaporation temperature T_{evap} of ammonia.

On the other hand, the high-pressure level is evaluated at the condenser by fixing the saturated liquid condition at T_{cond} for ammonia. The flow rate of the ammonia-water mixture is evaluated in relation to the energy, mass and ammonia balance in the generator.

$$R = \frac{m_{cycle}}{m_{geo}} = \frac{(h_{geo,in} - h_{geo,out})}{x_7 * h_1 + (1 - x_7) * h_7 - h_0}$$
(E10)

$$Q_{gen} = m_{geo} * (h_{geo,in} - h_{geo,out}) = m_{cycle} * x_7 * h_1 + m_{cycle} * (1 - x_7) * h_7 - m_{cycle} * h_0$$
 (E11)

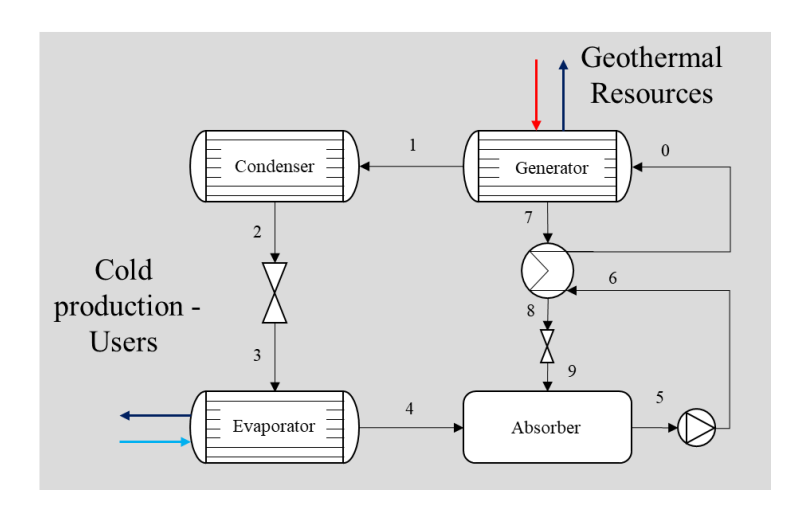


Figure 8: Refrigeration Absorption System layout

2.3 Economic Evaluation

The economic evaluation comprises two stages. Firstly, the cost analysis of individual plant components is conducted using thermo-economic correlations established by Turton (2008). The thermodynamic analysis provides essential parameters required for thermo-economic correlations, including the surface area required for the condenser and evaporator, compressor and valve handling flow rates, and separator volume. For the separator, the thermo-economic correlation referenced from Mosaffa et al. (2017) is adopted. Table 4 outlines the component types and the equations utilized for each one. Various economic equations exist for geothermal wells, often following linear or exponential



or logarithmic correlations. In this study, the correlation for the African application proposed by Shamoushaki et al., (2021) is adopted.

Table 4: Economic Correlation for machinery and wells

Component	Quantities	Relation	Reference
Condenser Heat Exchanger HRSG Recuperator Absorption vessel	S = Surface of thermal exchange [m²] P = Operating pressure [bar]	$C_{HE} = 10^{K_1 + K_2 * log_{10} S + K_3 * log_{10} S^2}$ $F_P = 10^{C_1 + C_2 * log_{10} P + C_3 * log_{10} P^2}$ $C_{BM} = C_{HE} * (B_1 + B_2 * F_M * F_P)$	Turton, 2008
Cooling Tower	$Q_{COND} = condense$ r heat exchanged $T_{Cw} = temperatur$ e of inlet air $T_{wb} = temperature$ of wet bulbe	$C_{tower} = 70.5 * Q_{COND} * (-0.6936 * ln(T_{Cw} - T_{wB}) + 2.1898)$	Roosen et al., 2003
Pump	W _p = Pump absorbed power [kW] P = pressure side [bar]	$C_{pump} = 10^{K_1 + K_2 * log_{10}} W_p + K_3 * log_{10}} W_p^2$ $F_P = 10^{C_1 + C_2 * log_{10}} P + C_3 * log_{10}} P^2$ $C_{BM} = C_{pump} * (B_1 + B_2 * F_M * F_P)$	Turton, 2008
Steam separator	Mass flow rate [kg/s]	$C_{sep} = 280.3 * m_{geo}^{0.67}$	Mosaffa et al., 2016- 2017
Turbine	$c_t = 3880.5 \\ [\$/kW^0.7] \\$ $W_{turb} = turbine \\ power [kW] \\$ $T_{in} = Inlet \\ turbine \\ temperature \\ \eta_t = Turbine \\ efficiency$	$C_{turb} = \left(c_t * W_{turb}^{0.7}\right) * \left[1 + \left(\frac{0.05}{1 - \eta_t}\right)^3\right] \\ * \left[1 + 5 * e^{\frac{T_{in} - 866K}{10.42 K}}\right]$	Roosen et al., 2003



The number of wells was evaluated with an empirical correlation based on the number of wells in relation to the size of power plants, by interpolating data available in the literature as showed in Figure 9. This equation is used in cases where no realistic data is available or data for power plants only are known. For other applications (as HTHP or ABS), one production well and one reinjection well per installed MW are considered.

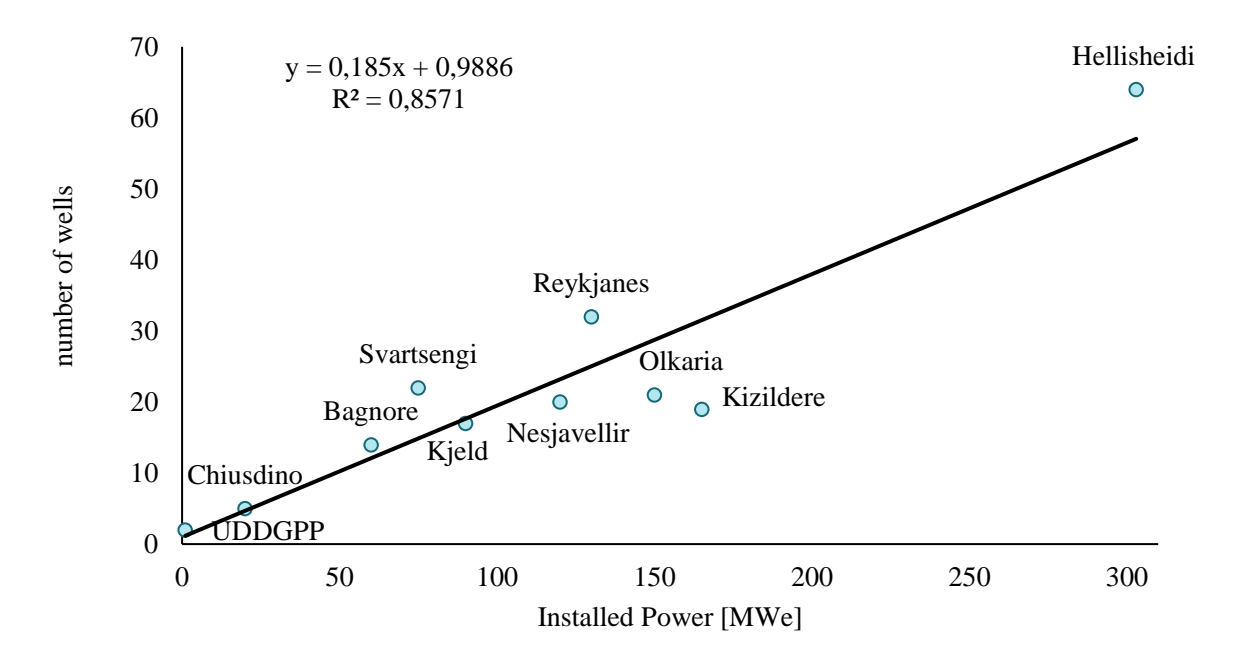


Figure 9: Correlation for number of geothermal wells

Secondly, the initial investment cost and the total O&M costs are assessed to determine the Levelized Cost of Energy (LCOEn). The LCOEn takes into account the complete cyclical costs (fixed and variable) of a generation technology per unit of energy, thus allowing comparison among different generators regardless of size, cost structure, and useful life. (Ueckerdt et al. 2013). The LCOEn provides a simple and quick procedure to measure the competitiveness of energy projects and is widely used for investments in conventional and renewable energies (Cory and Schwabe, 2009). However, it is important to note that the LCOEn is closely related to the quantities considered and the assumptions made and could lead to incomplete or misleading evaluations when used for absolute assessments (Ueckerdt et al. 2013). In the case of renewable energy systems, the value of the produced energy depends on the availability of resources and the intermittent nature of the source. Consequently, the LCOEn is related to the variability patterns, which determine the energy generation profile (Tran and Smith, 2018). This parameter is very important for this study, representing a significant economic indicator for multiple energy production systems, from electricity to heat and cold: Levelised Cost of Electricity (LCOE), Levelized Cost of Heat (LCOH), Levelized Cost of Cold (LCOC) (de Simón-Martín et al., 2022). This allows the evaluation of the economic feasibility of the production system to be expressed with a



single economic indicator. It quantifies the cost of electricity, thermal or cooling energy produced per kilowatt-hour (\$/kWh), as discussed by de Simón-Martín et al. (2022).

$$LCOEn = \frac{C_{TCI} + C_{WD} + \sum_{i=1}^{n} \frac{C_{pr}}{(1+r)^{i}}}{\sum_{i=1}^{n} \frac{E_{i}}{(1+r)^{i}}}$$
(E12)

The equation's parameters in (12) are: C_{TCI} is the total capital investment cost; C_{pr} for power plant is the Total Production Cost (C_{TPC}) for other application is the annual operating and maintenance cost ($C_{O&M}$); E_i is the annual thermal energy produced, it can be: electricity, heat or cold; r is the discount rate; n is the lifetime of the energy system. For the calculation of C_{TCI} , the method and parameters used in this work were taken from Karimi & Mansouri, (2018), Shamoushaki et al., (2022). For the evaluation of LCOEn with the integration of geothermal wells Hackstein & Madlener (2021) have been adopted. While for the evaluation of C_{TPC} , Shamoushaki et al. (2022) was followed. For $C_{O&M}$, literature reference values were taken (Beckers et al., 2021). The discount rate was set for each application at 7% (Beckers et al., 2021) and the lifetime varies between power plant and other application is fixed to 30 years (Shamoushaki et al., 2021; GECO project; Beckers et al., 2021). All correlations used and the general expression of the thermo-economic model are shown in Table 5.



Table 5: Economic correlations for Thermo-economic model

Cost type	Relation
Total Cycle Cost	$TC_B = \sum_{i=1 st \ component}^{i-th \ component} C_i$
Cost of site preparation	$C_{site} = 0.05 * TC_B$
Cost of service facilities	$C_{serv} = 0.05 * TC_B$
Allocated cost	$C_{alloc} = 0$
Total Direct Permanent Investment	$C_{DPI} = TC_B + C_{site} + C_{serv} + C_{alloc}$
Cost of contingencies and contractor's fee	$C_{cont} = 0.18 * C_{DPI}$
Total depreciable capital	$C_{TDC} = C_{DPI} + C_{cont}$
Cost of plant startup	$C_{startup} = 0.1 * C_{TDC}$
Permanent investment	$C_{TPI} = C_{TDC} + C_{startum}$
Working capital	$C_{WC} = 0$
Total Capital Investment	$C_{TCI} = C_{TPI} + C_{WC}$
Cost of wages and benefits	0.005
Cost of salaries and benefits	$C_{WB} = 0.035 * C_{TDC}$ $C_{SB} = 0.035 * C_{TDC}$
Cost of materials and services	$C_{TPI} = C_{WB}$ $C_{MO} = 0.05 * C_{WB}$
Cost of maintenance overhead	no wb
Direct Manufacturing costs	$C_{DMC} = C_{MO} + C_{TPI} + C_{SB} + C_{WB}$
Fixed Manufacturing Cost	$C_{FIX} = 0.02 * C_{TDC}$
Total annual cost of manufacture	$C_{COM} = C_{DMC} + C_{FIX}$
General Expense	$C_{GE} = 0$
Total production cost	$C_{pr} = C_{COM} + C_{GE}$
Annual Op. and Maint. cost (HTHP)	$C_{O\&M,HTHP} = 2.72 k \$/(kW * year)$
Annual Op. and Maint. cost (ABS)	$C_{0\&M,ABS} = 5.91 k \$/(kW * year)$



2.4 Environmental assessment

The environmental modelling approach complies to the Life Cycle Assessment (LCA) methodology, outlined by ISO 14040 and ISO 14044 standards (ISO, 2021a; ISO, 2021b). The typical LCA framework follows 4 structural steps: Scope and goal definition, Life Cycle Inventory, Life Cycle Impact Assessment, Interpretation. The goal and scope are statements of intent for the study. They explicitly state the reason why the study is being conducted, as well as the scope of the study. In the LCI analysis phase, data are collected and documented (e.g. energy use and material consumption) to fulfil the stated objective and scope. In the LCIA phase, the results of the inventory are converted into environmental impacts through the use of several environmental indicators. Finally, the interpretation phase looks at the results of the study, puts them into perspective, and may recommend improvements or other changes to reduce the impacts (Matthews et al. 2014).

The scope of this study is the assessment of the geothermal energy systems described in the previous paragraphs and the objective is to calculate an environmental indicator expressing their environmental impact. The boundaries encompass the construction, operation and maintenance phase of these systems, excluding all energy distribution infrastructure (thermal or electrical). The assessed environmental impact is Climate Change, by using the indicator of the Environmental Footprint 3.1 methodology. The functional unit is the electric or thermal energy unit (kWh), depending on the production system, and therefore the environmental indicator is expressed in terms of kg CO₂ eq/kWh. In this work, particular attention is paid to the LCI phase, since in order to characterize and evaluate such a large number of systems with different sizes, it is necessary to develop a parametric LCI (pLCI). The aim is to obtain a large number of cases of primary data in the literature, in order to develop a correlation between the size of a specific process and the materials and energy consumed in it. In other words, consumption of material and energy flows were connected to the following sizes of the different parts of the energy system:

- Geothermal wells: meters drilled (meters)
- Pipelines: meter of pipe (meters)
- Building: Power installed (kW) (only for power plant)
- Mechanical components: Power installed (kW)
- Operation: Annual consumption and emissions (years)
- Maintenance: annual consumption and replacements (years)

In the following sections, the process used for the realization of the pLCI and its validation are show.

2.4.1 Geothermal wells

The drilling and installation of a geothermal well is a time consuming process, which consumes many materials and a large amount of energy. Geothermal well drilling differ in geological and physical features such as rock types, reservoir pressure, temperature, casing, well cementing (Moya et al., 2018). Well Cementing has the aim to establish an annular barrier within the wellbore and casing to withstand specific environmental



conditions and maintain the casing in position. To prevent casing expansion during production in geothermal wells, it is necessary to fully cement the casing. In drilling operations, the casing plays a multifaceted role essential for the integrity and efficiency of the well (Applied Drilling Engineer, 1986). Firstly, the casing acts as a barrier, effectively isolating the well fluids from both the surrounding formation and any fluids of the formation. This isolation is crucial for maintaining the integrity of the well and preventing contamination or unwanted interactions between different fluid sources. Secondly, the casing serves as a structural support system, preventing borehole collapse during drilling operations. This function is vital for maintaining the stability of the wellbore and ensuring safe and efficient drilling operations. Additionally, the casing provides a clear pathway for the drilling fluid, facilitating the drilling process by allowing for the controlled circulation of fluids within the well. This ensures that the drilling fluid can effectively carry cuttings to the surface, facilitating the drilling process and minimizing downtime. Moreover, the casing plays a crucial role in minimizing damage to the subsurface environment. By providing a protective barrier between the wellbore and the surrounding formation, the casing helps prevent any potential environmental contamination or adverse effects on nearby geological formations (Allahvirdizadeh 2020). In the context of LCA for geothermal energy systems, wells have a great environmental impact involving several environmental indicators such as Climate Change, Acidification, Human Toxicity, Ecotoxicity freshwater (Zuffi et al., 2022). Depending on the type of technology used, the biggest impact factor for GWP is diesel consumption in the construction phase, mainly used for drilling wells (Tomasini-Montenegro et al., 2017). In some cases, it may also be the process with the highest impact on all environmental indicators (Menberg et al., 2016). it has been shown that the use of electrically powered drilling equipment can greatly reduce the environmental impacts (Karlsdottir et al., 2020)

A simplified model of geothermal wells has been created, based on two material flows, concrete and steel, and an energy flow represented by diesel consumption. Primary data were collected from multiple case studies, which are shown in Table 6. These data can be very variable for each case: for example, the level of difficulty in collecting data for casing steel is low, whereas for concrete it is very complex. This is due to LCIs, in which cement or in some cases concrete is reported, so a conversion must be made from all the data provided. In addition, a simplified model of geothermal drilling with diesel consumption was chosen as the data for electrical drilling were present in only a few plants (Karlsdottir et al., 2020; Orka, 2023a-2023b)



Table 6: Simplified LCI of geothermal wells in literature

Power Plant	Wells	Depth [m]	Casing [t]	Cement [t]	Diesel [m3]	Reference
Bagnore	Shallow	700	97.17	-	153.75	Tooti et al. 2020
	Deep	3394.5	278.35	-	539.38	Tosti et al., 2020
	Travale Sud 1B	3361	322.72	387.02	533.69	
	Montieri 5	3447	269	331	425.45	
Chiusdino	Travale Sud 1C	3713	336.11	273	188.10	Basosi et al., 2020; Fiaschi et al., 2021
	Montieri 5A	4137	265.96	388	472.12	
	Travale Sud 1D	4432	264.4	358	550.36	
Hellisheidi	average	2200	220.44	81.332	139.90	Karlsdottir et al., 2015
	Shallow	1312	136.43	120.893	96.23	Mainar-Tolodo et al
Kizildere	Deep	3127	276.54	204.187	303.02	Mainar-Toledo et al., 2023
Theistareykir	average	2400	176	248	183	Kjeld et al., 2022
Lacrignola	average	5000	556.5	228	561.20	Lacrignola & Blanc, 2013
The Banchory Geothermal project	Case 1	2000	200	200	236.56	
	Case 2	1800	50	180	189.25	McCay et al., 2019
	Case 3	3000	300	400	473.12	



Kirchstockach	production	4214	524.22	-	-	Menberg et al., 2021
	renjection	4452	553.82	-	-	
Olkaria	average	3000	170.673	197.6	320	KenGen
Reykjanes	average	2228.25	447.34	307.67	199.59	Orka, 2023a
Svartsengi	average	1206.16	213.90	141.45	115.79	Orka, 2023b
United Down Deep	Injection	1780	237.031	79.38	403.10	Paulillo et al.,
Geothermal Project	production	3985	407.073	181.56	888.57	2020a, 2020b

These data were collected and divided by the 3 pLCI flows and were interpolated with respect to the depth of each well, to obtain a function which is shown in Table 7 for each material type. Three linear correlations were obtained for each stream, and a the statistical indicator coefficient of determination R² expresses the degree of accuracy of the correlation. The correlation related to cement seems to exhibit a notably low coefficient of determination, likely attributable to less precise data with inherent uncertainties. Additionally, in contrast to the other two streams, geothermal wells drilling employs various types of cement, each with different specific weights, potentially introducing distortions to this correlation. In the results validation section, a comparison is done between other correlations expressed in the literature (Treyer et al., 2015; Hirschberg et al., 2014; Paulillo et al. 2021; Vito et al., 2020) according to different statistical indicators such as: Mean Square Error (MSE), Mean Absolute Error (MAE), Median Absolute Error (MdAE), Mean Absolute Percentage Error (MAPE), Root Mean Square Error (RMSE).

Table 7: Environmental correlation for pLCI

Flows and providers	Correlation
market for reinforcing steel reinforcing steel Cutoff, S - GLO	$y = 0.886 * z + 24.235 [ton]$ $R^2 = 0.615$
market for cement, Portland cement, Portland Cutoff, S - RoW	$y = 0.0624 * z + 55.47 [ton]$ $R^2 = 0.47$



diesel, burned in building machine | diesel, burned in building machine | Cutoff, S

y = 0.1296 * z + 1.2854 [ton] $R^2 = 0.72$

2.4.2 Machinery

The pLCI approach establishes correlations between material and energy usage in the production phase of the Machinery's systems. In the case of HTHP and ABS, disposal of the components themselves is also taken into account in the process, and thus also in the end-of-life phase. The correlation obtained is determined by the system's size, as indicated by the thermodynamic metamodel. During the construction phase, primary data was gathered from commercially available units of machinery. A relationship was established between the system's thermal power (in kW) and its total weight, using the collected data. Following this approach, reference processes were selected. For individual components, these processes are represented as material flows, drawing from existing models in the literature. However, for complex systems like ABS and HTHP, processes are directly taken as references, modeled from the Ecoinvent 3.7.1 database. Material percentage compositions are determined and calculated based on the obtained correlations. This approach enables the development of a new environmental model, incorporating adjusted input and output values, which are then multiplied by the correlation obtained. In the subsequent sections, all references and models are presented as implemented.

2.4.2.1 Power plant

The mechanical components of power plants were individually selected and evaluated based on their dimensions. The separator is modeled according to a flow of chromium steel (Tosti et al. 2020) and the correlation is obtained from the Gestra catalogue (Gestra, 2023). The reference parameter is the fluid flow rate that the separator can withstand. The turbine is modeled using flows of chromium steel (Tosti et al., 2020; Basosi et al., 2020; Fiaschi et al., 2021; Mainar-Toledo et al., 2023), and two different catalogs are utilized: The first is provided by Shinko Industrial steam Turbines for turbine sizes up to a maximum of 30 MW (Shinko, 2023), and the second is Siemens, which covers systems up to 120 MW (Siemens, 2023). The condenser is also modeled with chromium steel (Tosti et al., 2020; Wessel company, 2023), and the linear correlation is obtained from two different catalogs: The first is for smaller sizes and is provided by Wessel company (2023), while for larger sizes of heat exchangers, it is Quiri Echanges Thermiques (2023). Three flows are used for modeling the evaporative tower: Chromium steel, glass fiber, and plastic pipe (Basosi et al., 2020; Fiaschi et al., 2021). The SPX Technologies Marley Record SGS catalog is used for this component (SPX technologies, 2023). For the pumping system, the ecoinvent process is used as a reference, which models with cast iron (50%), copper (10%), and chromium steel (40%) of the total weight. The correlation for the weight is obtained from FRUNZE (2023). For binary ORC power plants, the only difference in components lies in the heat exchanger and the condenser, which are modeled with a flow of chromium steel (Tosti et al., 2021; ONDA, 2023). The correlation is obtained from two sources: Alfalaval, 2023 and ONDA, 2023. In Figure 10 the correlations obtained are shown.



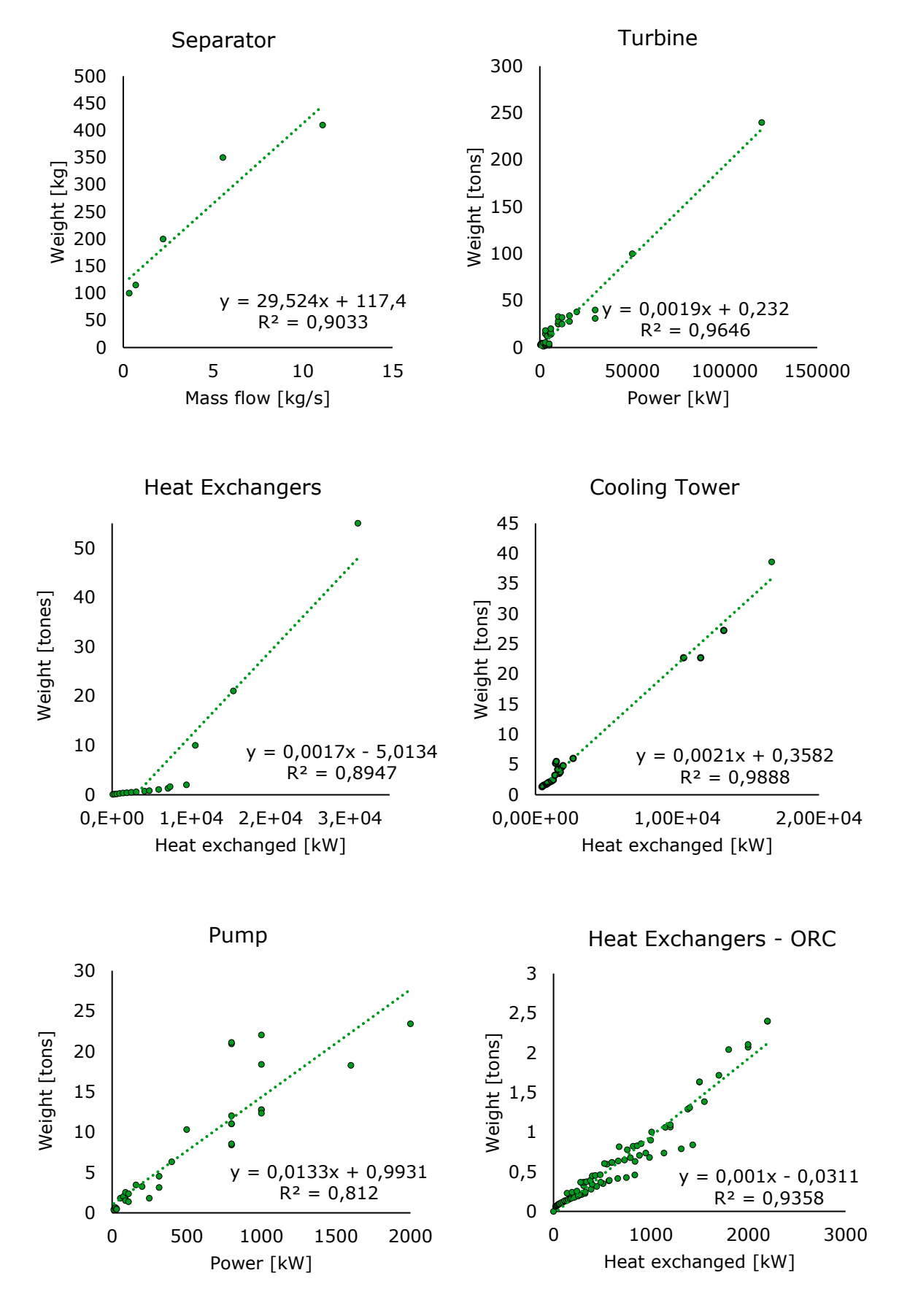


Figure 10: Material correlation for power plant machinery.



2.4.2.2 HTHP

During the construction phase of the system, primary data was collected from commercially available HTHP models sourced from TRANE (2022). A correlation was established between system thermal power (kW) and total weight, as depicted in Figure 11, based on the collected data. Subsequently, the production process for process *heat pump production, brine-water, 10kW* (heat pump, brine-water, 10kW) from the Ecoinvent database was selected as a reference model. Inputs and outputs of this process were categorized into materials and energy utilized during construction. Percentages for each material and energy consumption were determined, with energy normalized to the total mass of the element. This allows the creation of a new environmental model for the HTHP, incorporating adjusted input and output values multiplied by the correlation obtained.

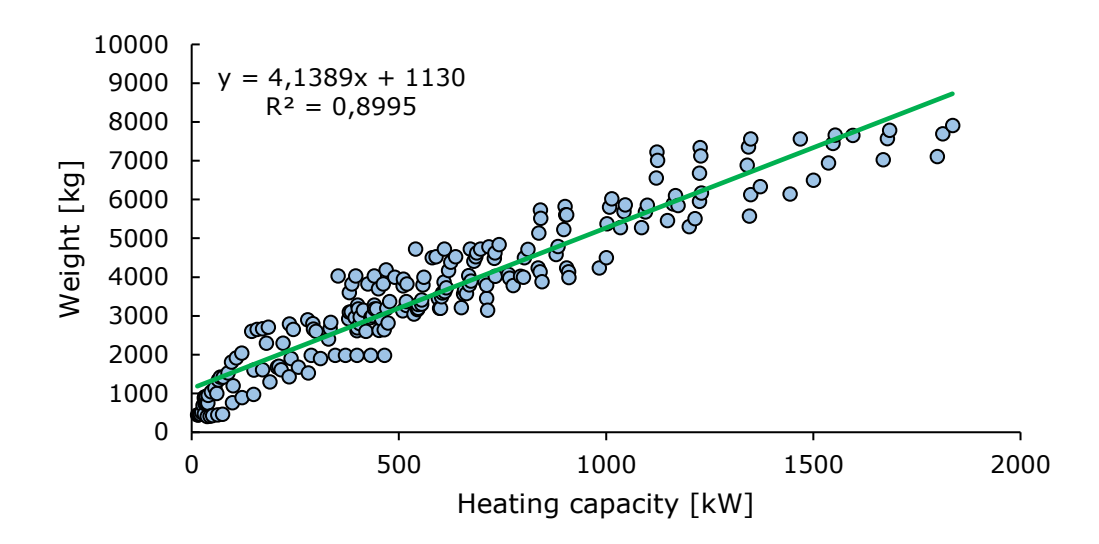


Figure 11: Material correlation for High Temperature Heat Pump

To ensure consistency, the process of the Absorption cycle provided by the Ecoinvent 3.7 database was adopted as a reference model. This process served as the starting point to derive the typical composition of materials for the devices in the case study. By excluding materials not closely related to the construction phase of the devices, a relative mass fraction (%) of construction materials was determined for each considered unit. The next step involved finding reliable catalogues of Absorber manufacturing companies to obtain information on weight and cooling power. Utilizing data obtained from the World Energy Absorption Chillers Europe Ltd catalogues, a total of 140 data points were obtained. With this data distribution, a satisfactory second-degree polynomial fitting function was achieved (WEACH, 2022). The choice of a second-degree function aimed to balance complexity, which increases with polynomial degree, without significantly increasing uncertainty. Figure 12 illustrates the distribution of points and the related 2nd-degree polynomial power-weight fitting function.



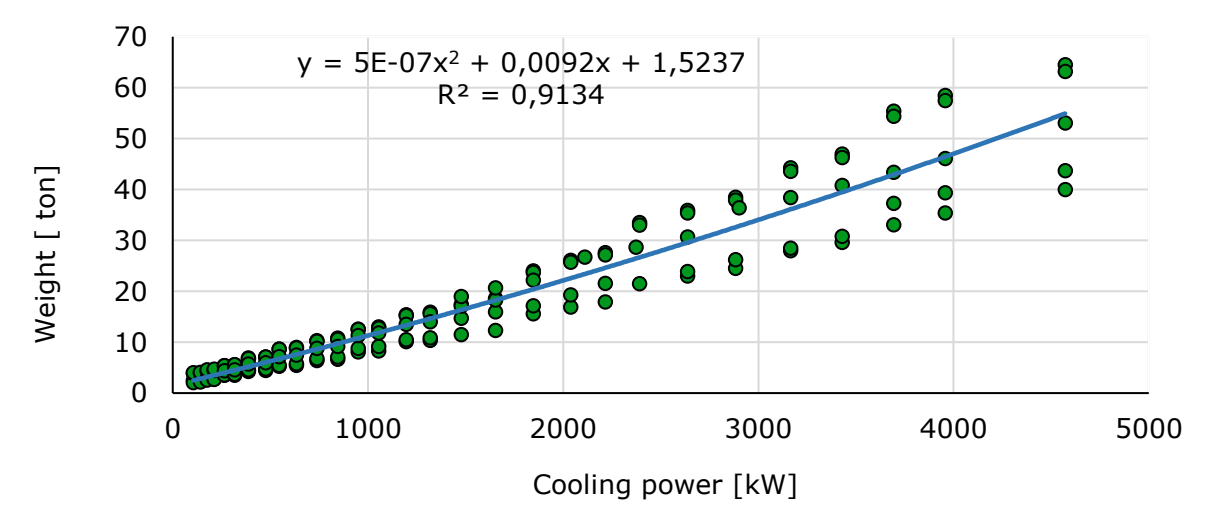


Figure 12: Material correlation for Absorption System

2.4.3 Pipeline and Building

For pipeline and building modelling, limited data are available in the literature, and in some cases very different from each other, so that it is not possible to develop a reliable correlation. For this reason, the buildings provided by Karlsdottir et al., (2015) are taken as a reference process, which provide the amount of materials per MW installed in the plant. This process only applies to power plants as the building for the containment of the turbomachinery assembly is considered (Table 8). For pipelines, the process provided by Karlsdottir et al. 2015 per pipeline meter is taken. In addition, the piping length is correlated with the relationship obtained by Paulillo et al.(2021), of about 500 m per well (Table 9).

Table 8: material and energy consumption for Building (LCI Building)

Building						
material	Amount [kg/MW]	material	Amount [kg/MW]			
Aluminium	578	Copper	152			
Concrete	206′400	Plastic	702			
Steel	11′943	Stainless steel	517			



Table 9: material and energy consumption for Pipeline (LCI Pipeline)

Pipeline					
material	Amount [kg/m]	material	Amount [kg/m]		
Aluminium	6.2	Mineral wool	4.3		
Steel	197				

2.4.4 Operation and Maintenance

As far as the operation and maintenance phase is concerned, the data is highly variable in each specific case and no unambiguous correlation could be found to describe this trend. The operation phase is considered by the thermodynamic model to be the share of electricity consumed by the recirculation pumps and is considered to be drawn from the national grid. In addition, the only available African reference, Olkaria IV, is considered for the power plants. Thus, atmospheric emissions are modelled in relation to the kWh produced and the share of water used for cooling systems. For a detailed reference, please refer to the Olkaria IV inventory section. Regarding the maintenance phase, 5% annual replacement of the materials used in the construction phase is assumed (GEOENVI project).

2.4.5 Case studies: Olkaria IV power plant

Among the numerous collaborations with WP9 partners, the one standing out is the joint effort with Strathmore University and KenGen. This partnership has led to a significant milestone in geothermal energy: completing the first-ever Life Cycle Assessment (LCA) of an African geothermal plant, Olkaria IV. It's worth noting that no such assessment has been conducted for any geothermal plant in Africa before (Mukoro et al., 2021). Currently, the Olkaria geothermal field is the second most productive worldwide, surpassed only by the geysers in the USA (Renkens, 2019). The field has five plants, with Olkaria IV being the latest addition (Renkens, 2019; Koissaba, 2017; Kong'ani et al., 2021). The first 45 MWe plant comprising of three 15 MWe turbines, Olkaria I, was developed between 1981 and 1985 by KenGen. Olkaria II comprises three turbines, each with 35 MWe, totaling 105 MWe. The units were developed between 2003 and 2010. OrPower Inc. owns Olkaria III, which comprises 151 MWe developed between 2013 and 2022. Olkaria IV and Olkaria I Additional Units 4 & 5, comprising four turbines totaling 300 MWe, are owned by KenGen and were commissioned in 2014 and 2015. KenGen also owns Olkaria V, which comprises 172 MWe and was commissioned in 2019. KenGen also owns Olkaria IAU 6, which has an installed capacity of 86 MWe. Oserian Flower Farm generates 4MWe from a binary power plant using steam leased from KenGen. It was commissioned in July 2014.



The LCA study focused on the Olkaria IV power plant. The plant comprises two turbines, each with a rated capacity of 75 MWe, totaling 150 MWe. Olkaria IV draws its steam from the Olkaria Domes segment of the greater Olkaria geothermal field. The segment is situated on the eastern portion of the greater Olkaria geothermal area. The larger Olkaria geothermal area project is in the Naivasha Sub-County, Nakuru County, Kenya. The project area is located in the Hell's Gate National Park (HGNP). The Olkaria area is home to approximately 20,000 pastoralists, whose primary source of income is derived from pastoralism and livestock trading. Moreover, a portion of the community relies on income generated from tourism activities (Kong'ani et al., 2021).

The power plant is a single flash with an installed capacity of 150 MWe. The net output capacity is 140 MWe and exploits a vapor-dominant resource hosted in Trachyte formation between 1.2 to 3 km below the surface. The cap rock is a thin layer of basaltic rock (Musonye, 2015). The plant is served by 21 wells: 18 production wells and 3 re-injection wells. The two plant turbines are each fed by a steam line at an intake flowrate of 135 kg/s, 180° C temperature, and pressure in the 9-12 bar range. The geothermal fluid comprises 1% Non-Condensable Gases (NCG), composed of 95.96 % CO₂, 0.49 % N₂, 1.11 % CH₄, and 2.28 % H₂S.

Here, the analysis is to assess the environmental impact of the Olkaria IV power plant and compare it to other geothermal power plants and other production systems has been carried out. The approach used for this analysis is cradle-to-gate type. The system boundaries encompass all processes related to the construction, operation, and maintenance phases. The end-of-life phase is not considered due to the lack of a disposal program. Interviews with the stakeholders indicated that drawing from the previous plants, for instance, Olkaria I, the plant under study might not be decommissioned once they reach their technical end of life. On the contrary, it will be rehabilitated to hold on operation. The production wells will, thus, continue producing steam and in case any well declines in pressure, it is converted to either a hot or cold re-injection well, depending on its location in the geothermal field. Thus, the decommissioning program was not considered for the plant under study. Further, this study did not consider the transmission system because it does not solely serve Olkaria IV but also other geothermal plants in the Olkaria geothermal field. The functional unit selected is the electrical energy produced by the plant in kWh, considering a useful life of 30 years and a capacity factor of 0.94, which is 8234 hours/year of operation.

2.4.5.1 Life Cycle Inventory: Olkaria IV

The modelled processes for the construction phase in this installation are the geothermal wells and wellheads; the building hosting the plant, and the collection pipelines. The geothermal wells are 3000 m deep on average. The collection pipelines are divided into 28 km of production line and 5 km of re-injection pipe. The building houses the machinery and control rooms. The machinery and plant have not been modelled with primary data from KenGen because it was difficult to obtain data from the contractors who built the power plant. Resultantly, machinery and plant data were adopted from the model proposed by Karlsdottir et al. (2015). The only known data for the Olkaria IV plant is the turbine rating, which is 75 MW for each of the two turbines. All inventory data are reported in **Table 10-Table 15**.

The operation phase consists in the consumption of 40.4 m³ of water per day for plant operations and approximately 126 MWh for heat distribution, of which 16% is taken from the national grid and 84% is taken directly from plant production. Direct emissions to the



atmosphere are mainly CO2, H2S, H2 and CH4. Six make-up wells are expected to be built in 25 years to maintain the geothermal steam flow rate at the required level. In addition, lubricant oil is consumed for the machinery, while Sodium Carbonate is used for anticorrosion and anti-scaling of the pipes. The plastic components of the cooling tower are replaced.

Table 10: LCI drilling geothermal wells

Drilling geothermal wells						
Material	Unit	Amount	Material	Unit	Amount	
Well cleaning (Tel- Polymeride)	kg/well	5800	Silica sand	kg/well	69040	
Soduim carbonate	kg/well	200	Diesel (drilling)	l/well	320000	
Steel	kg/well	170673	Water	l/well	110000	
Portland cement	kg/well	197600	NaOH	l/well	3200	
Accelerator	kg/well	300	HCI	l/well	2000	
Deformer	kg/well	640	Oil/lubricant	l/well	2000	
Fluid loss agents	kg/well	280	Excavation	m3/well	1500	
Dispersant	kg/well	60	Drilling sludge (to treatment/lan dfill)	kg/well	0	
Retarder	kg/well	280	Barite	kg/well	200	
Bentonite	kg/well	30000				



Table 11: LCI wellhead

Wellhead						
Material	unit	amount	Material	Unit	Amount	
Steel	kg/well	1 261	gravel/sand	kg/well	16 363	
Portland cement	kg/well	2 539	Excavation	m3/well	80	
Diesel	l/well	300	Filling	m3/well	49	

Table 12: LCI pipeline

Pipeline					
Material	unit	amount	Material	Unit	Amount
Steel	kg/m	113	Portland cement	kg/m	179
Stainless steel	kg/m	212			



Table 13: LCI Building

Building					
Material	unit	amount	Material	Unit	Amount
Steel	kg	117 712	Glass	kg	296
Stainless steel	kg	54	Wood	kg	10 400
Concrete	kg	159 000	Diesel	kg	19 070
Plastic	kg	31 900	Excavation	m3	425
Aluminum	kg	41	Filling	m3	897
Inert material (Copper)	kg	170			

Table 14: LCI Maintenance

Maintenance Maintenance						
Material	unit	amount	Material	Unit	Amount	
make-up wells	number	6.00	Anticorrosion and antiscaling	kg/year	14400	
Lubricant	l/year	3200	Plastic	kg	162201.6	
Na ₂ CO ₃	kg/year	14400				



Table 15: LCI operation

Operation					
Material	unit	amount	Emissions	Unit	Amount
Tap water	m³/year	177000	CO ₂	g/kWh	50.40
Electricity consumption	GWh/year	45.99	H ₂ S	g/kWh	1.54
			CH ₄	g/kWh	0.07

3. Results

The results section is structured into subsections based on high and medium enthalpy thermodynamic -. Within each sub-section, the validation of the metamodels is addressed first, covering thermodynamic, economic, and environmental aspects. Following this, the results of the complete metamodel are discussed, exploring the performance of the outputs as certain parameters change. Subsequently, case studies are analyzed using the geothermal tool. Finally, the data collection of plants in Kenya and some application cases were evaluated in the collaboration with Strathmore University – KenGen is presented.

3.1 High Enthaply validation

3.1.1 Thermodynamic

The thermodynamic metamodel's validation entails analyzing several known plants, with turbine size (i.e., installed power) serving as a reference parameter. The selected plants include Single Flash (SF), Double Flash (DF), Triple Flash (TF), Dry Steam (DS), and Binary system Organic Rankine Cycle (ORC) types, each characterized by distinct features. Plant selection primarily hinges on data availability, encompassing Bagnore 4 (SF), Nesjavellir, Olkaria IV (SF), Olkaria wells, Hellisheidi (DF), Kizildere (TF), Chiusdino (DS), Qualtra (ORC), Bagnore (ORC), and Meskoutine (ORC). It's worth noting that Olkaria wells data pertain to a well with a 5 MW potential, not yet used by a power plant, as it is in the testing phase. Additionally, Bagnore houses both flash and binary cycle plants of varying sizes. Figure 13 illustrates a column chart depicting the plant sizes in MW percentage, highlighting the percentage difference between the two values.

The analysis reveals that the tool's predictions significantly overestimate the installed capacity, ranging from 3.9% for Bagnore to 7.5% for Olkaria IV. Notably, Nesjavellir, Hellisheidi, and Kizildere exhibit larger assessment errors, with overestimations of 17.2%, 12.4%, and 22.2%, respectively. Nesjavellir's high error stems from condenser set at a temperature beyond the tool's evaluated range, leading to an exaggerated enthalpy drop and consequent plant size overestimation. Correcting this parameter enhances the



prediction accuracy level to about 2.33%. Conversely, for Hellisheidi and Kizildere, the evaluation of double or triple flashes enhance the prediction errors, reaching 6-7.5% per each flash. The input data for each flash were adjusted, leading to a remarkable reduction in prediction errors. For Hellisheidi plant, the tools achieved a reduction of the error to 4.02%, while for Kizildere the reduction was equally impressive at 6.62%. Figure 13 highlights the critical importance of conducting thorough investigations, especially when using this tool in scenarios with unknown variables. It is fundamenta to recognize that parameter optimization is not a one-size-fits-all solution. It is not a process that occurs automatically; rather, it demands meticulous examination and fine-tuning. Our study brings to light the need of such diligence in ensuring the accuracy and reliability of these predictions. However, it is crucial to acknowledge the limitations of our tool. When analyzing a single flash in the initial stages, a deviation in the range of 6-7% is observed. While this may seem acceptable in certain contexts, it highlights the need for further refinement. In cases where multiple flashes are possible, a more complicated process ensues. Achieving a reduction in prediction error needs the integration and optimization of various thermodynamic blocks. This puts in evidence the complexity of the task at hand and emphasizes the need for a meticulous approach to parameter adjustment and data analysis.

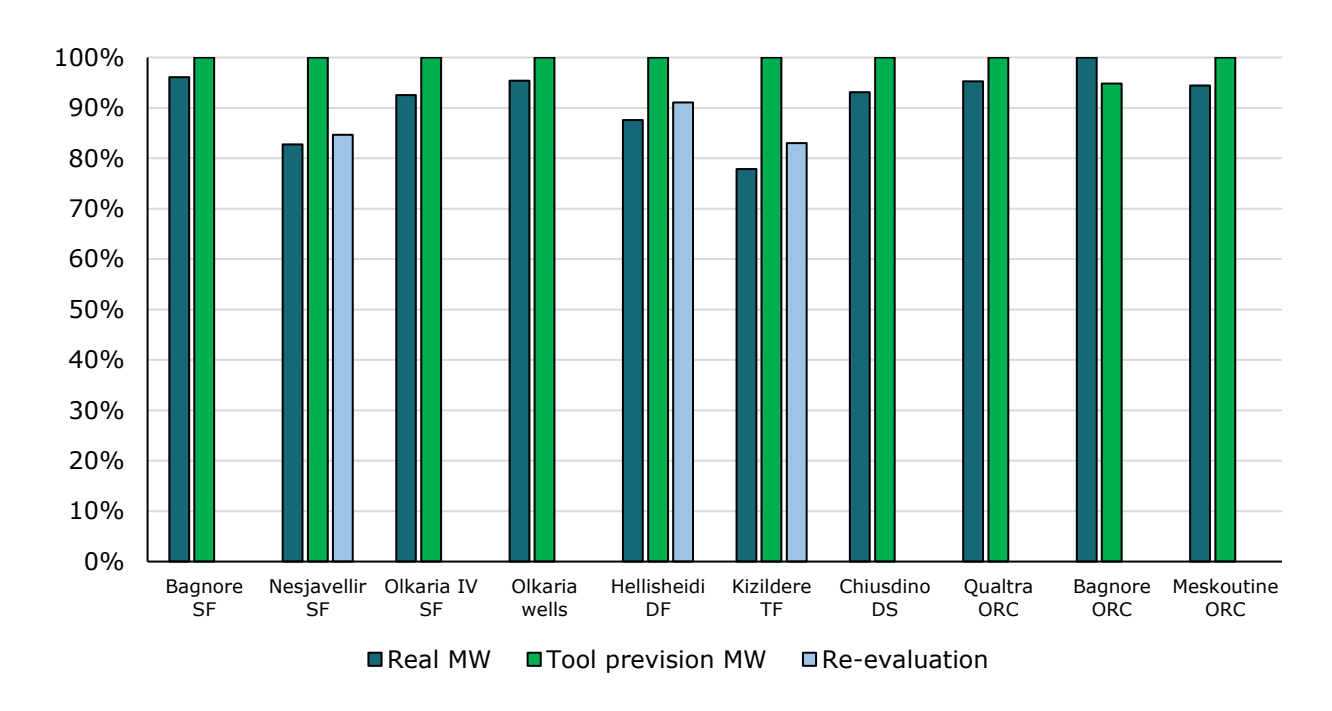


Figure 13: thermodynamic power plant validation

3.1.2 Economic analysis

As above outlined, the validation of the thermoeconomic metamodel is conducted with a limited number of real case studies for comparison. This limitation arises due to the scarcity of available data on the coupling of thermodynamic and economic parameters, particularly the Levelized Cost of Energy (LCOE). It is worth noting that the selected known cases, including Qualtra, Kizildere, Nesjavellir, and Hellisheidi from the GECO project, offer valuable insights to the validation process. However, the analysis reveals a rather intriguing observation: no definitive trend in cost prediction is found (Figure 14). This lack of a clear behavior suggests the complexity inherent in accurately predicting the LCOE of



geothermal plants. Indeed, the findings indicate that certain plants, such as Kizildere and Nesjavellir, tend to overestimate the LCOE, while others, like Qualtra and Hellisheidi, reveal an underestimation. Furthermore, the relative errors observed in the estimation process is significant, reaching up to 44% for Hellisheidi and notable values for other plants, showing that achieving precise economic predictions is a challenging task. These errors are evident also in absolute terms, with the maximum values in estimation being approximately 2.48 c \in /kWh for Hellisheidi and around 1 c \in /kWh for other cases. Consequently, the estimated error for unknown cases is expected to be approximately \pm 2.5 c \in /kWh. This margin of error highlights the inherent uncertainty in predicting the LCOE of geothermal plants using the current thermoeconomic metamodel.

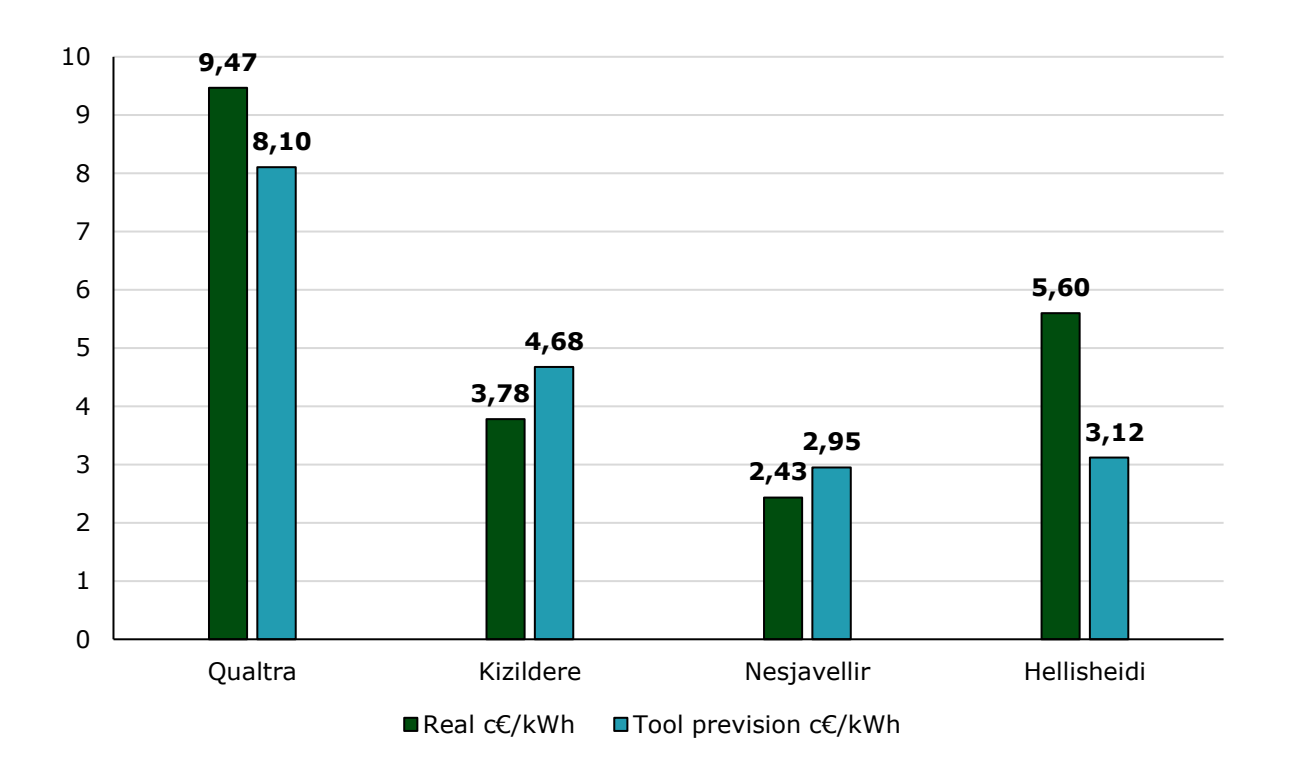


Figure 14: LCOE metamodel validation

3.1.3 Environmental impact assessment

One of the primary hurdles stems from the variability inherent in results evaluated through Life Cycle Assessment (LCA) methodologies. Different databases and methodologies can yield considerably different results, making direct comparisons arduous. Moreover, the availability of detailed benchmarking data for validation purposes is limited, which further complicates the process. In place of directly comparing results with literature data, an analysis is conducted initially at the inventory level, followed by an examination at the Life Cycle Impact Assessment (LCIA) level using a specially crafted model. This methodology enables a focused validation of specific processes, such as the well drilling process in this case, where detailed data allows for meaningful comparisons. The initial results showed in Figure 15 at the LCI level reveal intriguing insights. Despite the inherent variability, a discernible behavior emerges, particularly concerning the consumption of diesel during well



drilling. The distribution of points suggests a linear trend, albeit with some scatter. This contrasts with existing correlations found in literature by Paulillo et al. 2021, which either overestimate or underestimate diesel consumption. The correlation of Vito, (2020), on the other hand, has a non-linear trend, far below the distribution of points and its inflection point where a rapid increase begins is around 3800 m depth. Therefore, this correlation underestimates the diesel required for drilling in almost all cases. The correlation developed within this study presents a novel approach. Positioned between existing correlations proposed by Paulillo et al. (2021), it demonstrates a more accurate prediction of material consumption, as evidenced by various statistical parameters as shown in Table 16:. Notably, it is evident that the coefficient of determination stands out as the highest among them. This observation is particularly relevant, especially when juxtaposed with the findings of Paulillo et al. (2021) on EGS and the study by Vito (2020). In contrast to these, where the coefficient appears negative, indicating potential limitations in their predictive capabilities, the positive coefficient in our analysis means a more favorable outcome. Furthermore, delving deeper into the statistical metrics, it becomes clear that the lowest value corresponds to the Trend-line. Despite its seemingly inferior position in terms of numerical magnitude, this observation is paradoxically indicative of its superior accuracy. The juxtaposition of these statistical parameters highlights the importance of not solely relying on numerical values, but also considering the broader context and implications of the obtained results.

This accuracy is crucial in ensuring the reliability of the metamodel in predicting environmental impacts associated with geothermal well processes. Similar analyses are extended to other materials such as steel and cement, further enriching the validation process. Through meticulous examination and comparison, the study strives to enhance the robustness and accuracy of the environmental metamodel, laying the groundwork for comprehensive assessments of geothermal energy systems.

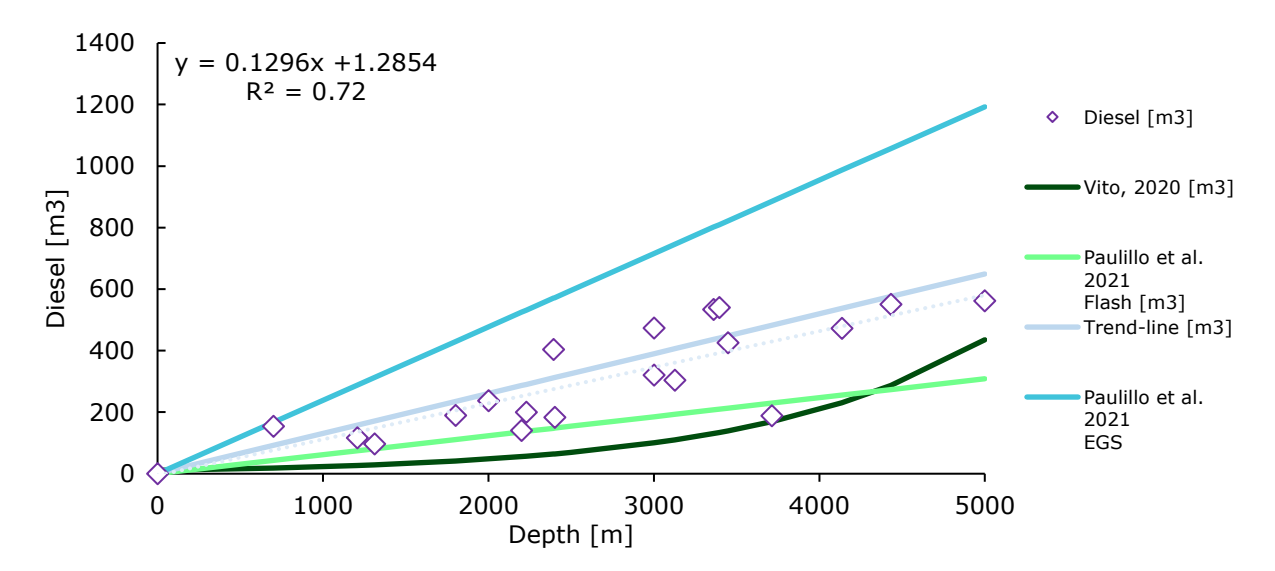


Figure 15: Comparison between Trend line, correlation proposed in the literature and primary data of Diesel consumption



Table 16: Comparison of statistical parameter of trend line against correlations in the literature

Statistic	Vito, 2020	Paulillo et al. 2021 FLASH	Paulillo et al. 2021 EGS	Trend- line
R ² coefficient of determination	-0.49	0.03	-3.01	0.72
MSE Mean Square Error	4.89E+04	3.28E+04	1.48E+05	1.50E+04
MAE Mean Absolute Error	186.79	145.60	338.96	94.27
MdAE Median Absolute Error	147.75	113.10	331.87	83.04
MAPE Mean Absolute Percentage Error	0.59	0.38	1.19	0.35
RMSE Root Mean Square Error	221.11	181.24	384.57	122.63

A comparison was also made at LCIA level, in particular, the analysis focuses on the six high-priority categories identified by the GEOENVI project, with Climate Change emerging as the indicator selected to express the final result for the metamodel.

In examining the data, it becomes evident that the values obtained in absolute terms, as depicted in Figure 16, provide a comprehensive perspective, not related to the functional kWh energy unit, but in terms of CO_2 equivalent emissions. The crosses represent benchmark values derived from the implementation of data collected from all sinks in the database, serving as a point of reference against the correlations documented in the literature.

The trends observed mirror those identified in the LCI analysis. Notably, as observed by Paulillo et al. (2021), the correlation associated with EGS tends to overestimate impacts, while the Flash correlation tends to underestimate them. However, a nuanced exploration reveals that the Flash correlation exhibits a trend closely aligned with real cases for well depths ranging from 1000m to 3000m. The comparison between different correlations further elucidates the nuances of their predictive capabilities. Vito's (2020) correlation, for instance, consistently lies below Paulillo's (2021) Flash correlation, suggesting different magnitudes of impact estimation. Meanwhile, the trend line, serving as an overarching descriptor, encapsulates a trajectory that lies between Paulillo's EGS and Flash correlations. Delving into the statistical parameters further enriches our understanding of



these trends. The table accompanying this analysis highlights the trend-line as the function that most accurately describes this process. This observation highlights the importance of not only identifying trends but also quantifying their accuracy through robust statistical analysis (Appendix).

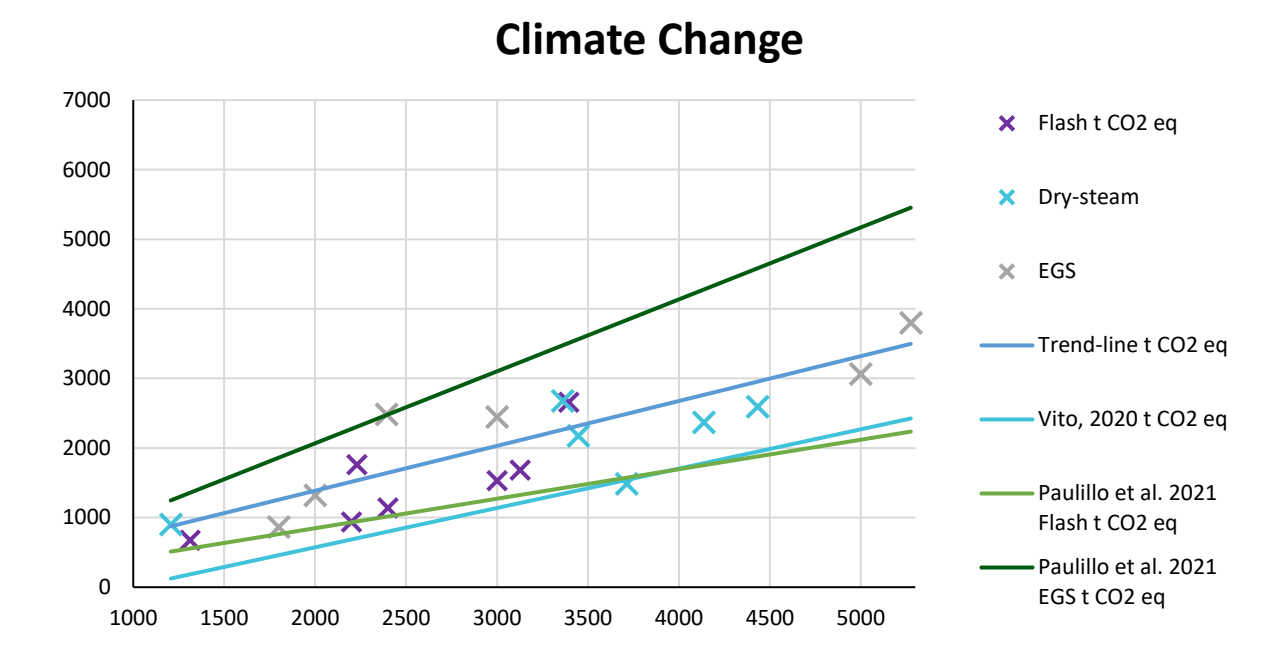


Figure 16: comparison with literature, primary data and trend-line of Climate change indicators.

3.1.4 Metamodel results

This section presents the findings derived from the economic and environmental metamodels. In both cases, an analysis was conducted across four scenarios, each varying solely with the depth of the wells. This parameter holds significant sway over both metamodels' outcomes. Thus, wells at depths of 1000 m, 2000 m, 3000 m, and 4000 m were selected for examination. Figure 17 showcases the Levelized Cost of Energy (LCOE) depicted in c\$/kWh, as the flow rate and temperature of the geothermal resource undergo variation. The flow rate spans from 1 to 80 kg/s. Additionally, reference values for the LCOE of photovoltaic (yellow line), wind (blue line), and gas turbine (red line) plants are provided, standing at 8.7 c\$/kWh, 8.4 c\$/kWh, and 18 c\$/kWh respectively, sourced from Trinomics, B. V. (2020). A maximum of 30 c\$/kWh is imposed, beyond which the technology ceases to be cost-effective. The resulting surface area demonstrates high values, translating to a higher cost per kWh produced for lower temperature and flow rate values. Conversely, as resource conditions improve, the LCOE decreases rapidly. It is worth noting that as the depth of the wells increases, the area with very low LCOE shrinks significantly, shifting towards the right. It is important to highlight that the LCOE ranges provided by IEA website (2023) and IRENA (2017) stand at 12-8.8 c\$/kWh and 14-4 c\$/kWh respectively. Furthermore, it is essential to consider that the graphs depict a maximum flow limit of 80 kg/s, indicating that the analysis focuses on intermediate-sized plants, typically around 30-40 MW. Conversely, larger power plants capable of handling higher flow rates exhibit cost-effectiveness even at lower temperatures. This is particularly noticeable as the combinations of flow rate and temperature increase considerably.



Additionally, a graph in the appendix illustrates scenarios with higher flow rates, further corroborating these observations.

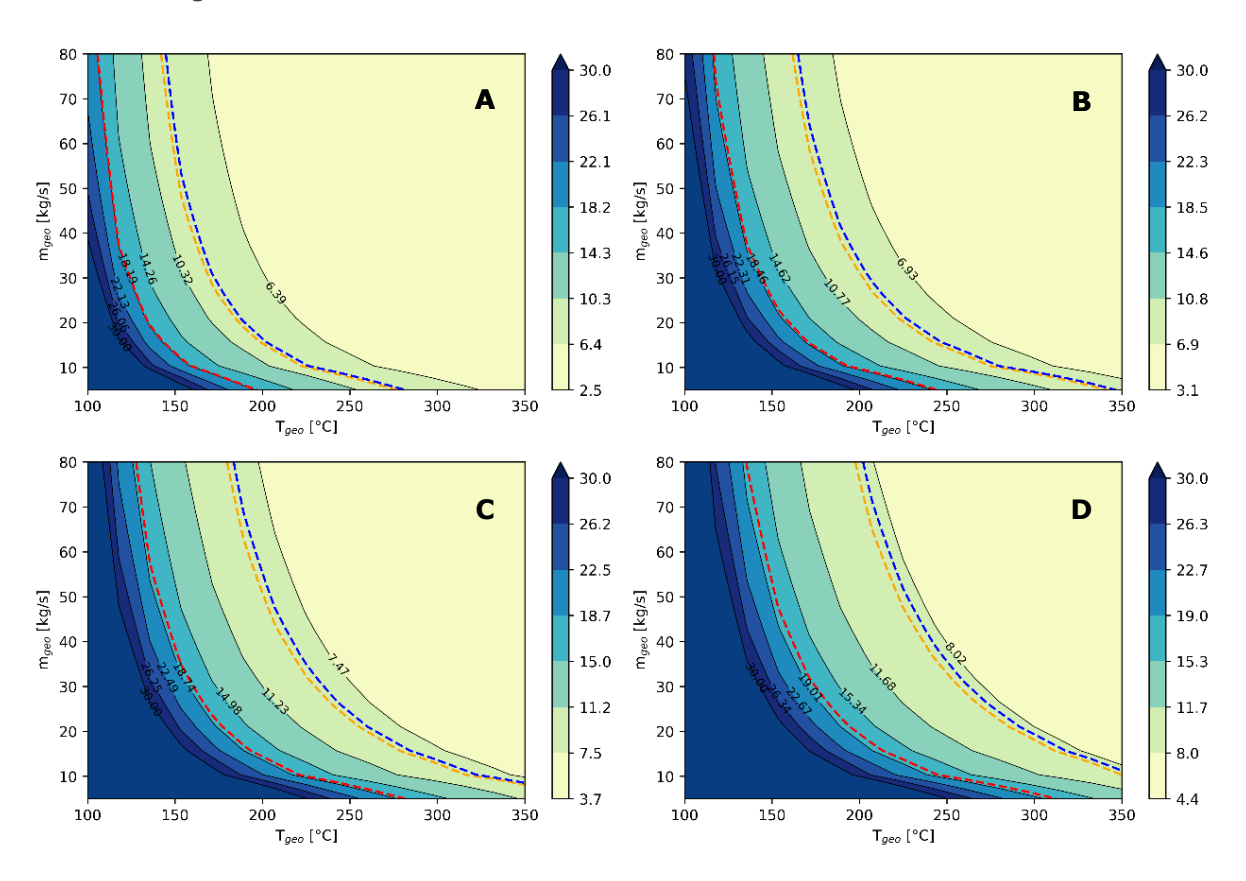


Figure 17: Levelized Cost Of Electricity [c\$/kWh] metamodel results for different well depth (wd). A: wd =1000m; B: wd = 2000m; C: wd = 3000m; D: wd= 4000m (Power Plant)

The environmental metamodel exhibits a pattern analogous to that of the economic metamodel, as illustrated in Figure 18. Specifically, equivalent CO2 emissions are notably high for low values of T_{geo} and m_{geo}. To delineate the environmental non-feasability threshold, a limit of 100 gCO₂ eq/kWh was established. Similar to the LCOE, an increase in well depth exerts a significant influence on Climate Change (CC) impacts. However, despite this influence, the impact is relatively restrained compared to other geothermal plants, owing to the considerable variability inherent in the system. Figure 18 illustrates this with a dark blue line representing equivalent emissions assessed by the Geothermal Kenya process in ecoinvent 3.7.1, while a dashed yellow line represents emissions from a photovoltaic plant. Notably, even in cases of deep wells, combinations of Tgeo and mgeo surpassing both the photovoltaic and Geothermal Kenya lines are manifold, indicating a considerable environmental benefit. It is important to note that comparisons to other lowemission geothermal plants, such as Hellisheidi, emitting around 16g CO2 eq/kWh (Zuffi et al. 2022), or wind power plants emitting 34q CO2 eg/kWh (Ecoinvent 3.7.1), are not yet viable. Conversely, the system under consideration demonstrates high performance compared to geothermal plants with high natural emissions, such as Bagnore, approximately 400g CO2 eq/kWh (Tosti et al., 2020), or gas turbine electricity production emitting approximately 740 g CO2 eq/kWh (Ecoinvent 3.7.1). Thus, across all depth cases, environmentally aligned and beneficial solutions are discernible for various combinations of T_{geo} and m_{geo}. Furthermore, it's crucial to emphasize that both LCOE and CC surfaces



presented here are based on a flow rate limit of 80 kg/s. In cases where the flow rate exceeds this threshold, both LCOE and CC experience a significant reduction, reaching levels of 2.3 - 3.9 c\$/kWh and 54-56 gCO₂ eq/kWh as illustrated in Appendix B..

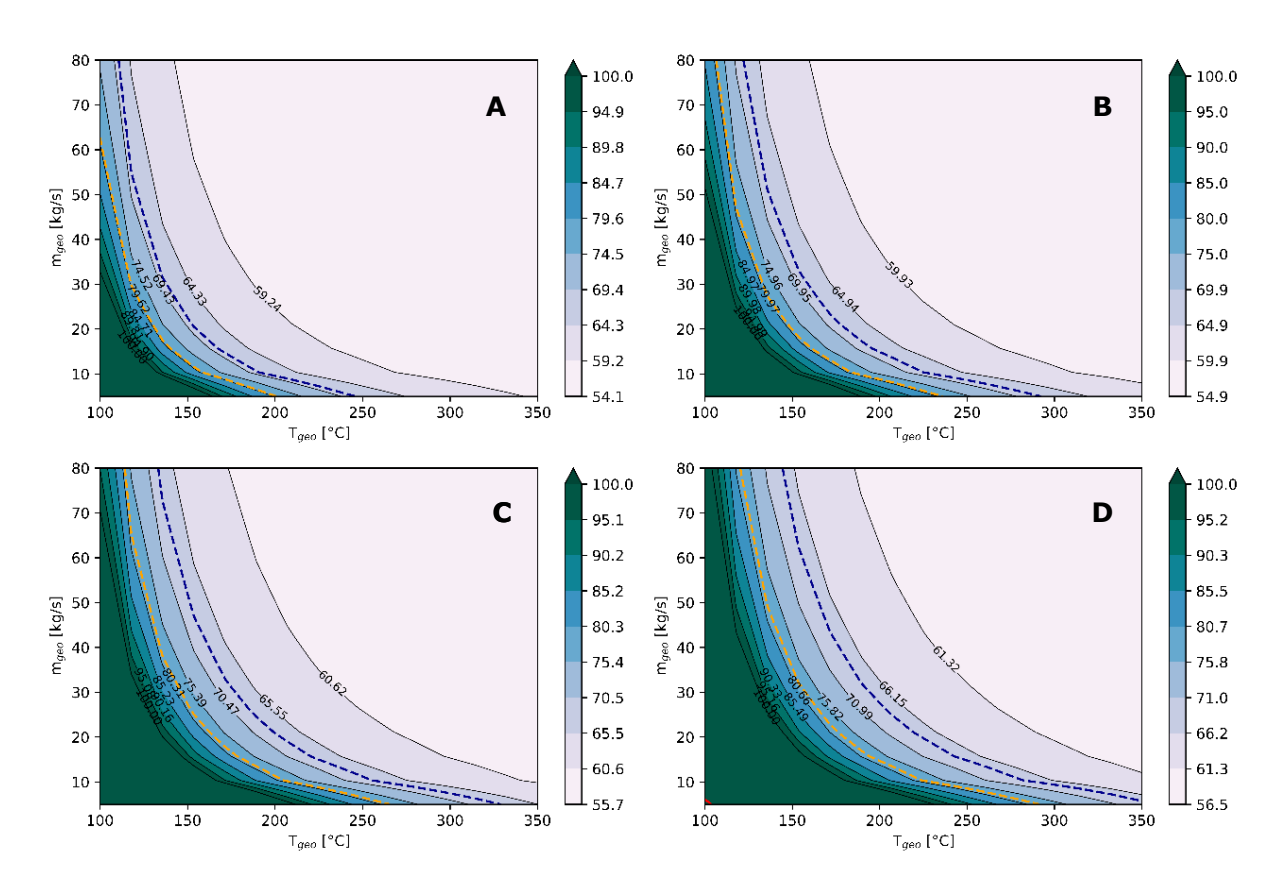


Figure 18: Climate Change metamodel results for different well depth (wd): A:wd = 1000m; B: wd = 2000m; C: wd = 3000m; D: wd= 4000m (Power Plant)

3.2 Medium and Low Enthalpy validation

The validation of metamodels for low- and medium-enthalpy geothermal resources faces significant challenges due to the scarcity of benchmarking data available in the literature. Specifically, the validation process for the thermodynamic and economic metamodel is primarily limited to absorption cycles, with only three case studies serving as reference points. Moreover, in the case of High Temperature High Pressure (HTHP) systems, the absence of literature values further compounds the challenge of consolidating data with realistic scenarios, as this technology remains relatively underexplored in the context of geothermal systems. Similar constraints apply to the validation of Life Cycle Assessment (LCA) analyses, which encounter additional hurdles due to the afore mentioned limitations. Consequently, greater attention has been devoted to interpreting results derived from metamodels and surfaces that delineate the trends of potential concerning the geothermal resource. This approach involves the comparison of these results with the limited number of known cases available in the literature. To facilitate this comparative analysis, four distinct scenarios concerning geothermal wells are proposed, each one evaluated with one production well and one re-injection well. However, the evaluation will focus solely on



varying depths in 500m or 1000m increments: starting from 0m (no wells), progressing to 500m, 1000m, and finally reaching 2000m. This methodological assumption is grounded in the understanding that such systems are typically deployed in scenarios where waste heat from a power plant is utilized or in the context of shallow wells. Consequently, a maximum depth of 2000 m has been selected, aligning with the typical operational parameters observed in these applications.

3.2.1 Thermodynamics

For the thermodynamic validation of the system, the installed cooling capacity of the absorption system (ABS) serves as the benchmark output parameter. This is evaluated against three reference cases sourced from Ylmaz et al. (2017), Wu et al. (2021), and Beckers et al. (2021), with reported capacities of 3.71 MW, 0.36 MW, and 11 MW, respectively. A bar diagram, depicted in the Figure 19, portrays the comparison between the real case and the tool's prediction, with the maximum value normalized to 100%. Notably, the tool exhibits a tendency to overestimate the installed cold power, consistently yielding the highest values across all cases. Upon closer examination, it becomes evident that the tool's predictions are highly accurate for the Ylmaz et al. (2017) and Beckers et al. (2021) cases, with prediction errors approximately 6.27% and 6.78%, respectively. Conversely, in the case of Wu et al. (2021), the prediction error is notably higher, approximately 22.88%. This discrepancy arises due to differences in the flow rate assumptions used in the tool compared to the real case scenario. Notably, the flow rate parameter evaluated in the tool uses distinct assumptions which cannot be modified within the metamodel. Thus, while the overall estimation is accurate, there is way for improvement in enhancing the metamodel's adaptability to varying parameters in different scenarios. So promising accuracy in predicting the installed cooling capacity, there remains potential for refinement to ensure greater flexibility and precision across diverse operational contexts. By incorporating adjustments to accommodate varying parameters, the metamodel can further enhance its utility and reliability in real applications.

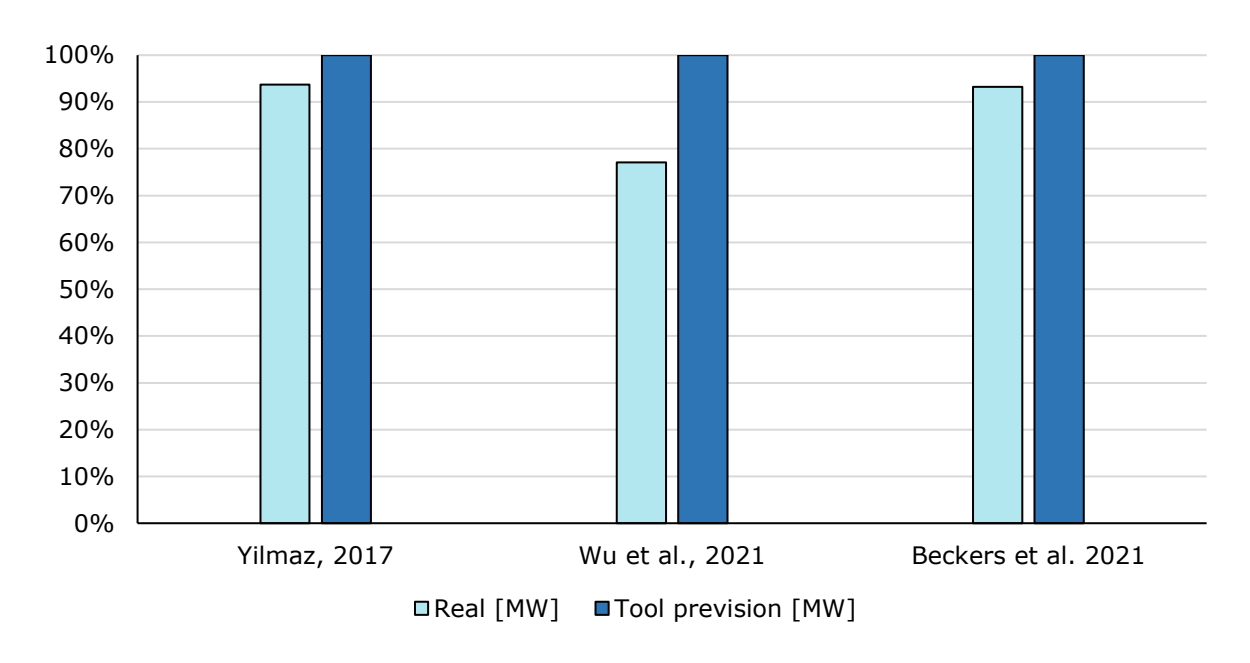


Figure 19: Column diagram of the validation of thermodynamic metamodel for the absorption cycle



3.2.2 Economics

For the economic validation aspect, it has only been able to access two cases of Levelized Cost of Cooling (LCOC) from Yilmaz (2017) and Beckers et al. (2021). Despite the limited dataset, the tool demonstrates a trend to overestimate the real case, albeit to a very marginal extent, resulting in highly accurate predictions. Specifically, the error margin for both cases stands at a mere 7.2%. It is worth noting that while this validation doesn't guarantee absolute precision due to the constrained dataset, the maximum difference observed in absolute terms is approximately 0.15 c\$/kWh. Such a negligible discrepancy indicates a remarkably low margin of error and thus states the reliability of tool prediction. while the validation process is somewhat constrained by the limited availability of data in the literature, the observed discrepancies between the tool's predictions and the real cases are minimal. However, it is important to acknowledge the need for continued validation efforts as more data becomes available, which can further refine and improve the accuracy of tool economic predictions.

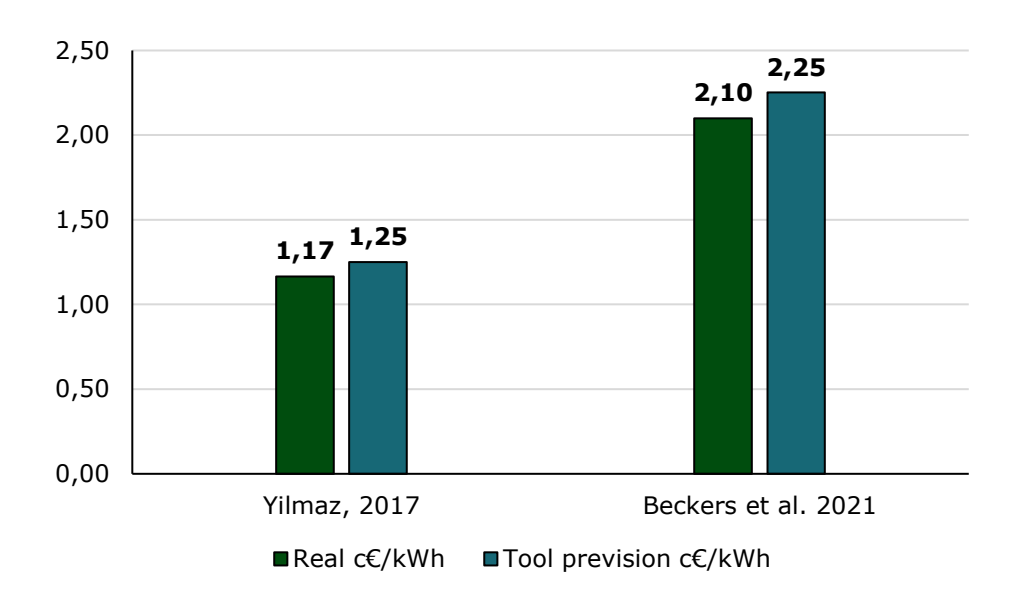


Figure 20: Column diagram for validation of the economic metamodel for the absorption cycle

3.2.3 Metamodel results

Figure 21 depicts the results obtained from the analysis of the energy metamodel, focusing on the evaluation of the system's energy performance characterized by the Coefficient of Performance (COP) and the evaporator temperature (T_{evap}). Notably, the evaporator temperature (T_{evap}) is closely tied to the target temperature for the end user, differing by only 5 degrees. One significant observation is that the Coefficient of Performance (COP) and T_{evap} , due to the inherent structural characteristics of the energy metamodel, exhibit minimal sensitivity to the mass flow rate (m_{geo}) for each parameter. This occurs because on the one hand, as already mentioned in the methodology, the T_{evap} is linked by a correlation to the $T_{geo,in}$; on the other hand, the COP as it is calculated takes into account the mass flow rate of the cycle that maintains the same ratio.

Distinct trends emerge, revealing contrasting aspects depending on the temperature of the geothermal resource (T_{geo}). At lower T_{geo} levels, the system demonstrates a high COP,



peaking at 0.76. However, it's noteworthy that T_{evap} concurrently rises to excessively high levels, ranging between 16-20 °C, making the cooling effect unsuitable for typical cooling applications. Conversely, higher $T_{geo,in}$ values result in a remarkable decrease in COP, reaching a minimum at 0.38. Nevertheless, T_{evap} decreases to as low as -10 °C, facilitating applications in industrial refrigeration settings. An optimal performance range and potential applications are identified within the 80-110 °C T_{geo} range, where a balance between COP and T_{evap} is achieved, making it suitable for a variety of practical applications. the intricate interplay between T_{geo} , COP, and T_{evap} , highlighting the importance of considering these factors globally to optimize the energy performance of the system for diverse application scenarios.

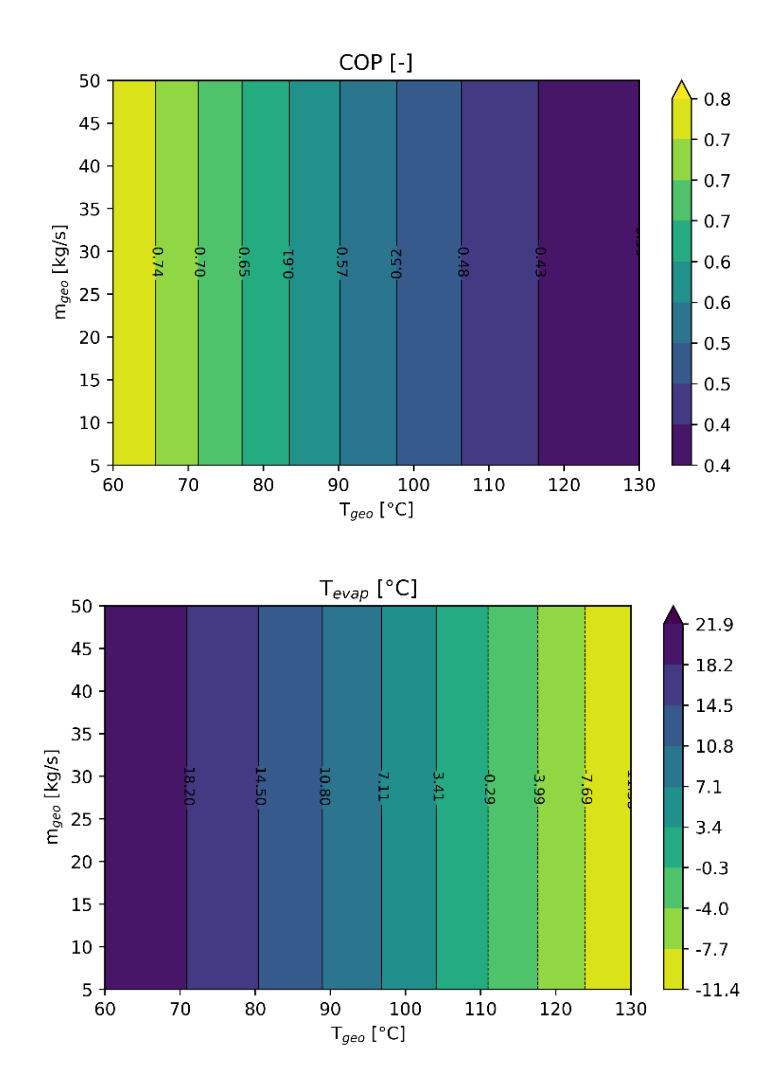


Figure 21: thermodynamic metamodels of Coefficient of Performance and Evaporation Temperature

The thermo-economic analysis, as represented by the Levelized Cost of Cooling (LCOC), delineates a crucial threshold where the cost of cooling energy becomes economically unfavorable beyond certain values. In Figure 22, two reference lines depicted in red and blue dashes correspond to literature values from Beckers et al. (2021) and Yilmaz (2017), standing at 21 c\$/kWh and 11.65 c\$/kWh, respectively.

A remarkable observation from the graph is that in scenarios where wells are absent, the LCOC remains remarkably low, with a maximum level of 10 c\$/kWh and a minimum of 1.4 c\$/kWh under the most favorable conditions. However, with the introduction of even two



wells (one production and one reinjection), the economic landscape undergoes a significant change. In fact, much higher ranges of variability occur, with a maximum of 43.6 c\$/kWh, 78.4 c\$/kWh, and 113.2 c\$/kWh as extreme values for the other three scenarios (wells at 500 m, 1000 m, and 2000 m). The range of high economic viability, outlined above the blue reference line, is significantly reduced by increasing the depth of the wells. Despite this, it can be observed that the red line remains in the low domain even in the case of deeper wells.

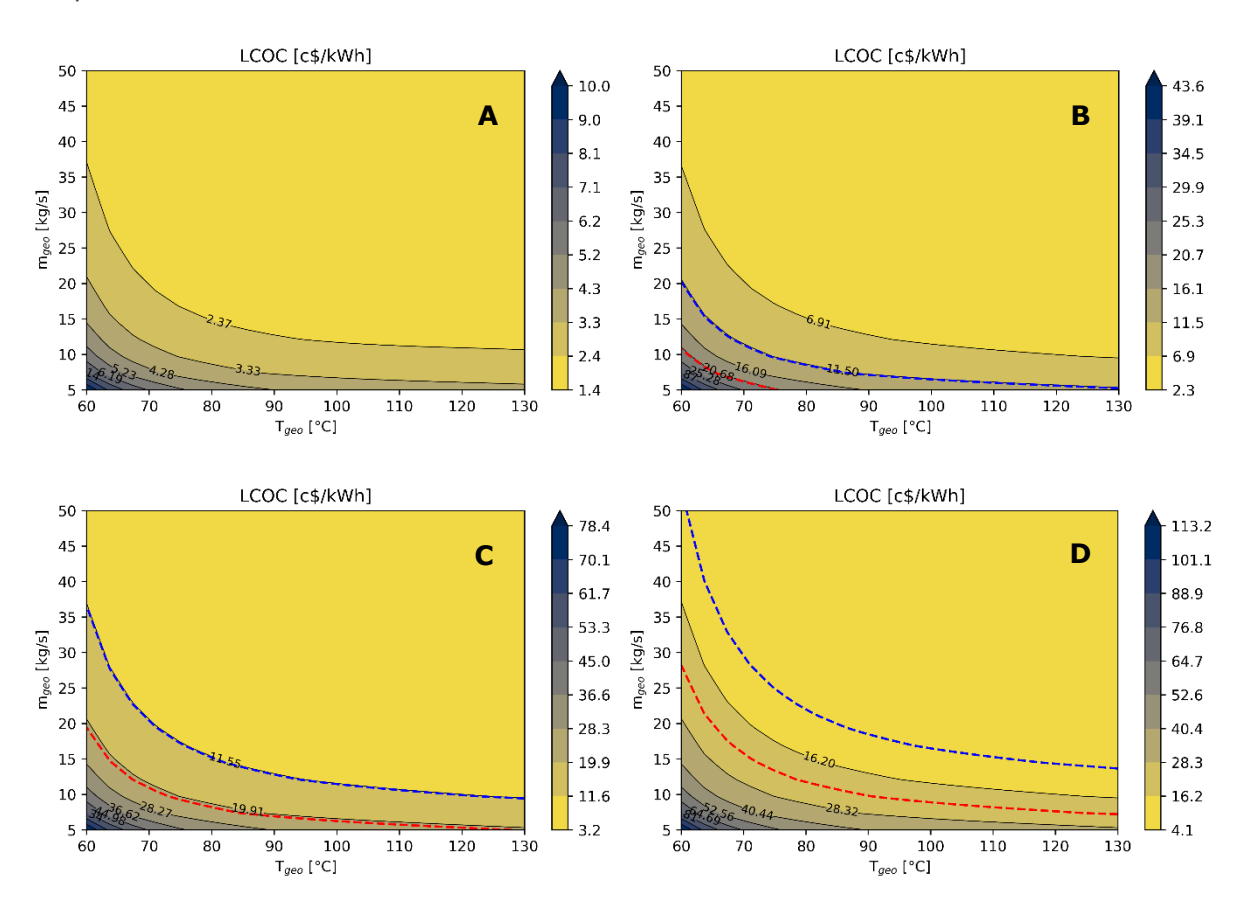


Figure 22: Levelized Cost of Cold economic metamodels for different well depth (wd): A:wd = 0m; B: wd = 500m; C: wd = 1000m; D: wd = 2000m (ABS)

On the other side, the environmental assessment provide a favorable picture for geothermal cooling systems. Despite the dearth of specific studies on Life Cycle Assessment (LCA) of geothermal Air-Conditioning and Refrigeration Systems (ARS), comparisons with data from the Ecoinvent database reveal substantially lower carbon emissions for geothermal cooling systems. In Figure 23, two dashed lines are depicted, one blue and one black, representing the environmental impact of two cooling systems (Pratiwi & Trutnevyte, 2021), which respectively register at 7.8 g CO2 eq/kWh and 10.2 g CO2 eq/kWh. As evidenced by the graphs, increasing the depth of the wells results in a significant rightward shift of these two lines, notably reducing the range where greater environmental benefits are achieved. However, compared to standard fossil-fuel-based refrigeration systems, there remains a considerable advantage, and in no depth scenario is there a situation of environmental disadvantage. To provide a more detailed analysis, consider the environmental impact of a provider from the Ecoinvent 3.7.1 database (cooling energy, from natural gas, at cogen unit with absorption chiller 100kW | cooling



energy). Here, the environmental impact is measured at 417 g CO2/kWh, significantly higher than the impact ranges evaluated using the tool. This comparison highlights the relevant environmental benefits of geothermal cooling systems, even as well depths increase. While the shift towards deeper wells may reduce the extent of environmental advantage, geothermal systems still maintain a significant edge over traditional fossil-fuel-based alternatives. Additionally, the stark contrast with the environmental impact of conventional cooling methods further emphasizes the importance and potential of geothermal technology in reducing carbon emissions and promoting sustainable practices. Furthermore, by correlating the results obtained between LCOC and CC, it is determined that in the decision-making phase, greater attention should be given to economic aspects, as environmental considerations provide a significant advantage in all cases compared to conventional systems.

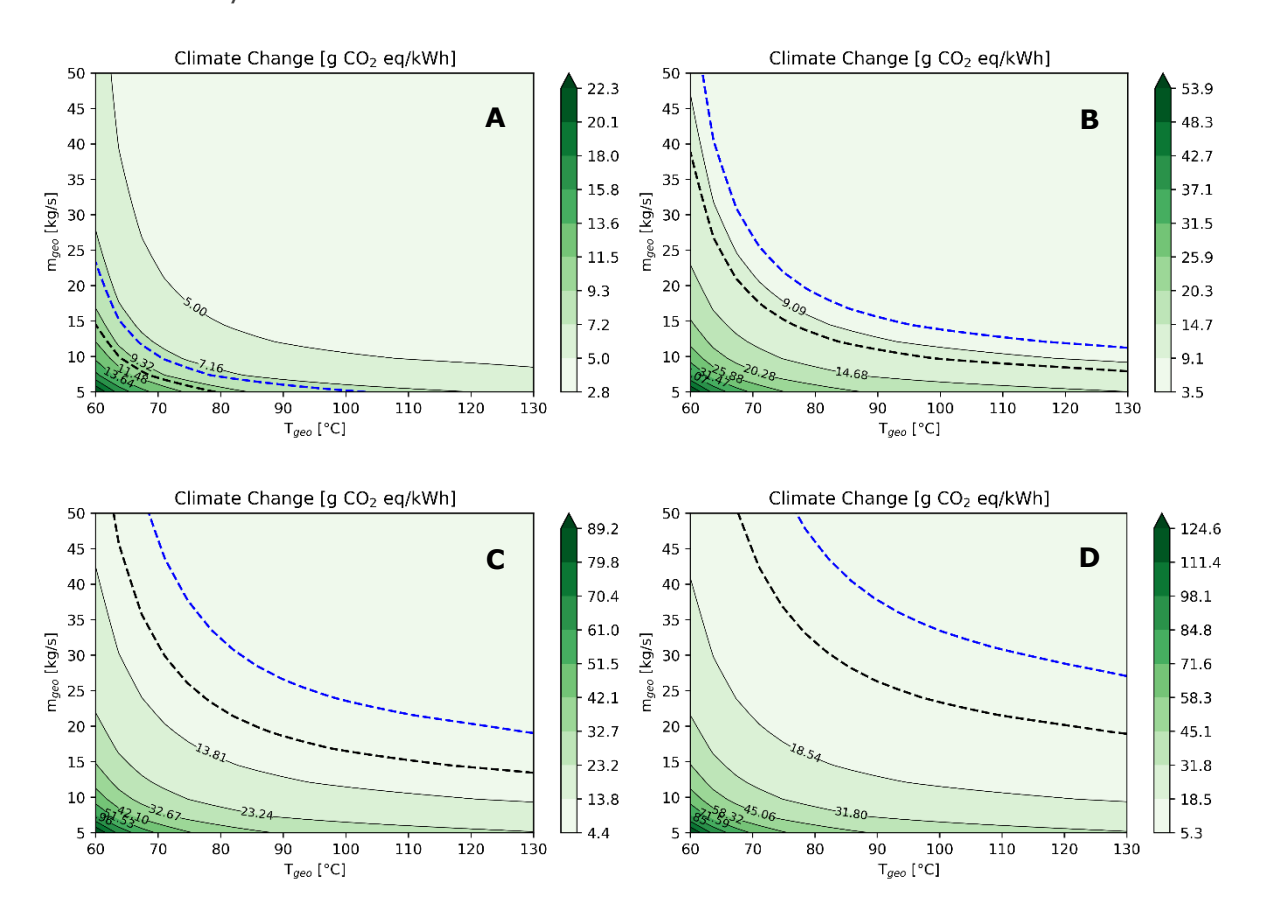


Figure 23: Environmental metamodels of climate change indicators for different well depth (wd): A:wd =0m; B: wd = 500m; C: wd = 1000m; D: wd=2000m (ABS)

The thermo-economic evaluation reveals significant variability in the Levelized Cost of Heat (LCOH) for HTHP, contingent upon resource conditions and well characteristics. Figure 24 illustrates LCOH, with different well depth scenario, as already shown for ABS thermodynamic blocks. The red dashed line denotes the reference LCOH value provided by IEA 2021 for heat generated from natural gas-fired boilers, approximately at 17 c\$/kWh, while the cost obtained for High-Temperature Heat Pumps (HTHP) is indicated as 22 c\$/kWh (Jeßberger, J et al. 2023). It is evident that there's a substantial increase in LCOH from 5a to 5c, underscoring the significant influence of drilling costs on this parameter. In 2000m depth scenarios LCOH is notably high for low values of T_{geo} and m_{geo} , reaching a maximum of 223 c\$/kWh, with economic feasibility only apparent at higher temperatures



or increased mass flow rates. Moving to 1000m or 500m depth, where the well depth is shallower, the maximum LCOH reduces to 156.8 c\$/kWh and 90.2 c\$/kWh, with more combinations of T_{qeo} and m_{geo} surpassing the red dashed line.

Lastly, in no well scenario, only a narrow range fails to yield an economic advantage. In fact, for all combinations of T_{geo} - m_{geo} above 62°C or above 17 kg/s, an LCOH below the boiler heat output is obtained. This highlights the dependence of LCOH on well costs, significantly impacting the parameter. Hence, for HTHP applications, scenarios where the geothermal reservoir is shallow or utilizes hot waste fluids from geothermal power plants would offer substantial economic benefits. However, if a greater number of wells or deeper drilling is necessary, the conditions for LCOH advantage diminish considerably. Therefore, a meticulous evaluation is imperative for each specific case based on the resource depth.

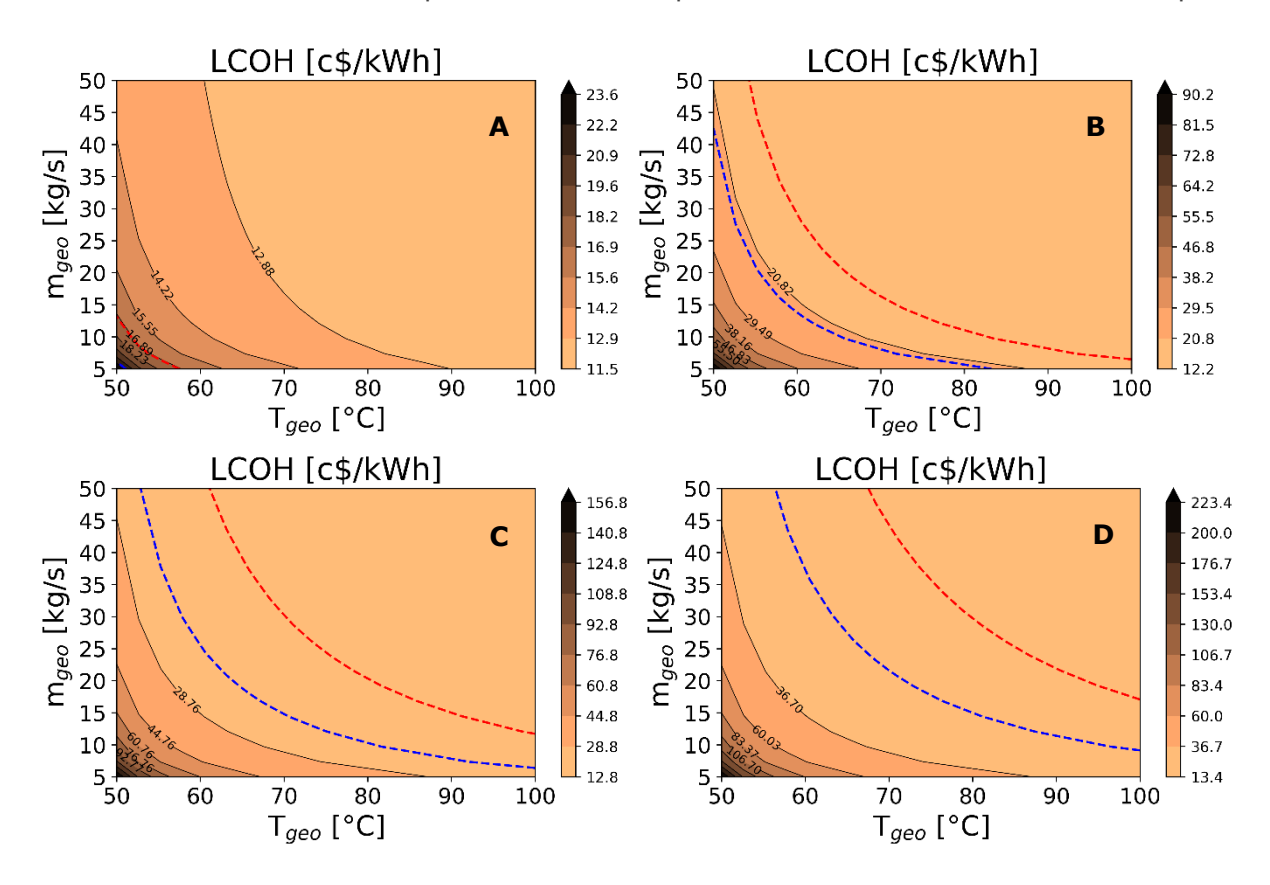


Figure 24: Levelized Cost of Heat economic metamodels for different well depth (wd): A:wd = 0m; B: wd = 500m; C: wd = 1000m; D: wd= 2000m (HTHP)

Figure 25 shows the metamodel of CC, equivalently for Figure 24. Given the limited literature on the environmental impact of geothermal High-Temperature Heat Pumps (HTHP), indicative limits are displayed. A red line represents the CC indicator for a kWh produced by a natural gas modulating condensing boiler, at 264.16 g CO2 eq/kWh, while a blue line denotes a kWh from a borehole heat exchanger brine-water, evaluated at 223.88 g CO2 eq/kWh by Ecoinvent providers. The trend express that of LCOH, wherein CC exhibits a higher impact for case (2000m depth), reaching 317 gCO2 eq/kWh for low $m_{\rm geo}$ and $T_{\rm geo}$, comparable to normal boiler emissions. Hence, temperatures above 60°C or $m_{\rm geo}$ above 15 kg/s are favored to minimize environmental impact. It's noteworthy that drilling also contributes significantly to CC, albeit less than to LCOH, owing to the strong influence of electricity production. The 1000m and 500m scenarios reveal even greater



potential for achieving low environmental impact, evidenced by a decrease in equivalent emissions. The limits provided for borehole heat exchanger brine-water in both scenario cover only a narrow range for temperatures below 60° C. Moreover, in the no-wells scenario all T_{geo} and m_{geo} combination are environmentally advantageous. Considering the insights from both LCOH and CC, economic viability emerges as the prevailing limiting factor. Therefore, for a comprehensive assessment of HTHP installation, priority should be given to economic feasibility over environmental concerns as the ABS evaluation. Optimal conditions defined by economic metamodels should guide decision-making processes to ensure the most advantageous outcomes.

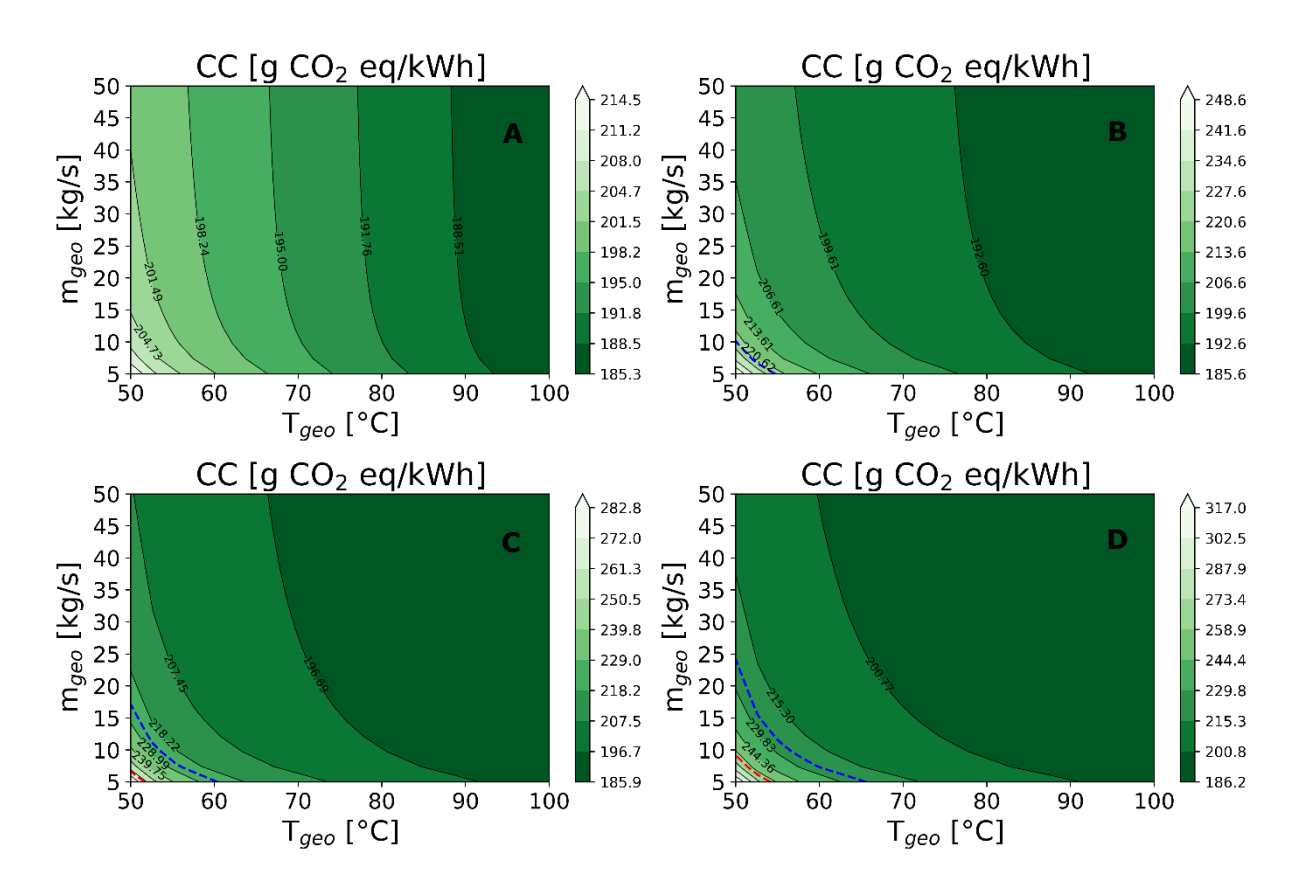


Figure 25: environmental metamodels of climate change indicators for different well depth (wd): A:wd = 0m; B: wd = 500m; C: wd = 1000m; D: wd= 2000m (HTHP)

3.2.4 Application and case studies

The case study evaluated in is the Malawi hot springs, coming from literature (Davalos et al., 2021) and Langano geothermal resources, coming from LEAP-RE partner collaboration (Addis Ababa Science and technology University, AASTU). Davalos et al., 2021 performed an extensive study on the geochemical characteristics of 27 hot springs in Malawi, distributed along north to south of the Malawi Rift Zone. In addition to characteristics related to the chemistry of the geothermal resource, the surface temperature assessment



is carried out by reporting the temperature of all 27 sites. The surface temperature ranges between 35-80°C, but only hot springs with a temperature above 50°C are taken into consideration in this work, as reported in Table 17.

On the other hand, AASTU analyzed, through a data acquisition campaign, the chemical and physical compositions of water in the areas surrounding Aluto-Langano for as many as 20 different sites in 2004. The temperature of this sample is variable as it is taken in different areas and at different depths. In fact, surface temperatures range between 23°C and 60°C, while hot spring samples with high mass flow rates reach temperatures from 60°C to a maximum of 95.2°C. For this area, only resources with temperature higher than 50 °C have been taken into account, which are 12 and are also shown in Table 17.

Unfortunately, the required mass flow rate measurements for the sustainability assessment of the use and replenishment of the resource are not available for Malawi area and and only a qualitative description in terms of low-medium-high for the Aluto-Langano area.

For this reason, three flow rate scenarios for each geothermal resource are defined - High 50 kg/s (Hm), Medium 20 kg/s (Mm), Low 8 kg/s (Lm).

Table 17: Hot spring from Malawi and Aluto-Langano

Malawi (Daval	os et al., 2021)	Aluto-Langano		
Hot Spring	Temperature [°C]		Temperature [°C]	
Ngala	54.9	Sp-2	66.2	
Chiweta	79.7	Sp-84	62.5	
Mphizi Stream	78.7	Sp-5 (new) Bole	94.3	
Mtondolo	64.77	Sh-1	95.2	
Mtondolo 2	72.9	Sh-2	94.6	
Chiwe	74.9	Wendo H.Sp	71.1	
Chombo	66.84	Belle H.Sp	73.1	
Madzimawira	63.73	Kenteri H.Sp	60.7	
Ling'ona	58.08	Chitu-1	61.3	



Chikwizi	52.17	Chitu-2	58.9
July Borehole	51.35	TG-32	68.4
		TG-30	60.1

Final applications have been defined for possible users for heat and cold production. For heat production possible uses:

- Cooking station (CS) supplying steam at 140 °C (HT condition) for cooking food, which requires about 2.89 GWh/year heat load for a group of 5'000 people, (CS_{5k}); 5.79 GWh/year for 10'000 people (CS_{10k}); 29.00 MWh/year for 50'000 people (CS_{50k}) (Kajumba et al. 2022).
- Cassava drying (CD) supplying steam at 100°C (LT condition) for drying vegetables.
 This process requires about 28 MWh/y, so three scenarios are assumed in which a
 company produces about 100 tonnes/year CD₁₀₀, 500 tonnes/year CD₅₀₀, and 1000
 tonnes/year CD₁₀₀₀ (Nwakuba et al. 2016).

Figure 26 shows the thermal energy produced by HTHP with R1234ze(Z) fluid, the corresponding LCOH and CC. The dashed red lines represent the heat demand for the three scenarios CS_{5k} , CS_{10k} , CS_{50k} . The graph shows that in the case where m_{geo} is Lm for all wells, it is possible to satisfy the heat demand for a community of 5 thousand people CS_{5k} . A community of 10 thousand people CS_{10k} can be satisfied for some wells even in the case of Lm (Mtondolo 2, Chiwe, Mphizi stream). For all other wells, it is possible to satisfy this demand only in the case of Mm. The heat load of the CS_{50k} scenario is only reached for some sites in the Hm case (Chombo, Chiwe, Motombolo, Motombolo2 and Mphizi stream). It can also be noted that the two Madzimawira and Chiweta sites where the flow rates are known can meet the CS_{10k} and CS_{50k} heat loads respectively.

All scenarios have an LCOH variable between 11.2 c\$/kWh and 12.5 c\$/kWh and are therefore very cost-effective. It is mainly due to the surface heat source, which allows for an extremely low LCOH. As far as CC is concerned, a larger variation is found, ranging between 197-186 gCO₂/kWh. It is found that for wells with low T_{geo} , CC increases, and this is the result of the cycle behaviour. In fact, the lower T_{geo} implies a larger difference between the low and high pressure of the cycle, which is reflected in a higher consumption of electricity by the compressor and thus a greater environmental impact.



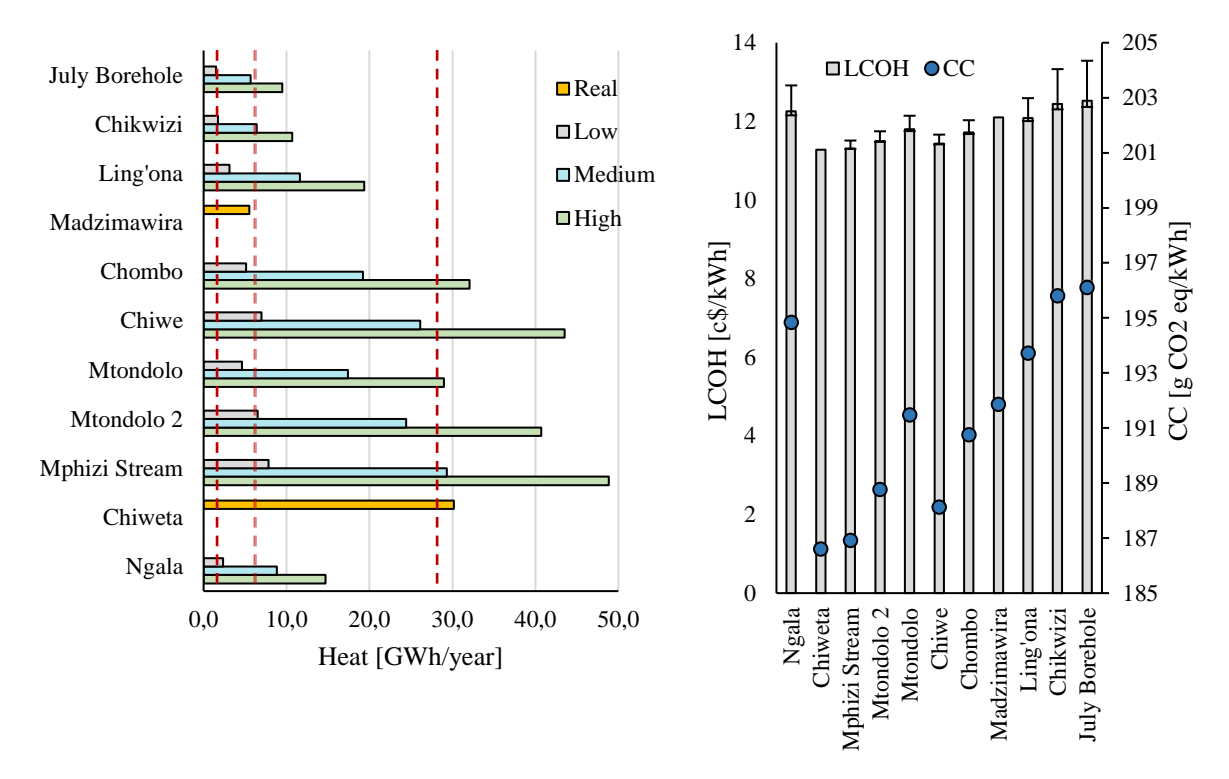


Figure 26: Potential exploitation for a cooking station in Malawi

For the Cassava drying application in Figure 27, it is shown that all wells even for Lm are able to meet the heat demand for drying of 100 ton/year CD100. As for the CD500 intermediate scenario, it is achieved with five wells in the case of Mm (Chombo, Chiwe, Motondolo, Motondolo 2 and Mphizi Stream).

In the Hm scenario, only three wells could reach the CD1000 production level. For the Madzimawira and Chiweta cases, they can meet more than the heat demand of the CD100 and CD500 cases respectively. LCOH is for all scenarios between $6.8 - 8 \, \text{c} \, \text{kWh}$, therefore an extremely low value leading to strong cost-effectiveness. The LCOH variation from Lm and Hm is between $1 - 6 \, \%$ for all scenarios excluding Chikwizi and July Borehole, which have a variation in the order of $10 \, \%$.

For CC it again turns out to be more variable, in the range of 130 to 139 gCO2/kWh which is far below the limits observed in the previous section.

The considerations done for the previous figure (Figure 26) can be extended here as well, since the higher T_{geo} allows a reduction in environmental impact by reducing electrical energy consumption.



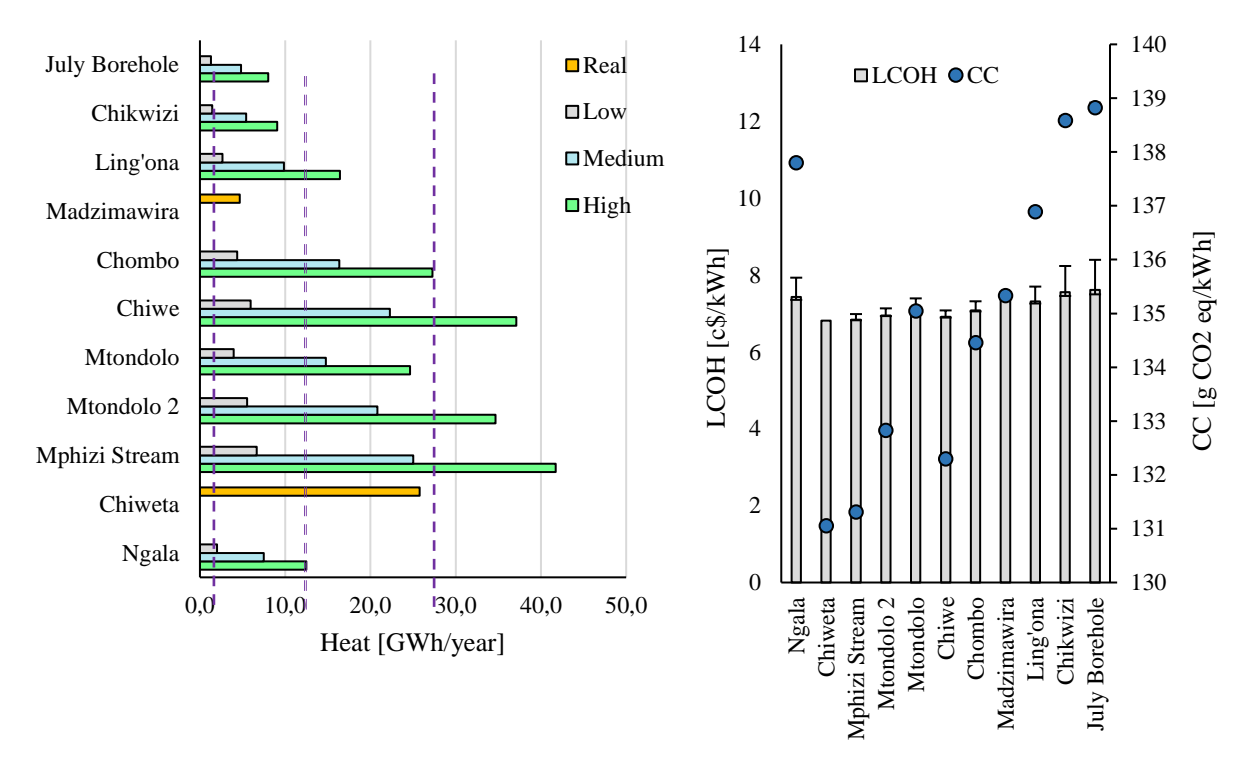


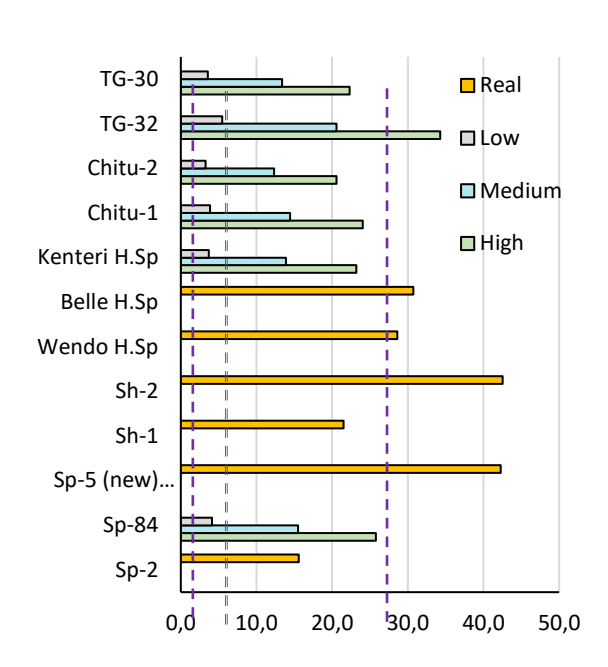
Figure 27: Potential exploitation for Cassava Drying in Malawi

On the case of Ethiopian area (Aluto-Langano), the results illustrated in Figure 28 reveals a significant potential for sustaining cooking stations to serve communities of 5,000 or 10,000 residents across all examined wells. Notably, in scenarios with high flow rates, only the TG-32 well exhibits capacity to not only meet but surpass the heat load requirements for a community of 50,000 individuals. Of particular interest is the performance of the Belle H. Sp, Wendo H. Sp, Sh-2, SP-5 (new), and Bole wells. These wells, characterized by flow rates determined through qualitative ground measurements, demonstrate the capability to fulfill the thermal needs of a community of 50,000 inhabitants, with Sh-2 and Sp-5 even exhibiting a notable margin for expansion.

In terms of Levelized Cost of Heat (LCOH), the collective average among all wellshovers around 10-12 c\$/kWh, a remarkably competitive results primarily attributable to the absence of drilling expenses. The abundance of surface resources yielding such elevated temperatures underscores the exceptional cost-effectiveness of the system.

This principle extends to environmental considerations as well. Carbon footprint data indicates that the wells maintain a range of 182-193 gCO2 eq/kWh, notably lower in comparison to alternative systems. Moreover, it's emphasized that wells boasting higher temperatures contribute significantly to reducing carbon emissions by approximately 5-8 gCO2 eq/kWh when contrasted with those operating at lower temperatures.





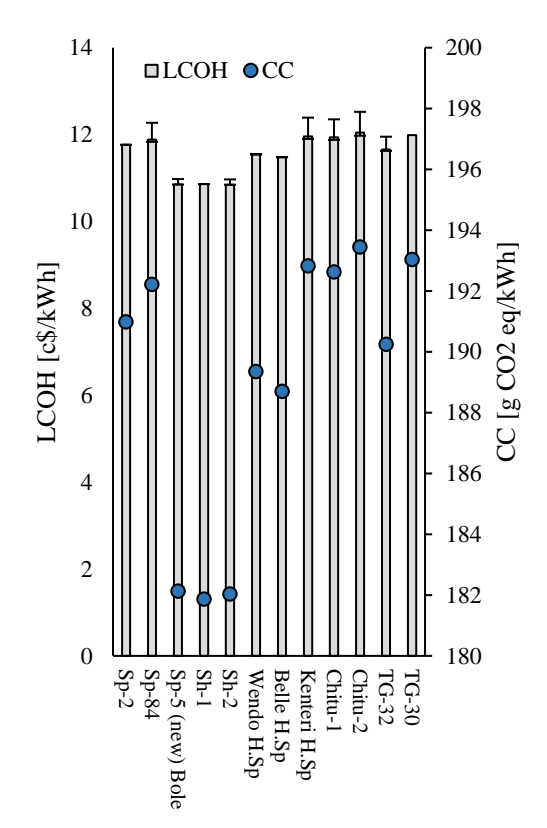


Figure 28: Potential exploitation for a cooking station in Ethiopia

4. Strathmore - KenGen Collaboration

4.1 LCA Olkaria IV

The life cycle impact assessment was conducted using the methodology in Environmental Footprint 3.0 on the Ecoinvent 3.7.1 database. All environmental indicators proposed by the methodology were analysed. Table 18 highlights the highest priority categories in a geothermal field (GEOENVi project, 2023). The results are retrieved in the unit of measurement of each indicator and presented per kWh. The study also uses the Climate Change (CC), 56 gCO2 eq/kWh, to benchmark this analysis with the other energy producing technologies. This benchmark is far below the Kenyan medium-voltage energy mix that impacts 249 gCO2 eq/kWh. Another indicator that appears to be decidedly high is the ecotoxicity of fresh water (Ecf). The following is a detailed analysis of the CC and ECf indicators and all other high-priority indicators with a contribution analysis to determine which process is causing these impacts.



Table 18: Life Cycle Impact Assessment of Olkaria IV

Unit	Indicator name		Impact assessment results	Priority level
mol H+ eq	Acidification	Ac	2.22E-05	High
kg CO2 eq	Climate change	СС	5.60E-02	High
CTUe	Ecotoxicity, freshwater	Ecf	2.27E+01	High
kg P eq	Eutrophication, freshwater	Euf	7.24E-07	Low
kg N eq	Eutrophication, marine	Eum	6.41E-06	Low
mol N eq	Eutrophication, terrestrial	Eut	6.90E-05	Low
CTUh	Human toxicity, cancer	НТс	2.57E-11	High
CTUh	Human toxicity, non-cancer	HTnc	5.40E-11	High
kBq U-235 eq	Ionising radiation	IR	1.90E-04	Medium
Pt	Land use	LU	7.49E-03	Medium
kg CFC11 eq	Ozone depletion	OD	3.73E-10	Medium
disease inc.	Particulate matter	PM	3.87E-10	Medium
kg NMVOC eq	Photochemical ozone formation	POF	2.00E-05	Low
MJ	Resource use, fossils	Ruf	3.52E-02	High
kg Sb eq	Resource use, minerals and metals	Rumm	5.91E-08	High
m3 depriv.	Water use	WU	4.88E-04	Medium

From the contribution analysis shown in Figure 29, the first aspect that is highlighted is that the contribution of well drilling is not the most impactful process in absolute terms, as is the case in many other analyses of geothermal plants [REF]. In fact, it has a maximum contribution of 34.12~% and 31.6~% for Ac and Ruf due to diesel consumption, while for Htnc and Htc it impacts 7.48~% and 16.05~% respectively due to the use of chromium steel for casing.

One process that stands out is the impact of steam pipline. Steam pipeline has a very high contribution in the order of 80%, 55% and 50% for the Htc Rumm and Htnc indicators respectively due to the high use of chrome steel for the steam and reinjection line. This may at first glance appear to be a point of clarification, since a large amount of the same material is used for the casing of the wells. Inventory data show that approximately 3584 tonnes of steel is used for geothermal wells, while approximately 5936 tonnes of steel is used for pipelines. This means that the extent of the plant on the ground has a significant impact on the consumption of some very impactful materials. As far as the impact from the operation and maintenance phase is concerned, the maximum contribution is in Ac and Ruf with a contribution that is around 30 % due to electricity consumption from the grid and the construction of makeup wells. Plant machinery has a significant impact on Rumm and Htnc by 40.78% and 22.69% respectively due to the copper in the heat exchangers



and pumps and the titanium and steel in the various components. Finally, it is shown that the CC and Ecf indicators derive 94.54 % and 99.64 % from the plant's direct emissions. Each, however, derives from different causes; in fact, CC derives from CO2 emissions from the geothermal fluid, whereas Ecf derives from H2S emissions.

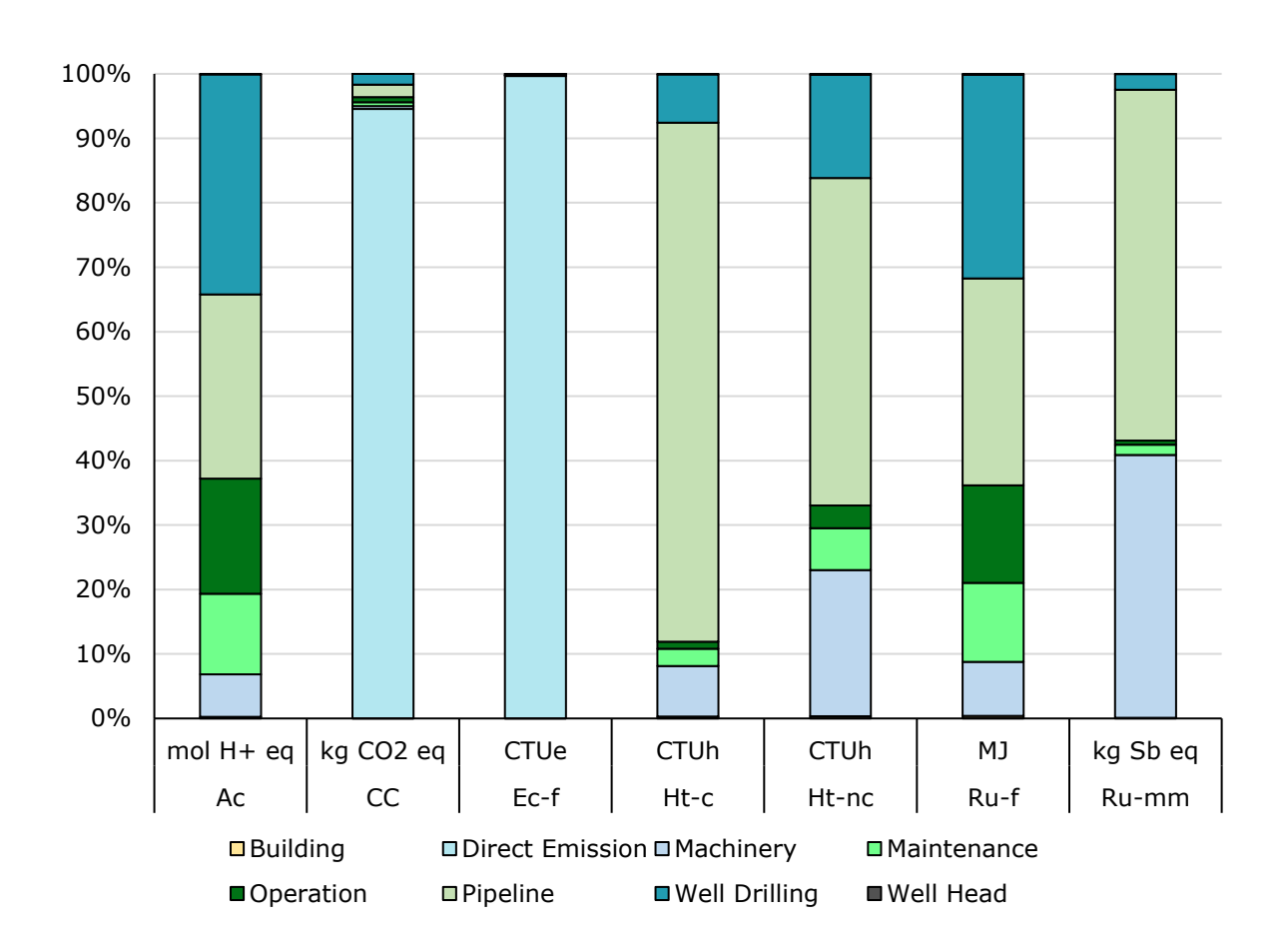


Figure 29: Contribution analysis of high priority indicators

Given the strong contribution of atmospheric emissions, a Monte Carlo simulation was performed considering a specific level of uncertainty for direct atmospheric emissions, with lognormal distribution. Four uncertainty scenarios were run with Sigma equal to 1.05, 1.25, 1.5 and 2 to understand what the effect on CC and Ecf categories might be in the case of uncertainty and variability in emissions. The median value of CC goes from 55.99 , 57.43 , 60.59 , 70.09 gCO2 eq and the minimum value goes from 46.59-68.04 (σ =1.05), 26.40-116.72(σ =1.25), 15.67-22.97(σ =1.50), 7.03-647.49 (σ =2.00) g CO2 eq and the median remaining for all 4 cases between 55.9 and 56.3 g CO2 eq. The median value of Ecf goes from 22.69, 23.19, 24.65, 28.71 CTUe and the minimum value goes from 18.67-27.83 (σ =1.05), 9.93-48.51 (σ =1.25), 5.46-96.88 (σ =1.50), 1.78-275.33 (σ =2.00) CTUe and the median remaining for all 4 cases between 22.66 and 22.85 CTUe. These results are showed in Figure 30 and Figure 31.



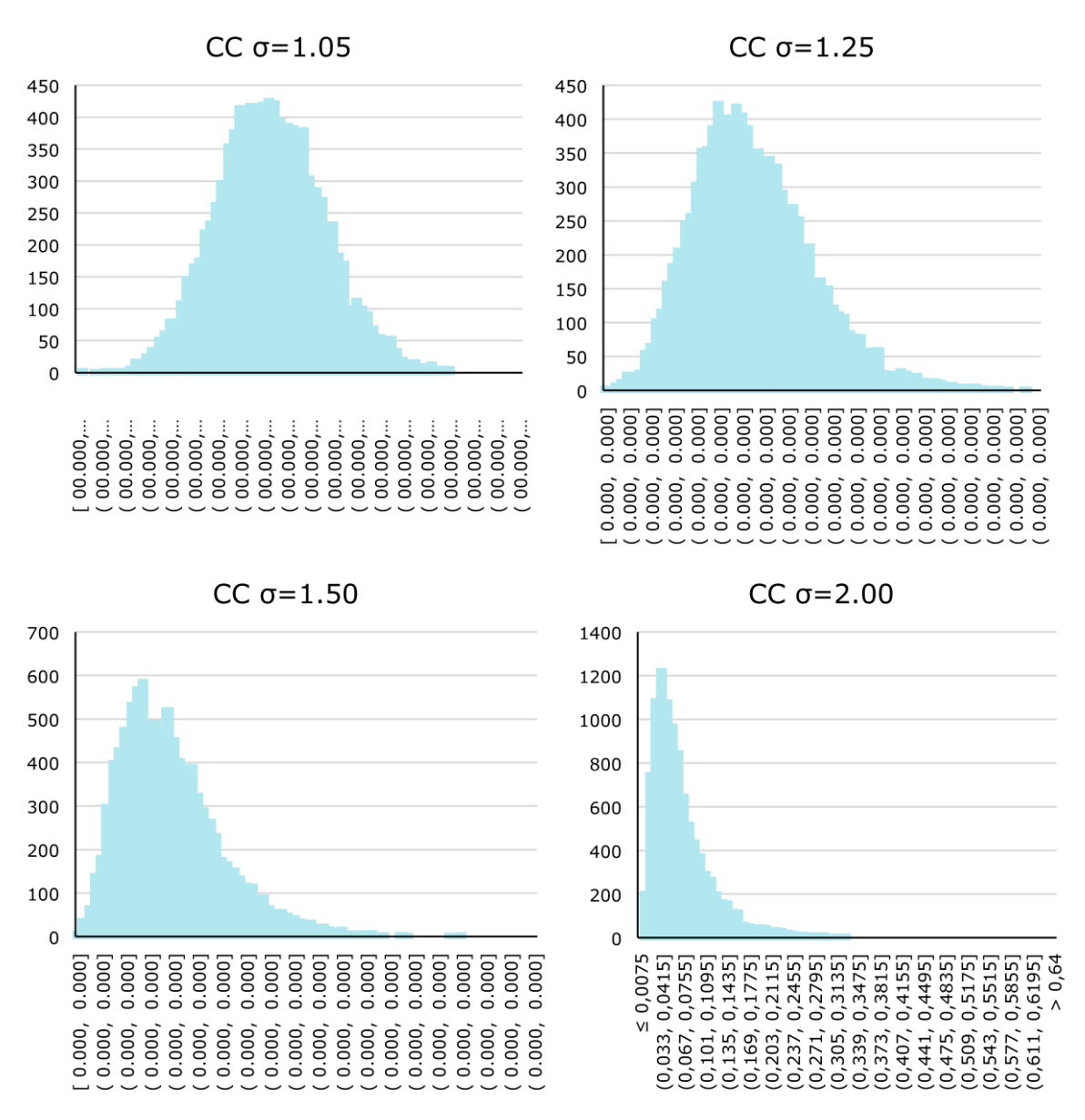


Figure 30: Monte Carlo analysis with different σ for Climate Change



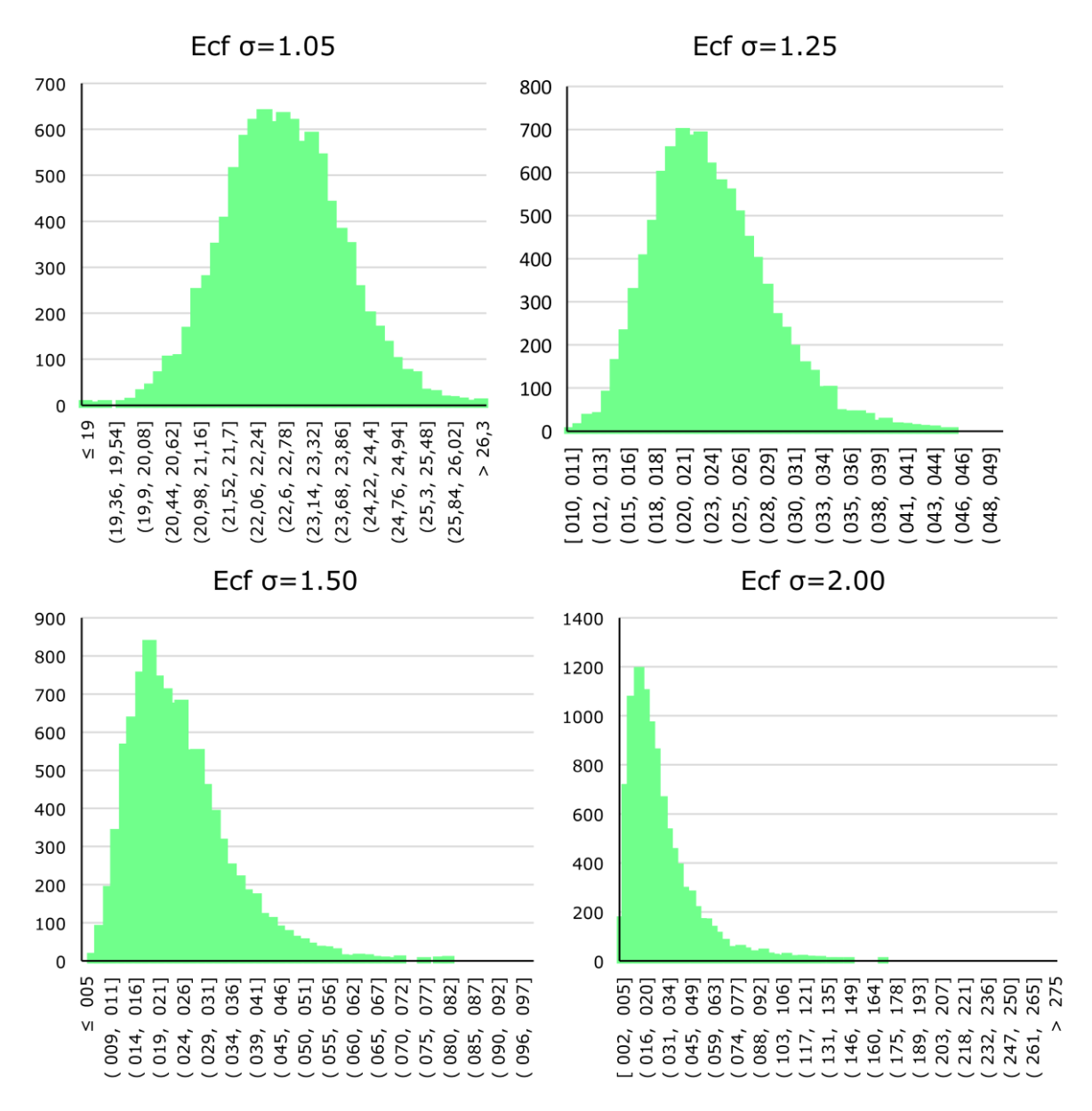


Figure 31: Monte Carlo analysis with different σ for Ecotoxicity freshwater

Finally, a single score comparison with other geothermal plants (Italian and Icelandic), other renewable energy systems (Photovoltaic and Wind) and the national energy mix of several countries (Kenya, Italy, Tanzania and South Africa) is made (Figure 32). In this case, the Ecoinvent 3.7.1 database does not have data on high-voltage electricity production, but only on medium voltage, so the realistic value is certainly higher, but it gives an idea of the order of magnitude of the impacts. As can be seen, the Olkaria plant has an environmental impact comparable to the Icelandic geothermal plant with low emissions into the atmosphere. Furthermore, it can be seen that the Olkaria plant is also more environmentally sustainable than a wind and photovoltaic plant. The environmental impact of national power grids must obviously have a greater contribution as all types of power production are considered, but in the case of Kenya, Olkaria's overall impact is less than half that of the medium-voltage kWh produced, and therefore very environmentally



beneficial. It is also much less impactful than the Italian, Tanzanian and much more the South Africa's national grids.

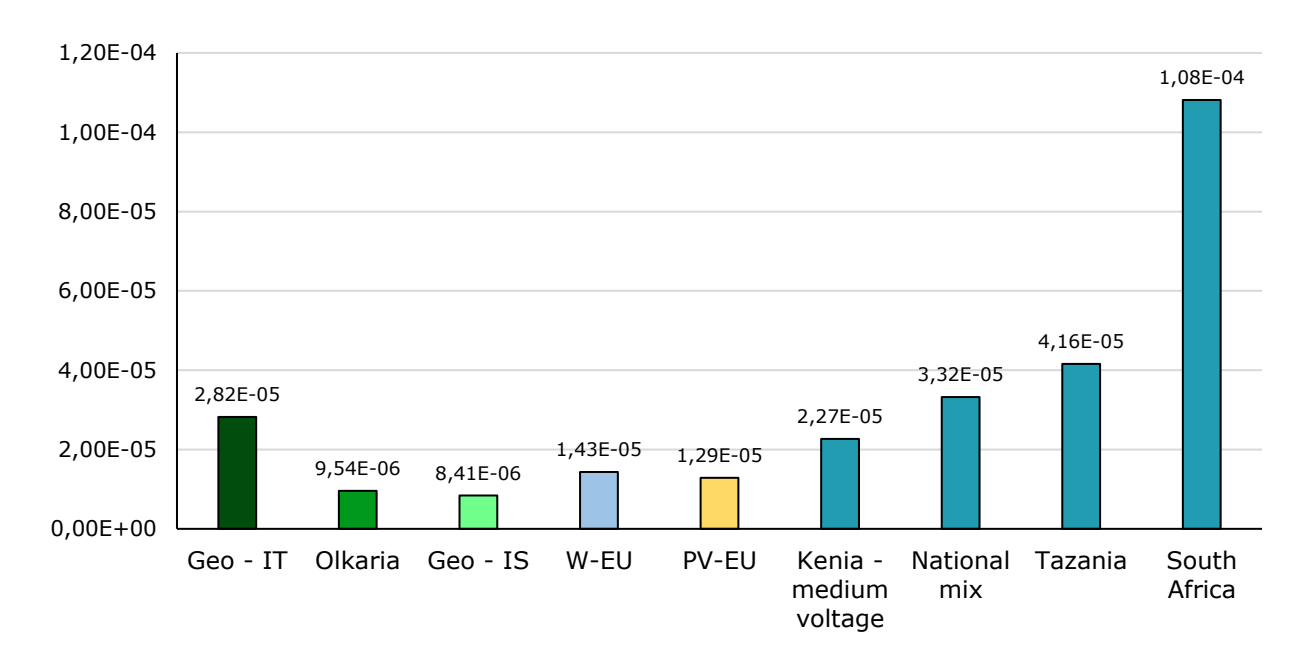


Figure 32: Comparison between: different geothermal, Photovoltaic, Wind power plant, and national electricity grid at single score level

4.2 Geothermal Power Plants in Kenya

An inventory of geothermal power plants used for electricity production or direct use utilization in Kenya was compiled, capturing essential data including the name, ownership, total installed capacity, year of commissioning, location, technology used, and a brief description of each facility: Olkaria I is closed for rehabilitation to increase capacity to 63 Mwe; Olkaria I (AU 4& 5) is funded by Japan's International Co-operation Agency (JICA); Olkaria I Unit 6 houses the largest single unit of turbine ever installed in a KenGen geothermal power plant; Olkaria II its reservoir is a two-phase liquid dominated one that is overlain by a thin steam-dominated zone 100-200m thick at 240°C; Olkaria III (OR power 4) is a subsidiary of Ormat Technologies or Power is the second largest power producer in Kenya and the largest IPP; Olkaria IV The geothermal plant is of single flash type; Olkaria V has 41 wells in total (33 production wells and 8 injection wells. Runs at a temperature of 270° C; Olkaria well heads a mix of directional and vertical wells. Well depths: 3000 m for appraisal and production wells and 2000 m for exploration wells; Menengai units (13) utilizes binary steam cycle technology; Eburru fields is an excellent example of the potential for applying wellhead geothermal power plants for economic advantage. It demonstrates that a small, single flash, condensing geothermal power plant can be a viable alternative to other technologies, such as binary, for medium to high enthalpy geothermal resources in a small-scale application; Oserian Development Company Ltd (ODLC) constructed a 2.0 MWe binary plant and a smaller 1.4 MWe back pressure turbine in Olkaria Central to utilize fluid from wells OW-306 and OW-202 respectively leased from KenGen. The plants provide electrical power for the farm's operations and were commissioned in 2004 and 2007, respectively. ODLC who grow cut flowers for export is also utilizing steam to heat fresh water through heat exchangers, enrich CO2 levels and to fumigate the soils utilizing H₂S. The heated fresh water is then



circulated through greenhouses. The use of geothermal energy for heating the greenhouses has resulted in drastic reduction in operating costs.

Table 19: Kenyan geothermal power plants

Name of facility	Ownership	Total Installed Capacity (MW)	Year of Commissio ning	Location	Technology
Olkaria I	KenGen	45	1981-1985	Naivasha	Flash
Olkaria I (AU 4& 5)	KenGen	150	2014	Naivasha	Flash
Olkaria I Unit 6	KenGen	86.88	Jun-22	Nakuru	Flash
Olkaria II	KenGen	105	2003-2010	Naivasha	Flash
Olkaria III (OR power 4)	OR Power 4 Inc.	150	2000-2016	Nakuru	Flash
Olkaria IV	KenGen	150	September 2014.	Naivasha	Flash
Olkaria V	KenGen	172	Aug-19	Nakuru	Flash
Olkaria well heads	KenGen	88.5	2010-2016	Naivasha	Flash
Menengai units (13)	IPPs	35	Aug-23	Nakuru	ORC
Eburru fields	KenGen	2.4	2011	Gilgil	Flash
Oserian	Oserian Development Company	3.6	2003	Nakuru	Flash (Backpressur e) and Binary-ORC

4.3 Knowledge transfer and application cases with Strathmore University

Strathmore University collaborates with the University of Florence in Engineering Sciences and Capacity building initiatives. The objectives include assessing electricity and heat utilization in African energy development, developing thermodynamic models, creating metamodels for thermodynamic variables, conducting Life Cycle Inventory data collection for geothermal facilities, and participating in capacity building events. To achieve these goals, Strathmore University has hired a geologist and mechanical engineer with expertise in various fields including research, energy auditing, geothermal resource development, and sustainability studies. The collaboration allowed for an exchange of knowledge on energy systems topics, and in the application of certain analyses for educational/scientific purposes, one of which is given below.



The analysis focused on the heat pump whose flow diagram is shown in Figure 33. The main applications analyzed were milk pasteurization, fruit drying, vegetable drying and grain drying.

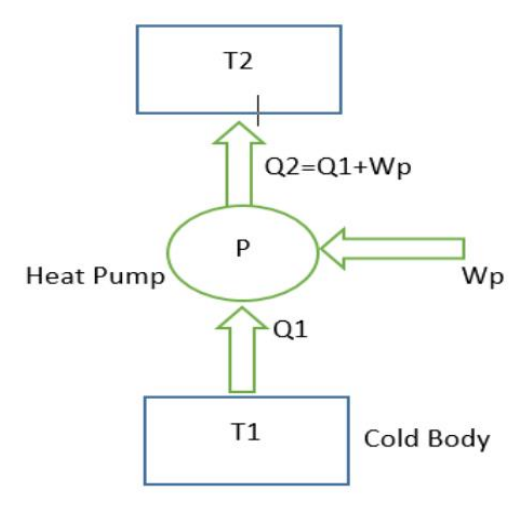


Figure 33: Direct use flow diagram

TABL	E I: EXTENT OF THE	ERMAL GROUND IN SE	CTORS OF OLKARIA AN	ID EBURKU
Sector	Area (km^2) with T $(1.0) > 30$ °C	Area (km 2) with T (1.0) > 50 "C	Area (km ²) with $T (1.0) > 70 ^{\circ}C$	Area (km²) IR - Anomalies
W Olkaria	5.45	0.69	0.10?	0.17
C.+NOlkaria	3.7	0.58	0.18	0.35
SOlkaria	3.45	0.48	0.13 1)	0.25
EDomes	2.0	0.30	0.07 1)	
NEburru	3.2	0.32	0.11	0.32
CEburru	1.35	0.11	0.03	0.13
SEburru	1.55	0.15	0.05	0.20

Figure 34: Extent of Thermal Ground in Sectors of Olkaria and Eburru (Hochstein & Kagiri, 1997)

The temperatures used in this analysis were based on literature on the Olkaria and Eburru sites showing the temperature variations at a depth of 1m. Tea drying temperatures range between $60^{\circ}\text{C}-100^{\circ}\text{C}$ (Kinyanjui, 2013). Heat treatment is a traditional method to ensure the quality and safety of milk, mainly including ultra-high temperature (UHT) instant inactivation (135–150 °C, 2–10 s) and pasteurization (72°C, 15 s, or 63°C, 30 min) (Yu et al. 2022). The temperature of the working fluid was set at a lower temperature of the geothermal heat source and higher than the temperature required for heating for effective heat transfer. The working fluid temperature range for heating and drying used in the analysis were between 20°C-151.3 °C at a pressure range of 1.079 bar and 28 bar for applications that require temperatures between 30°C and 150°C. Below were the results obtained:



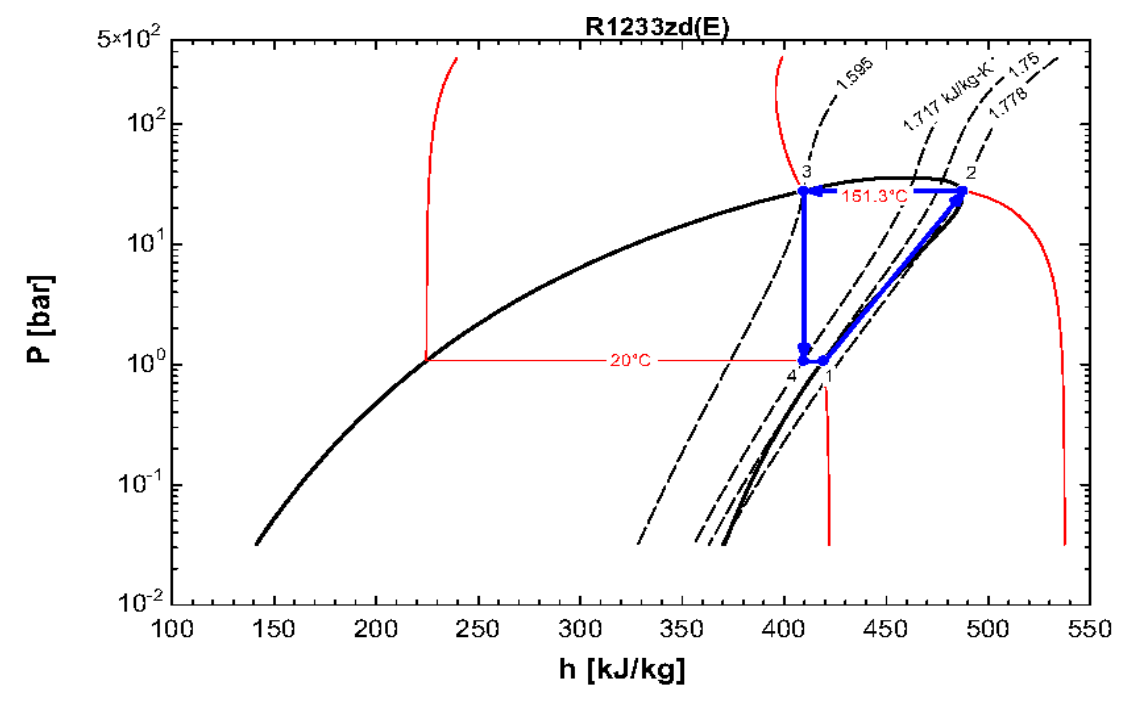


Figure 35: P-h diagram for milk pasteurization analysis on EES

	$COP_{hp,i}$	$\mathbf{T}_{\mathbf{cold},i}$	$\mathbf{T}_{hot,i}$	$\mathbf{Q}_{\mathrm{H,i}}$	$\mathbf{Q}_{L,i}$	$\mathbf{W}_{\mathbf{Comp},i}$
		[C]	[C]	[kj]	[kj]	[W]
1	3.526	30	150	5.672	-7.917	2.245
2	3.636	30	145	5.672	-7 .823	2.152
3	3.756	30	140	5.672	-7.73	2.058
4	3.887	30	135	5.672	-7.636	1.964

Figure 36: Analysis for different temperatures for UHT pasteurization process

The average COP obtained was 3.7 with heat drawn from the cold body at the evaporator as 5.672 kJ. The average heat dissipated to the space to be heated, in this case the milk, from the condenser was found to be 7.7765 kJ.



5. Conclusions

The report focuses on the implementation and analysis of the results obtained through the work conducted within the LEAP-RE project, with particular reference to Work Package 9 (WP9) Geothermal Atlas for Africa (GAA) and specifically Task 9.2 related to scientific technologies concerning geothermal resources. This work closely ties in with the activities carried out in Task 9.1, which addressed geological-geophysical issues and resource mapping. The objective is to create a tool that evaluates optimal engineering applications for sustainable resource exploitation, considering energy, economic, and environmental aspects. Several energy systems were analyzed concerning classic technologies outlined in the literature for geothermal resource exploitation, aiming at creating a geothermal tool enabling rapid evaluation using minimal input data.

The methodology used for assessing system performance in geothermal energy systems involves selecting key parameters like temperature, mass flow rate, and ambient air temperature. These parameters categorize geothermal resources based on temperature ranges, aiding in the selection of appropriate energy systems. Subsequently, various energy system models are formulated and validated, with output matrices used to develop meta-models. These meta-models, constructed using linear multidimensional interpolation, enable cost-effective evaluations of system performance. To enhance the accuracy, additional parameters like system lifespan and well depth are incorporated, ensuring thorough assessments for each application type.

Furthermore, economic modeling comprises two main stages. Firstly, individual plant component costs are analyzed using established thermo-economic correlations, derived from thermodynamic analysis. This provides essential values for components such as condensers, evaporators, compressors, and separators. The number of wells is then evaluated based on empirical correlations relative to power plant size. Secondly, initial investment and operation and maintenance (O&M) costs are assessed to determine the Levelized Cost of Energy (LCOEn).

In terms of environmental modeling, the approach adheres to the Life Cycle Assessment (LCA) methodology outlined by ISO 14040 and ISO 14044 standards. This model aims to evaluate the environmental impact of geothermal energy systems across their construction, operation, and maintenance phases. Particular attention is given to Climate Change as the assessed environmental impact, using the Environmental Footprint 3.1 methodology, expressed in kg CO2 eq/kWh. The focus lies on the Life Cycle Inventory (LCI) phase, aiming at developing a parametric LCI (pLCI) to characterize and evaluate systems with variable sizes. This involves correlating material and energy consumption with specific process sizes, such as geothermal wells, pipelines, mechanical components, and operational and maintenance parameters.



The validation of the thermodynamic metamodel involves analyzing various geothermal plants, with turbine size as a reference parameter. Plant selection includes Single Flash, Double Flash, Triple Flash, Dry Steam, and Binary Organic Rankine Cycle types, chosen based on data availability. The analysis indicates that the tool significantly overestimates the installed capacity, a deviation of 6-7% is observed, which, though tolerable in some scenarios, highlights the need for further enhancement. For scenarios involving multiple flashes, a more intricate procedure is required. Minimizing prediction errors demands the meticulous integration and optimization of different thermodynamic blocks. This highlights the complexity of the task and emphasizes the importance of a thorough approach to parameter adjustment and data analysis. The validation of metamodels for lowand medium-enthalpy geothermal resources faces challenges due to limited benchmarking data. Validation efforts for thermodynamic and economic metamodels focus mainly on absorption cycles, with few reference cases available. High Temperature High Pressure (HTHP) systems lack literature values, further complicating the validation. Similarly, validating Life Cycle Assessment (LCA) analyses encounters hurdles due to these limitations. To address this, a comparative analysis with known cases is proposed, focusing on geothermal wells at variable depths. The thermodynamic validation uses the installed cooling capacity of absorption systems as a benchmark, showing a tendency to overestimate. While the predictions are accurate for some cases, discrepancies arise due to differences in flow rate assumptions. Enhancing adaptability and precision across diverse scenarios remains a goal for improving metamodel utility and reliability.

The validation of the thermoeconomic metamodel is conducted meticulously, albeit with constraints imposed by the scarcity of available data on the coupling of thermodynamic and economic factors, notably the Levelized Cost of Energy (LCOE). Although insights from selected known cases provide some understanding, the analysis reveals a lack of definitive trends in cost prediction, highlighting the intricate nature of accurately forecasting LCOE for geothermal plants. Notably, some plants tend to overestimate LCOE, while others are subjected to underestimation, resulting in significant relative errors. The maximum observed error in estimation stands at approximately 2.5 c€/kWh or approximately 1 c€/kWh for some cases, yielding an estimated error margin of around ± 2.5 c€/kWh for unknown cases. This margin underscores the inherent uncertainty in LCOE prediction using the current thermoeconomic metamodel. In terms of economic validation for medium- and low-enthalpy application, the analysis is based on only two cases of Levelized Cost of Cooling (LCOC). Despite the limited dataset, the tool tends to marginally overestimate the real case, with an error margin of just 7.2% for both instances. Although this validation is constrained by data availability, the maximum absolute difference observed is approximately 0.15 c\$/kWh, indicating a remarkably low margin of error and confirming the reliability of the tool's predictions. Continuous validation efforts will be paramount as more



data become available, enabling further refinement and improvement in the accuracy of economic predictions.

The challenge of comparing results from Life Cycle Assessment (LCA) methodologies stems from their inherent variability due to diverse databases and methodologies, which complicates direct comparisons. Moreover, the limited availability of benchmarking data further complicates validation efforts. Instead of direct comparisons, our approach involves initial analysis at the inventory level and subsequent examination at the Life Cycle Impact Assessment (LCIA) level using a tailored model. This approach allows for focused validation of specific processes, such as well drilling, leading to intriguing insights, particularly concerning diesel consumption. A novel correlation developed in our study yields more accurate predictions compared to existing ones, as evidenced by statistical parameters. This enhanced accuracy is essential for ensuring the reliability of the metamodel in predicting environmental impacts associated with geothermal well processes. Similar analyses extend to other materials like steel and cement, enriching the validation process and laying the groundwork for comprehensive assessments of geothermal energy systems. At the LCIA level, our analysis focuses on high-priority categories, with Climate Change emerging as the selected indicator. Through comparative analysis, nuanced trends in impact estimation across different correlations are revealed, underscoring the importance of robust statistical analysis in quantifying accuracy. This meticulous approach is crucial for advancing our understanding and improving the reliability of environmental impact predictions in geothermal energy systems.

The obtained metamodels, considering potential prediction errors, effectively forecast the size, cost, and environmental impact of energy systems for geothermal resource exploitation. This outcome yields a tool facilitating the assessment of different systems' feasibility, thus revealing both favorable and unfavorable conditions for sustainable development. Furthermore, during the final project mapping phase, a geographical-level evaluation is conducted to pinpoint areas with production potential, economic viability, and environmental feasibility.

The analyzed case study on low and medium enthalpy resources in Malawi and the Ethiopian area of Aluto Langano showcases the ease with which significant results in producible energy, economic feasibility, and environmental impact were obtained through the analysis.

Additionally, collaboration with the Strathmore University-KenGen team enabled the first Life Cycle Assessment (LCA) of a geothermal plant in Africa and data collection on several geothermal plants in Kenya. This knowledge exchange facilitated a synthetic analysis of various applications for direct use.



Appendix A

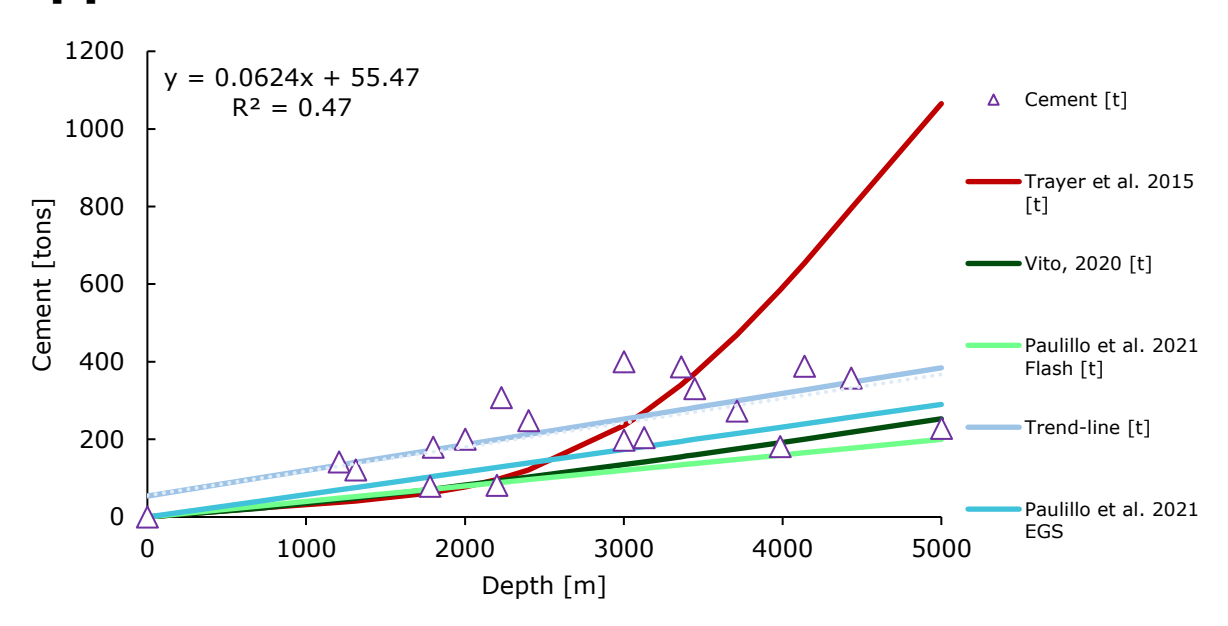


Figure A1: Comparison between Trend line, correlation proposed in the literature and primary data (Cement consumption)

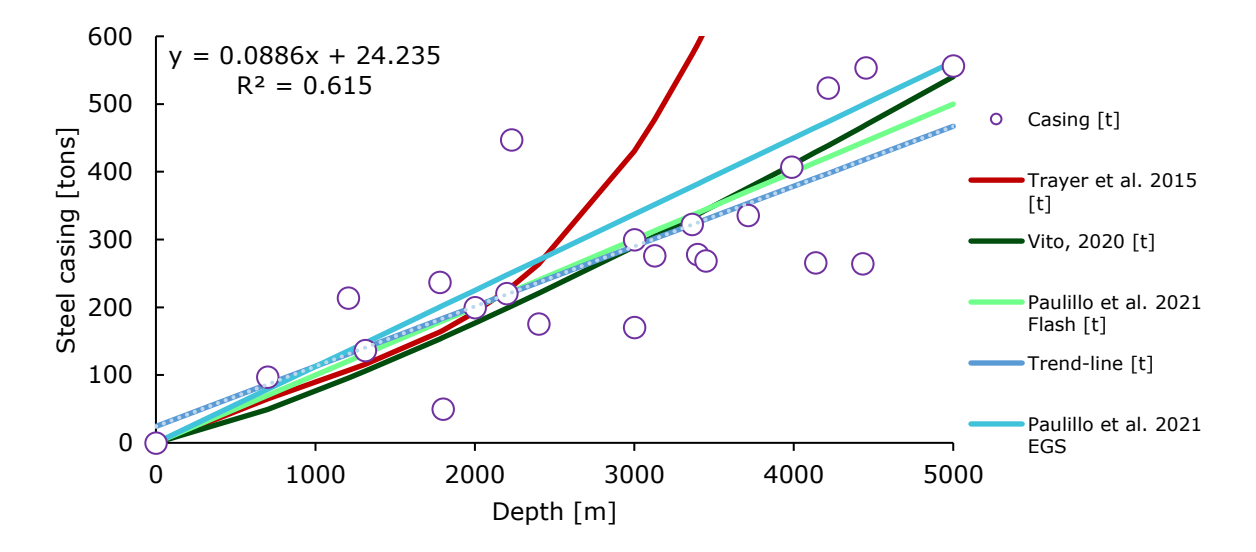


Figure A2: Comparison between Trend line, correlation proposed in the literature and primary data (Steel casing consumption)



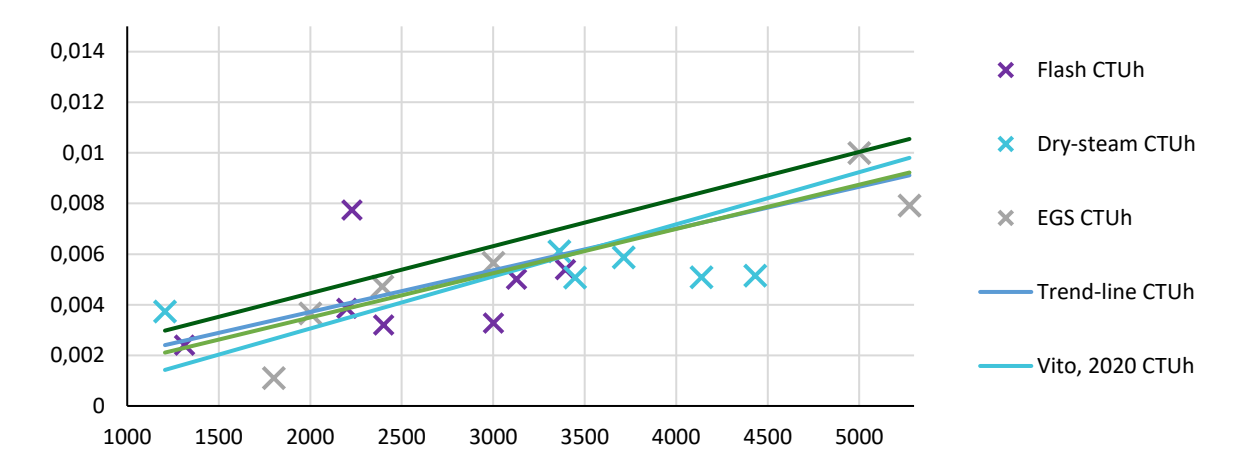


Figure A3: comparison with literature, primary data and trend-line of Human Toxicity, cancer indicators

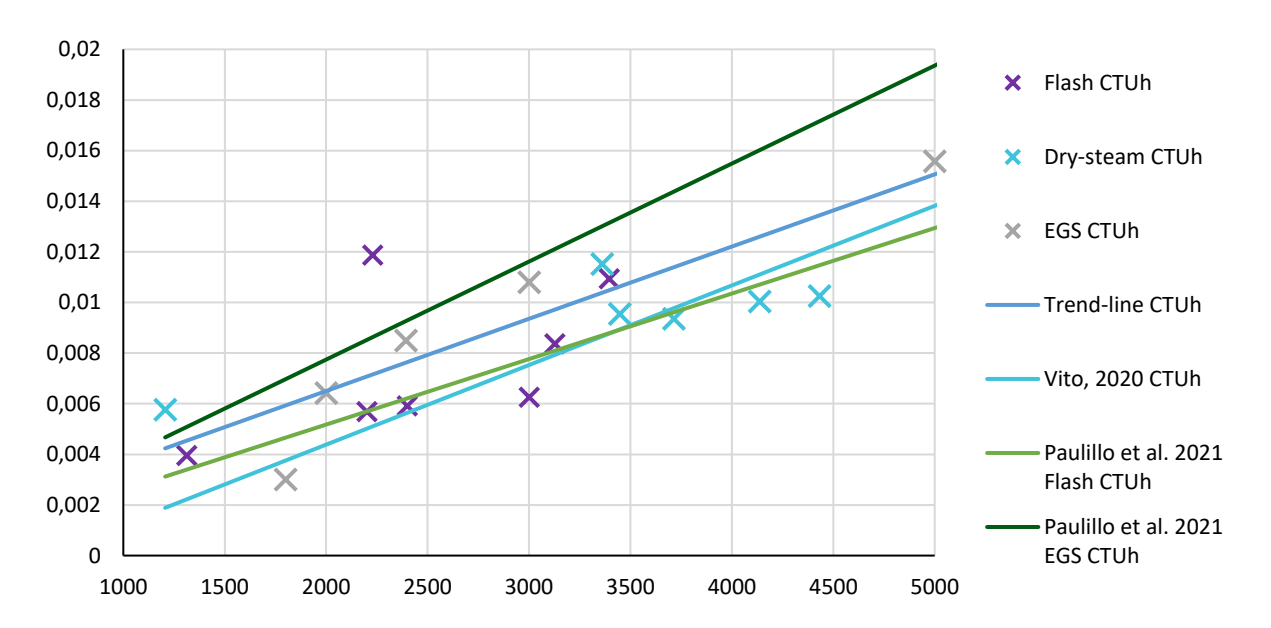


Figure A4: comparison with literature, primary data and trend-line of Human Toxicity, non-cancer indicators



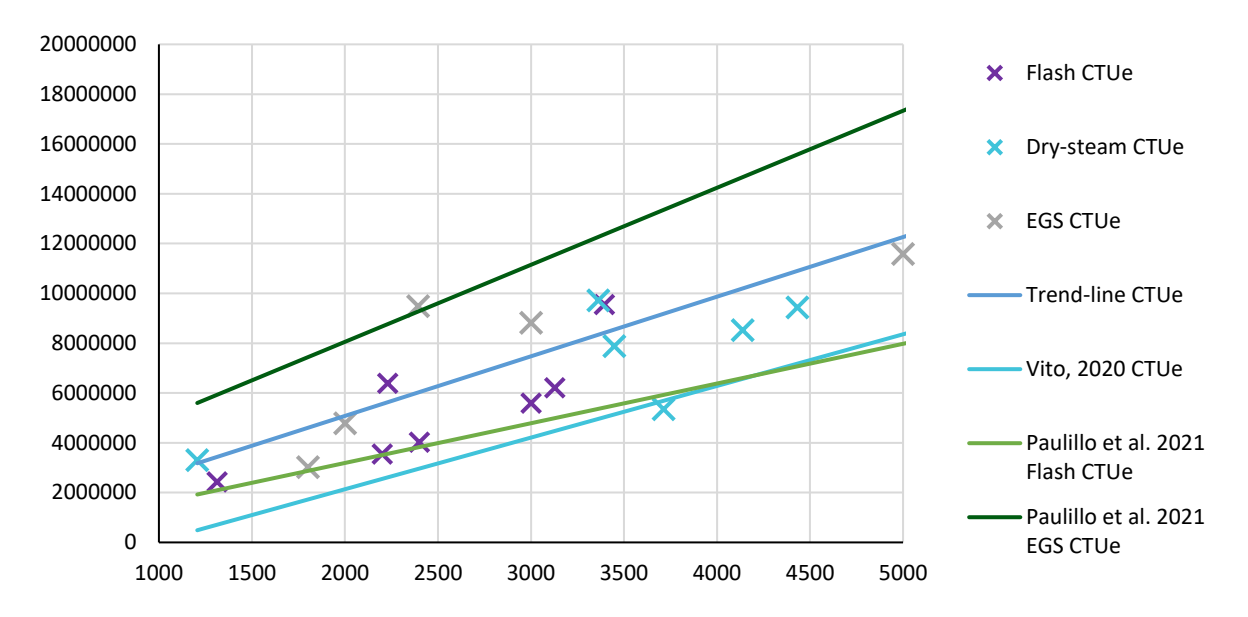


Figure A5: comparison with literature, primary data and trend-line of Ecotoxicity, freshwater indicators

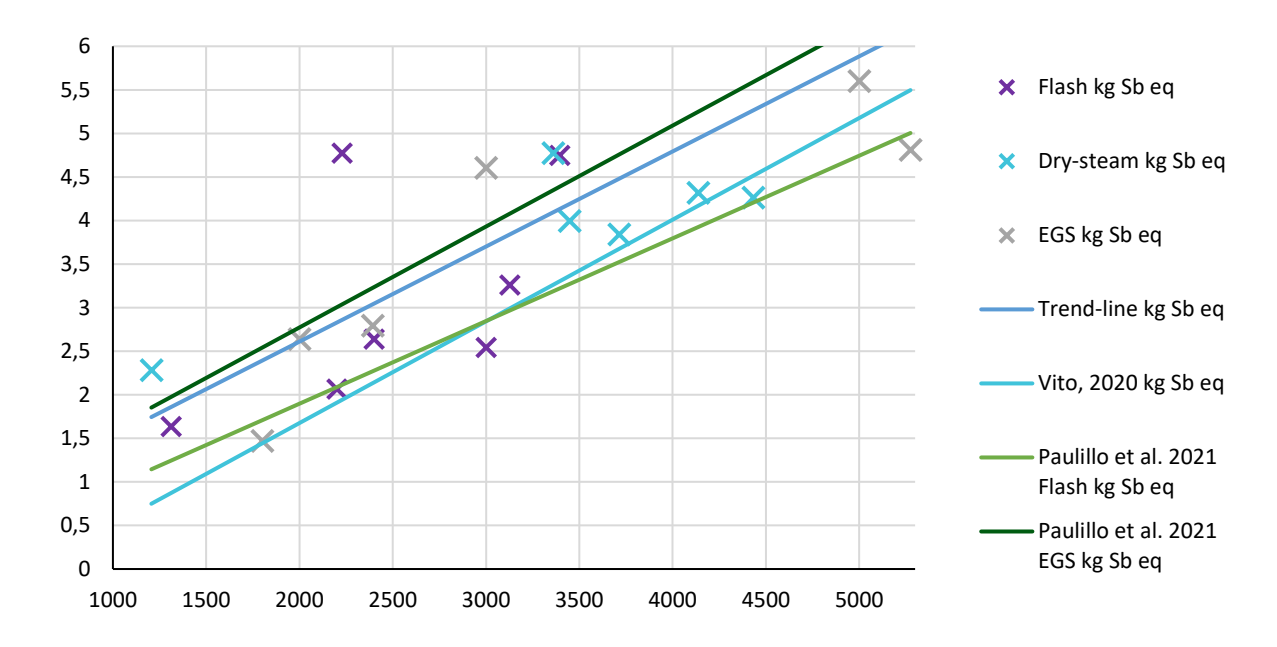


Figure A6: comparison with literature, primary data and trend-line of Material resource - mineral and metals indicators



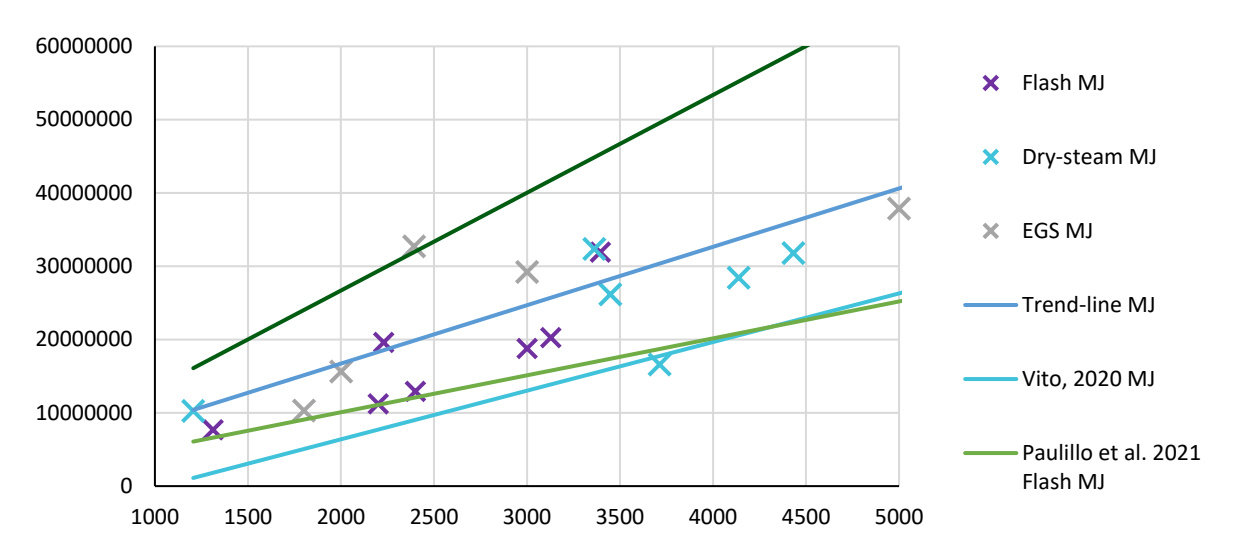


Figure A7: comparison with literature, primary data and trend-line of Energies resource - non-renewable indicators

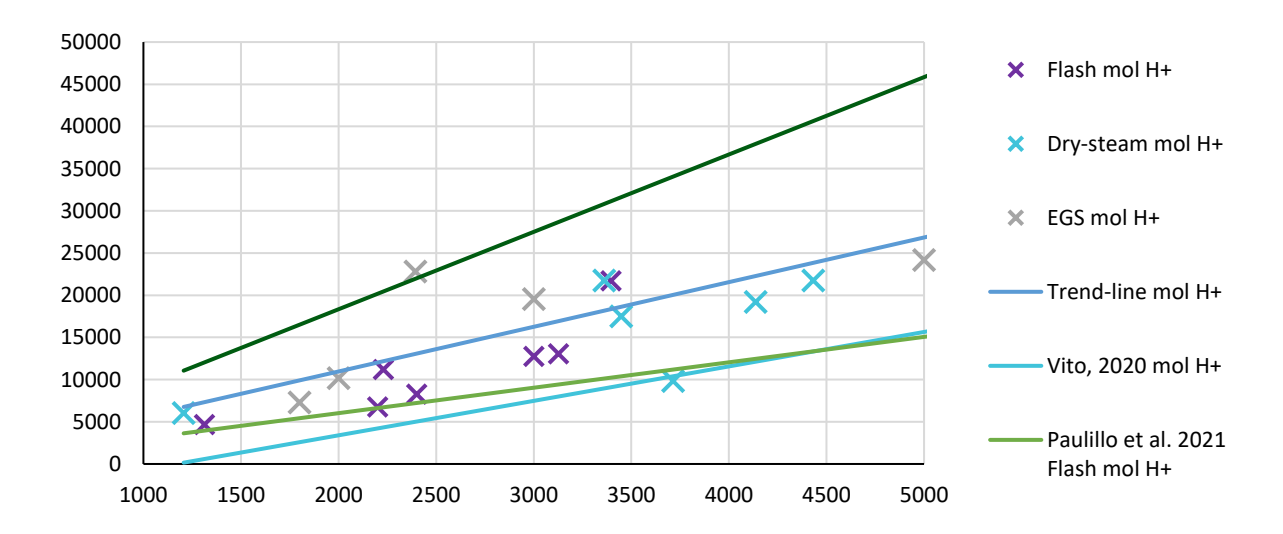


Figure A8: comparison with literature, primary data and trend-line of Acidification indicators



Appendix B

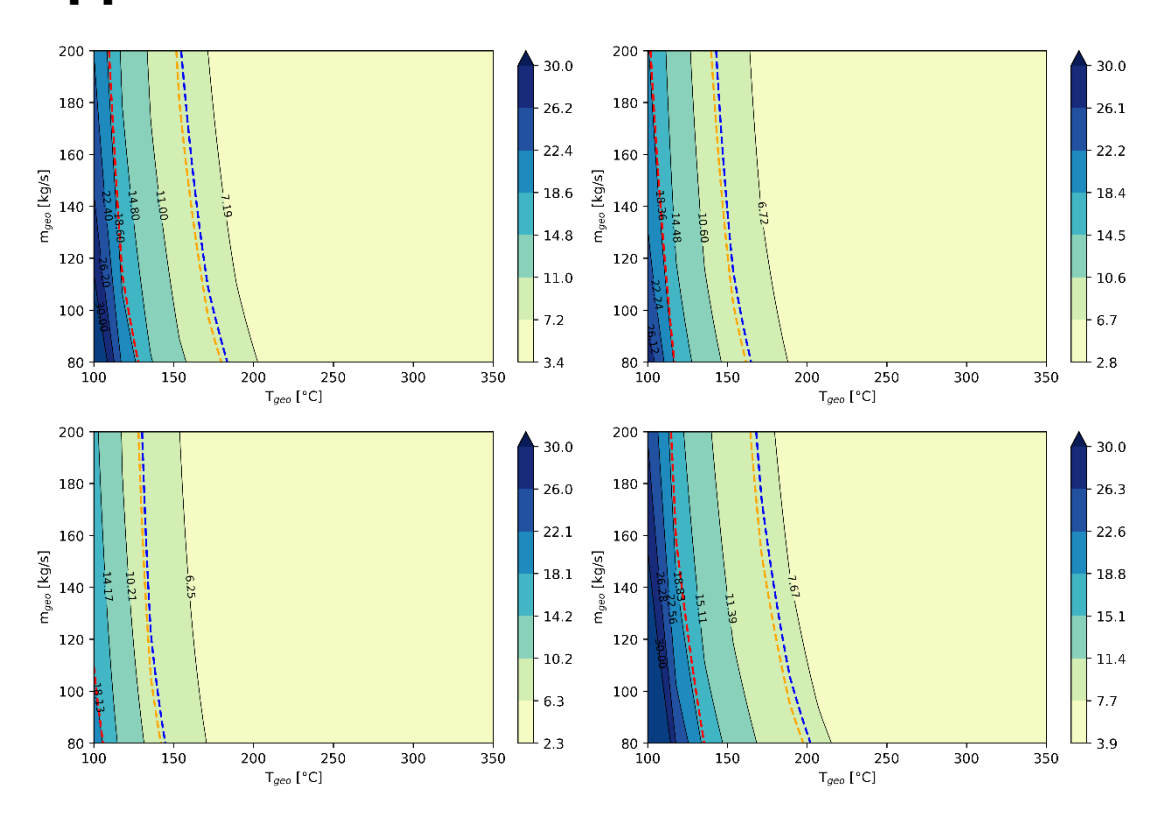


Figure B1: Levelized Cost Of Electricity metamodel results for different well depth (wd). A: wd =1000m; B: wd = 2000m; C: wd = 3000m; D: wd= 4000m (Power Plant)



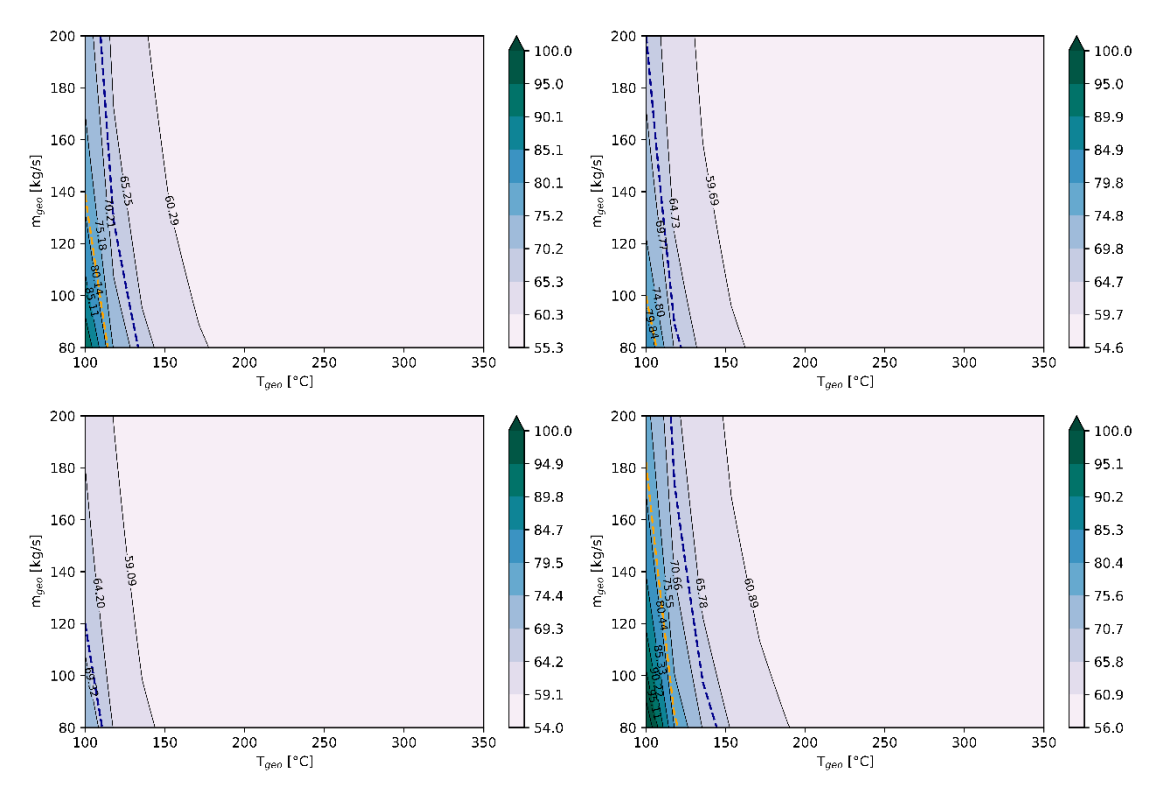


Figure B2: Climate Change metamodel metamodel results for different well depth (wd). A: wd = 1000m; B: wd = 2000m; C: wd = 3000m; D: wd= 4000m (Power Plant)



Appendix C

Steam flashing: The flashing process may occur in several places:

- in the reservoir as the fluid flows through the permeable formation with an accompanying pressure drop.
- in the production well anywhere from the entry point to the wellhead because of the loss of pressure due to friction and the gravity head; or
- in the inlet to the cyclone separator because of a throttling process induced by a control valve or an orifice plate.

Then data from actual production wells in the geothermal fields in Kenya used to model the energy output. The data from these fields gives the well head pressure, mass flow rate and enthalpy. The calculations based on this data are manually done using the established thermodynamic models and compared to the known output of the sampled wells. This serves to validate the thermodynamic models. The validated thermodynamic models are then coded in python. The coded model is run using the data collected from the field and results compared to values obtained from the manual calculations. The pyXsteam library in Python has been leveraged to extract data from the steam tables in Figure B2. This process has been completed for the single flash power geothermal plant. For the single flash geothermal power production plants, the thermodynamic models through the separator, turbine, and condenser were then translated into Python code. This coding process was automated to handle input data from an Excel file containing information on any geothermal production wells. The results obtained are given in Figure B2 below.

	Date	Whp(bar)	Enthalpy(a)Kj/Kg	steam(a)T/hr	brine(a)T/hr	Total flow(a)T/hr	Remark	X2	h3	h4	m4	wt
0	14/07/2009	5.40	1305.0	43.9	84.5	128.4	Discharge data	0.519527	2751.521781	1731.049879	240.145988	245062.233525
1	NaN	17.50	1420.0	36.1	94.6	130.7	commissioning data	0.381607	2795.281330	1086.724193	179.553615	306777.610897
2	05/04/2018	13.20	1735.4	40.6	47.6	88.2	NaN	0.852941	2786.997765	1283.475288	270.825882	407192.801676
3	03/05/2019	13.10	1345.1	40.7	114.1	154.8	NaN	0.356705	2786.747159	1288.314128	198.784365	297865.057956
4	28/10/2019	13.40	1308.2	43.1	134.9	178.0	NaN	0.319496	2787.489588	1273.840218	204.732987	309893.957429
5	16/04/2020	13.40	1145.6	25.9	130.0	155.9	NaN	0.199231	2787.489588	1273.840218	111.816277	169250.637140
6	12/12/2020	13.20	1422.5	42.2	93.6	135.8	NaN	0.450855	2786.997765	1283.475288	220.413846	331397.172101
7	26/05/2021	13.00	1418.6	35.9	80.6	116.5	NaN	0.445409	2786.493361	1293.167439	186.804715	278960.322825
8	20/11/2021	13.03	1744.0	36.4	41.0	77.4	NaN	0.887805	2786.569838	1291.709914	247.377951	369795.385480
9	29/09/2022	13.30	1493.7	36.7	71.8	108.5	NaN	0.511142	2787.245227	1278.650717	199.652089	301194.045592

Figure B2: Results for calculation in Python.



References

- Agoundedemba, M., Kim, C. K., & Kim, H. G. (2023). Energy Status in Africa: Challenges, Progress and Sustainable Pathways. Energies, 16(23), 7708. https://doi.org/10.3390/en16237708
- Alfalaval, 2023. Website: https://www.alfalaval.com/
- Allahvirdizadeh, P. (2020). A review on geothermal wells: Well integrity issues.
 Journal of Cleaner Production, 275, 124009.
 https://doi.org/10.1016/j.jclepro.2020.124009
- Anderson, A., & Rezaie, B. (2019). Geothermal technology: Trends and potential role in a sustainable future. Applied Energy, 248, 18-34. https://doi.org/10.1016/j.apenergy.2019.04.102
- Applied Drilling Engineering. s.l.: Society of Petroleum Engineers (SPE), 1986. pp. 300-350. 1555630014.
- Barbier, E. (2002). Geothermal energy technology and current status: an overview.
 Renewable and sustainable energy reviews, 6(1-2), 3-65.
 https://doi.org/10.1016/S1364-0321(02)00002-3
- Basosi, R., Bonciani, R., Frosali, D., Manfrida, G., Parisi, M. L., & Sansone, F. (2020). Life cycle analysis of a geothermal power plant: Comparison of the environmental performance with other renewable energy systems. Sustainability, 12(7), 2786. https://doi.org/10.3390/su12072786
- Beckers, K. F., Kolker, A., Pauling, H., McTigue, J. D., & Kesseli, D. (2021). Evaluating the feasibility of geothermal deep direct-use in the United States. Energy conversion and management, 243, 114335. https://doi.org/10.1016/j.enconman.2021.114335
- Bertani, R. (2016). Geothermal power generation in the world 2010–2014 update report.
 Geothermics, 60, 31-43. https://doi.org/10.1016/j.geothermics.2015.11.003
- Chan, J. Z., Allebach, J. P., & Bouman, C. A. (1997). Sequential linear interpolation of multidimensional functions. IEEE Transactions on Image Processing, 6(9), 1231-1245. DOI: 10.1109/83.623187



- Chen, J., & Jiang, F. (2015). Designing multi-well layout for enhanced geothermal system to better exploit hot dry rock geothermal energy. Renewable Energy, 74, 37-48. https://doi.org/10.1016/j.renene.2014.07.056
- Chitgar, N., Hemmati, A., & Sadrzadeh, M. (2023). A comparative performance analysis, working fluid selection, and machine learning optimization of ORC systems driven by geothermal energy. Energy Conversion and Management, 286, 117072. https://doi.org/10.1016/j.enconman.2023.117072
- Christensen, J. L., & Hain, D. S. (2017). Knowing where to go: The knowledge foundation for investments in renewable energy. Energy Research & Social Science, 25, 124-133. https://doi.org/10.1016/j.erss.2016.12.025
- Cory, K., & Schwabe, P. (2009). Wind levelized cost of energy: A comparison of technical and financing input variables (No. NREL/TP-6A2-46671). National Renewable Energy Lab.(NREL), Golden, CO (United States). https://doi.org/10.2172/966296
- de Simón-Martín, M., Bracco, S., Piazza, G., Pagnini, L. C., González-Martínez, A.,
 & Delfino, F. (2022). Levelized Cost of Energy in Sustainable Energy Communities:
 A Systematic Approach for Multi-Vector Energy Systems. Springer Nature.
 https://doi.org/10.1007/978-3-030-95932-6
- DiPippo, R., 2008. Geothermal power plants. Elsevier.
 https://doi.org/10.1016/B978-0-7506-8620-4.X5001-1
- DiPippo, R. (2012). Geothermal power plants: principles, applications, case studies and environmental impact. Butterworth-Heinemann.
- Eslami-Nejad, P., Ouzzane, M., & Aidoun, Z. (2014). Modeling of a two-phase CO2-filled vertical borehole for geothermal heat pump applications. Applied Energy, 114, 611-620. https://doi.org/10.1016/j.apenergy.2013.10.028
- Evans, J. A., Foster, A. M., Huet, J. M., Reinholdt, L., Fikiin, K., Zilio, C., Houska, M., Landfeld, A., Bond, C., Scheurs, M., Van Sambeeck, T. W. M. (2014). Specific energy consumption values for various refrigerated food cold stores. Energy and Buildings, 74, 141-151. https://doi.org/10.1016/j.enbuild.2013.11.075
- Fiaschi, D., Manfrida, G., Mendecka, B., Tosti, L., & Parisi, M. L. (2021). A comparison of different approaches for assessing energy outputs of combined heat



- and power geothermal plants. Sustainability, 13(8), 4527. https://doi.org/10.3390/su13084527
- FRUNZE. 2023. FRUNZE JSC "SMNPO-Engineering". Website: https://frunze.com.ua/en/
- GECO project website https://geco-h2020.eu/. [Accessed 14 February 2023].
- GEOENVI project website https://www.geoenvi.eu/. [Accessed 14 February 2023].
- Gestra, 2023. web site: https://www.gestra.com/global/it-IT/products/systemand-packaged-solutions/steam-driers
- Gupta, H., & Roy, S. (2007). Worldwide status of geothermal resource utilization.
 Geotherm Energy, 199-229. DOI:10.1016/B978-044452875-9/50008-3
- Hackstein, F. V., & Madlener, R. (2021). Sustainable operation of geothermal power plants: why economics matters. Geothermal Energy, 9, 1-30. https://doi.org/10.1186/s40517-021-00183-2
- Hirschberg, S., Wiemer, S., & Burgherr, P. (Eds.). (2014). Energy from the Earth:
 Deep Geothermal as a Resource for the Future? (Vol. 62). vdf Hochschulverlag AG.
- Hochstein, M. P., & Kagiri, D. (1997). The role of 'steaming ground'over high temperature systems in the Kenya Rift. In Proceedings (pp. 29-35).
- IEA, International Energy Agency. 2023. Website: https://www.iea.org/reports/projected-costs-of-generating-electricity-2020
- International Organization for Standardization (ISO), "ISO 14040:2021— Environmental management — Life cycle assessment — Principles and framework.
 Environ. Manage.," Geneva, Switzerland, 2021a.
- International Organization for Standardization (ISO), "ISO 14044:2021 Environmental management - Life cycle assessment - Requirements and guidelines. Environ. Manage.," Geneva, Switzerland, 2021b.
- IRENA (2017), Geothermal Power: Technology Brief, International Renewable Energy Agency, Abu Dhabi.
- Johansson, T. B., Kelly, H., Reddy, A. K., & Williams, R. H. (1993). Renewable energy: sources for fuels and electricity.



- Karimi, S., & Mansouri, S. (2018). A comparative profitability study of geothermal electricity production in developed and developing countries: Exergoeconomic analysis and optimization of different ORC configurations. Renewable Energy, 115, 600-619. https://doi.org/10.1016/j.renene.2017.08.098
- Karlsdóttir, M. R., Pálsson, Ó. P., Pálsson, H., & Maya-Drysdale, L. (2015). Life cycle inventory of a flash geothermal combined heat and power plant located in Iceland. The International Journal of Life Cycle Assessment, 20, 503-519. https://doi.org/10.1007/s11367-014-0842-y
- Karlsdottir, M. R., Heinonen, J., Palsson, H., & Palsson, O. P. (2020). Life cycle assessment of a geothermal combined heat and power plant based on high temperature utilization. Geothermics, 84, 101727. https://doi.org/10.1016/j.geothermics.2019.101727
- Kinyanjui, S. (2013). Direct use of geothermal energy in Menengai, Kenya: proposed geothermal spa and crop drying. Geothermal Training Programme, (9).
- Kjeld, A., Bjarnadottir, H. J., & Olafsdottir, R. (2022). Life cycle assessment of the Theistareykir geothermal power plant in Iceland. Geothermics, 105, 102530 https://doi.org/10.1016/j.geothermics.2022.102530
- Koissaba, B. R. O. (2017). Geothermal Energy and Indigenous Communities. https://eu.boell.org/sites/default/files/geothermal-energy-and-indigenous-communities-olkariaproject-kenya.pdf
- Kong'ani, L. N. S., Wahome, R. G., & Thenya, T. (2021). Variety and management of developmental conflicts: the case of the Olkaria IV geothermal energy project in Kenya. Conflict, Security & Development, 21(6), 781-804. https://doi.org/10.1080/14678802.2021.2000806
- Kong'ani, L. N. S., & Kweyu, R. M. (2022). Toward Sustainable Implementation of Geothermal Energy Projects; the Case of Olkaria IV Project in Kenya. DOI: 10.5772/intechopen.107227
- Lacirignola, M., & Blanc, I. (2013). Environmental analysis of practical design options for enhanced geothermal systems (EGS) through life-cycle assessment.
 Renewable energy, 50, 901-914. https://doi.org/10.1016/j.renene.2012.08.005



- Lund, J. W., & Toth, A. N. (2021). Direct utilization of geothermal energy 2020 worldwide review. Geothermics, 90, 101915.
 https://doi.org/10.1016/j.geothermics.2020.101915
- Mainar-Toledo, M. D., Halaçoğlu, U., Sahiller, H. A., Hazar, T., Zuffi, C., Díaz-Ramírez, M., & Manfrida, G. (2023). Environmental benefits for a geothermal power plant with CO2 reinjection: case study of the Kizildere 3 U1 geothermal power plant. Energy Storage and Saving, 2(4), 631-638. https://doi.org/10.1016/j.enss.2023.08.005
- Manfrida, G., Talluri, L., Ungar, P., Zuffi, C., Díaz-Ramírez, M., Leiva, H., Mainar-Toledo, M. D. & Jokull, S. (2023). Exergo-economic and exergo-environmental assessment of two large CHP geothermal power plants. Geothermics, 113, 102758. https://doi.org/10.1016/j.geothermics.2023.102758
- Matthews, H. S., Hendrickson, C. T., & Matthews, D. (2014). Life cycle assessment: quantitative appro aches for decisions that matter. Open access textbook. https://www.lcatextbook.com/
- McCay, A. T., Feliks, M. E., & Roberts, J. J. (2019). Life cycle assessment of the carbon intensity of deep geothermal heat systems: A case study from Scotland. Science of the total environment, 685, 208-219. https://doi.org/10.1016/j.scitotenv.2019.05.311
- Menberg, K., Pfister, S., Blum, P., & Bayer, P. (2016). A matter of meters: state of the art in the life cycle assessment of enhanced geothermal systems. Energy & Environmental Science, 9(9), 2720-2743. https://doi.org/10.1039/C6EE01043A
- Menberg, K., Heberle, F., Bott, C., Brüggemann, D., & Bayer, P. (2021). Environmental performance of a geothermal power plant using a hydrothermal resource in the Southern German Molasse Basin. Renewable Energy, 167, 20-31. https://doi.org/10.1016/j.renene.2020.11.028
- Mosaffa, A. H., Farshi, L. G., Ferreira, C. I., & Rosen, M. A. (2016). Exergoeconomic and environmental analyses of CO2/NH3 cascade refrigeration systems equipped with different types of flash tank intercoolers. Energy Conversion and Management, 117, 442-453. https://doi.org/10.1016/j.enconman.2016.03.053
- Mosaffa, A. H., Mokarram, N. H., & Farshi, L. G. (2017). Thermoeconomic analysis
 of a new combination of ammonia/water power generation cycle with GT-MHR cycle



- and LNG cryogenic exergy. Applied Thermal Engineering, 124, 1343-1353. https://doi.org/10.1016/j.applthermaleng.2017.06.126
- Moya, D., Aldás, C., & Kaparaju, P. (2018). Geothermal energy: Power plant technology and direct heat applications. Renewable and Sustainable Energy Reviews, 94, 889-901. https://doi.org/10.1016/j.rser.2018.06.047
- Mukoro, V., Gallego-Schmid, A., & Sharmina, M. (2021). Life cycle assessment of renewable energy in Africa. Sustainable Production and Consumption, 28, 1314-1332. https://doi.org/10.1016/j.spc.2021.08.006
- Noailly, J., & Shestalova, V. (2017). Knowledge spillovers from renewable energy technologies: Lessons from patent citations. Environmental Innovation and Societal Transitions, 22, 1-14. https://doi.org/10.1016/j.eist.2016.07.004
- ONDA. 2023. Website: https://www.onda-it.com/eng/
- Orka, H. S. (2023a). LIFE CYCLE ASSESSMENT OF A GEOTHERMAL POWER PLANT.
 https://www.hsorka.is/media/as2mickl/l%C3%ADfsferilsgreining-fyrir-reykjanes.pdf
- Orka, H. S. (2023b). LIFE CYCLE ASSESSMENT FOR SVARTSENGI GEOTHERMAL POWER PLANT.https://www.hsorka.is/media/a30hr1on/l%C3%ADfsferilsgreining-fyrir-svartsengi.pdf
- Palar, P. S., Liem, R. P., Zuhal, L. R., & Shimoyama, K. (2019, July). On the use of surrogate models in engineering design optimization and exploration: The key issues. In Proceedings of the Genetic and Evolutionary Computation Conference Companion (pp. 1592-1602). https://doi.org/10.1145/3319619.3326813
- Paulillo, A., Cotton, L., Law, R., Striolo, A., & Lettieri, P. (2020a). Geothermal energy in the UK: The life-cycle environmental impacts of electricity production from the United Downs Deep Geothermal Power project. Journal of Cleaner Production, 249, 119410. https://doi.org/10.1016/j.jclepro.2019.119410
- Paulillo, A., Cotton, L., Law, R., Striolo, A., & Lettieri, P. (2020b). Life-cycle inventory data and impacts on electricity production at the United Downs Deep Geothermal Power project in the UK. Data in brief, 29, 105117. https://doi.org/10.1016/j.dib.2020.105117
- Paulillo, A., Kim, A., Mutel, C., Striolo, A., Bauer, C., & Lettieri, P. (2021). Influential parameters for estimating the environmental impacts of geothermal power: A global



- sensitivity analysis study. Cleaner Environmental Systems, 3, 100054. https://doi.org/10.1016/j.cesys.2021.100054
- Pratiwi, A. S., & Trutnevyte, E. (2021). Life cycle assessment of shallow to medium-depth geothermal heating and cooling networks in the State of Geneva. Geothermics, 90, 101988 https://doi.org/10.1016/j.geothermics.2020.101988
- Quiri Echanges Thermiques. 2023. Web site: https://www.quiri.com/en/thermalexchanges/
- Renkens, I. (2019). The impact of renewable energy projects on indigenous communities in Kenya. IWGIA: Denmark, December. https://www.iwgia.org/images/publications/new-publications/IWGIA_report_28_The_impact_of_renewable_energy_projects_on_In digenous_communities_in_Kenya_Dec_2019.pdf
- Semmari, H., Bouaicha, F., Aberkane, S., Filali, A., Blessent, D., & Badache, M. (2024). Geological context and thermo-economic study of an indirect heat ORC geothermal power plant for the northeast region of Algeria. Energy, 290, 130323. https://doi.org/10.1016/j.energy.2024.130323
- Shamoushaki, M., Fiaschi, D., Manfrida, G., Niknam, P. H., & Talluri, L. (2021). Feasibility study and economic analysis of geothermal well drilling. International Journal of Environmental Studies, 78(6), 1022-1036. https://doi.org/10.1080/00207233.2021.1905309
- Sharmin, T., Khan, N. R., Akram, M. S., & Ehsan, M. M. (2023). A state-of-the-art review on geothermal energy extraction, utilization, and improvement strategies: conventional, hybridized, and enhanced geothermal systems. International Journal of Thermofluids, 18, 100323. https://doi.org/10.1016/j.ijft.2023.100323
- Shinko Ind. LTD. 2023. web site: https://www.shinkohir.co.jp/en/product.html
- Shortall, R., Davidsdottir, B., & Axelsson, G. (2015). Geothermal energy for sustainable development: A review of sustainability impacts and assessment frameworks. Renewable and sustainable energy reviews, 44, 391-406. https://doi.org/10.1016/j.rser.2014.12.020
- Siemens. 2023. Web site: https://www.siemens.com/global/en/industries/power-utilities.html?gclid=CjwKCAiA1-6sBhAoEiwArqlGPklww8eeeDwqR90yu1FfGhx-GAXjHIC3Jftt04aQBjSGDQnN3__3fBoCol0QAvD_BwE&acz=1&gad_source=1



- Simiyu, S. M., & Keller, G. R. (2000). Seismic monitoring of the Olkaria Geothermal area, Kenya Rift valley. Journal of Volcanology and Geothermal Research, 95(1-4), 197-208. https://doi.org/10.1016/S0377-0273(99)00124-9
- Soelaiman, T. A. F. (2016). Geothermal energy. Electric Renewable Energy Systems, 114-139.
- SPX technologies. 2023. SPX technologies Marley Recold SGS. Website: https://spxcooling.com/it/
- Templeton, J. D., Ghoreishi-Madiseh, S. A., Hassani, F., & Al-Khawaja, M. J. (2014). Abandoned petroleum wells as sustainable sources of geothermal energy. Energy, 70, 366-373. https://doi.org/10.1016/j.energy.2014.04.006
- Tole, M. P. (1996). Geothermal energy research in Kenya: a review. Journal of African Earth Sciences, 23(4), 565-575. https://doi.org/10.1016/S0899-5362(97)00019-5
- Tomasini-Montenegro, C., Santoyo-Castelazo, E., Gujba, H., Romero, R. J., & Santoyo, E. (2017). Life cycle assessment of geothermal power generation technologies: An updated review. Applied Thermal Engineering, 114, 1119-1136. https://doi.org/10.1016/j.applthermaleng.2016.10.074
- Tosti, L., Ferrara, N., Basosi, R., & Parisi, M. L. (2020). Complete data inventory of a geothermal power plant for robust cradle-to-grave life cycle assessment results. Energies, 13(11), 2839. https://doi.org/10.3390/en13112839
- Tran, T. T., & Smith, A. D. (2018). Incorporating performance-based global sensitivity and uncertainty analysis into LCOE calculations for emerging renewable energy technologies. Applied energy, 216, 157-171. https://doi.org/10.1016/j.apenergy.2018.02.024
- Treyer, K., Oshikawa, H., Bauer, C., & Miotti, M. (2015). WP4: environment. Energy from the Earth. Deep Geothermal as a Resource for the Future.
- Trinomics, B. V. (2020). Final Report Cost of Energy (LCOE). Energy costs, taxes and the impact of government interventions on investments. https://energy.ec.europa.eu/system/files/2020-10/final_report_levelised_costs_0.pdf
- Tryggvadóttir, L., Chatenay, C., Sigurðardóttir, V. Y., Jóhannesson, Þ.,
 Hallgrímsson, J. H., Tulinius, H., ... & Efla, I. S. O. R. (2020, November). Direct



- utilization of geothermal resources: overview with focus on Africa. In Proceedings, 8th African Rift Geothermal Conference. Nairobi, Kenya (pp. 2-8).
- Ueckerdt, F., Hirth, L., Luderer, G., & Edenhofer, O. (2013). System LCOE: What are the costs of variable renewables?. Energy, 63, 61-75. https://doi.org/10.1016/j.energy.2013.10.072
- Vito, SpA RINA Consulting, EY, 2020. Study on 'Geothermal plants' and applications' emissions: overview and analysis: final report., Publications Office of the European Union.
 Belgium.
 Retrieved
 from https://policycommons.net/artifacts/294394/study-on-geothermal-plants-and-applications-emissions/1183716/
 on 05 Mar 2024. CID: 20.500.12592/4xktt6. https://doi.org/10.2777/755565
- WEACH, 2023. Word Energy Absorption Cooling & Heating. Website: https://www.worldenergyeurope.eu/
- Wessels company, 2023. Web site: https://www.westank.com/
- Williams, C. F., Reed, M. J., & Anderson, A. F. (2011, January). Updating the classification of geothermal resources. In Proceedings, Thirty-Sixth Workshop on Geothermal Reservoir Engineering (p. 2011).
- Yang, S. Y., & Yeh, H. D. (2009). Modeling heat extraction from hot dry rock in a multi-well system. Applied Thermal Engineering, 29(8-9), 1676-1681. https://doi.org/10.1016/j.applthermaleng.2008.07.020
- Yu, T., Zhang, X., Feng, R., Wang, C., Wang, X., & Wang, Y. (2022). Comparison of the effects of high hydrostatic pressure and pasteurization on quality of milk during storage. Foods, 11(18), 2837. https://doi.org/10.3390/foods11182837
- Zarrouk, S. J., & Purnanto, M. H. (2015). Geothermal steam-water separators: Design overview. Geothermics, 53, 236-254. https://doi.org/10.1016/j.geothermics.2014.05.009
- Zarrouk, S. J., & Moon, H. (2015). Response to the Comments by Ronald DiPippo on "Efficiency of geothermal power plants: A worldwide review". Geothermics, 53, 550-553. https://doi.org/10.1016/j.geothermics.2014.08.009
- Zhai, H., Shi, L., & An, Q. (2014). Influence of working fluid properties on system performance and screen evaluation indicators for geothermal ORC (organic Rankine cycle) system. Energy, 74, 2-11. http://dx.doi.org/10.1016/j.energy.2013.12.030



Zuffi, C., Manfrida, G., Asdrubali, F., & Talluri, L. (2022). Life cycle assessment of geothermal power plants: A comparison with other energy conversion technologies. Geothermics, 104, 102434. https://doi.org/10.1016/j.geothermics.2022.102434